

Seton Hall University

eRepository @ Seton Hall

Seton Hall University Dissertations and Theses
(ETDs)

Seton Hall University Dissertations and Theses

Spring 5-1-2020

Electrical and Chemical Characterization of a Helium-Air Non-Thermal Atmospheric Pressure Plasma Jet

Adam Zandani

adam.zandani@student.shu.edu

Follow this and additional works at: <https://scholarship.shu.edu/dissertations>



Part of the [Engineering Commons](#), and the [Physics Commons](#)

Recommended Citation

Zandani, Adam, "Electrical and Chemical Characterization of a Helium-Air Non-Thermal Atmospheric Pressure Plasma Jet" (2020). *Seton Hall University Dissertations and Theses (ETDs)*. 2801.
<https://scholarship.shu.edu/dissertations/2801>

Electrical and Chemical Characterization of a Helium-Air Non-Thermal Atmospheric Pressure
Plasma Jet

By

Adam Zandani

Submitted in partial fulfillment of the requirements for the degree
Master of Physics
Department of Physics
Seton Hall University
May 2020

© 2020 Adam Zandani

SETON HALL UNIVERSITY
COLLEGE OF ARTS AND SCIENCES
DEPARTMENT OF PHYSICS

APPROVAL FOR SUCCESSFUL DEFENSE

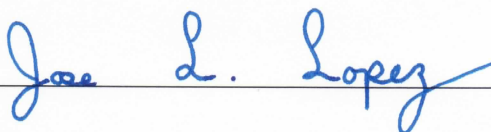
Adam Zandani has successfully defended and made the required modifications to the text of the master's thesis for the **M.S.** during this **Spring Semester 2020**

MASTER'S COMMITTEE

(please sign and date beside your name)

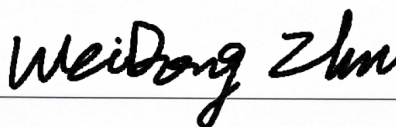
Mentor:

Dr. Jose L. Lopez



Committee Members:

Dr. Wei-Dong Zhu



Dr. M. Alper Sahiner



The mentor and any other committee members who wish to review revisions will sign and date this document only when revisions have been completed. Please return this form to the Office of Graduate Studies, where I will be placed in the candidate's file and submit a copy with your final thesis to be bound as page number two.

Acknowledgements

I would personally like to thank Dr. W Zhu the guidance and support during my undergraduate years in physics. I would also like to thank him for the use of equipment to make this possible. My utmost gratitude goes to Dr. J Lopez for having faith in me and accepting me into the Master's program at Seton Hall and making this study possible. I am grateful for the guidance and encouragement provided. I would also like to thank Dr. M Sahiner for being a part of my committee and providing priceless feedback and support since arriving in Seton Hall University.

TABLE OF CONTENTS

Acknowledgements.....	i
Abstract.....	iii
Chapter 1: Introduction.....	1
Chapter 2: DBD and Literature Review.....	15
Chapter 3: Experimental Setup and Method.....	21
Chapter 4: Results and Discussion.....	24
4.1: Species Production.....	25
4.1.1 Hydroxyl Radical.....	26
4.1.2 N ₂ (Second Positive System).....	37
4.1.3 N ₂ ⁺ (First Negative System).....	47
4.1.4 N ₂ (First Positive System).....	56
4.1.5 Helium Metastable.....	64
4.1.6 Atomic Oxygen.....	72
4.1.7 Reynold's Number.....	80
4.2 Electrical Characteristics.....	81
4.3 Gas Temperature Fit.....	90
Chapter 5: Conclusion.....	97
References.....	98

ABSTRACT

Plasma is one of the most complicated, yet promising fields in physics due to its high efficiency and multitude of crucial applications such as biological sterilization, polymer modification, surface treatments, etching, agriculture, and facilitation of selective catalytic processes to name a few. With these advantages, mysteries still remain. With this in mind, in order to accurately gauge the total influence of the plasma applied in various processes, understanding what is being produced and how the production occurs is vital. To understand this, optical emission spectroscopy was used to gauge how the species generated are influenced by operation parameters such as voltage, frequency, flow rate, and distance along the effluent. It was found that increasing voltage increased the intensity of all species generated. The emission of OH (308 nm), He (706nm) and atomic O (777nm) were found to decrease as it got further away from the exit, while the emission of N₂ (337nm), N₂⁺ (391nm), and N₂ (631nm) increased due to the increased air interaction. With an increase in flow rate, all species benefitted except N₂ (337nm) and N₂ (631nm) which peaked around 5 L/min due to increasing ionization of N₂⁺ (391nm) at higher flow rates. Analysis of generation mechanisms show the significance of the Penning effect between metastable He and air molecules on specie production while electron impact mechanisms are heavily dependent on power coupling of the system. Reaction rates and loss mechanisms explain the temporal evolution of the plasma jet and its effect on specie production. Gas temperature was found to deviate slightly regardless of operational parameters.

CHAPTER 1: INTRODUCTION

Although it is more convenient to refer to plasma as the first state of matter due to its significance in the universe, plasma is frequently defined as the fourth state of matter, with the other three being the commonly taught solid, liquid and gas. To explain, plasma is the most abundant form of matter in the universe making up more than 99% of visible matter including stars but it is seen as the fourth state on an energy scale. For example, a solid contains particles that are tightly packed, contain the least amount of kinetic energy, and have a definite shape and volume. As sufficient energy is applied, the particles begin to loosen their structure and transition into a state of matter where they do not have a definite shape but still contain a definite volume known as a liquid. Similarly, as more energy is applied the particles gain kinetic energy and as a result, they move freely. This state is known as a gas state where the particles of the gas are not defined by a shape or volume. The amount of energy needed for these state transitions is referred to as latent heat. When a substantial amount of energy is applied to a gas state, the electrical properties of the gas changes and creates a state of free moving charged particles, ions, and neutral particles which is defined as a plasma. Plasmas are electrically neutral due to the similar electron and ion concentrations on average; however, it is actually electrically conducting due to the free moving electrons available throughout the plasma. With this information, we define plasma as a quasi-neutral state that contains electrons, neutral particles, positive and negative ions that interact to create a form of matter.

In order to characterize plasma, it can be placed in one of two categories: thermal equilibrium (hot) or non-thermal equilibrium (cold). A plasma in thermal equilibrium means that the temperature of the neutral particles in the gas, T_n , and the temperature of the electrons, T_e , are close to each other. This is due to the electron gaining more energy through the plasma

generation process than it is losing due to collisions with the neutral particles, which are much heavier than the electron. In this instance, the temperatures of both the neutral particles and the electrons can reach several thousand Kelvin and, in some cases, the temperatures can get high enough to result in thermonuclear fusion. These plasma energies are usually in the range of fifty to hundreds of eV (electron-volts). Typical uses for thermal equilibrium plasmas include welding and cutting where such high temperatures are needed to influence the material. On the other hand, a plasma is considered to be non-thermal equilibrium when T_n is much lower than T_e because the method of plasma generation does not allow the electrons to transfer the kinetic energy gained to the heavier neutral particles during the collisions. Because of this, the plasma energy usually ranges from 1 to tens of eV while the neutral particles stay near room temperature.

Both types of plasmas are naturally occurring and can also be manmade. In the case of manmade forms, there are many different methods of generating it including through pulsed DC (direct-current), RF (radio-frequency), and AC (alternating-current) power. For this paper, generating the plasma via AC power is of particular interest. Regardless of method of generation, certain stipulations must be satisfied in order to be considered a plasma. Because this form of matter is defined by the interaction and movement of charged particles and neutrals in the medium, this leads to the formation of Coulombic forces and electromagnetic fields. The creation of the forces and fields then concentrates the charges to a range of λ_D , where outside of the range is electrically neutral and inside the range is not. λ_D is known as the Debye length and is mathematically defined as:

$$\lambda_D = \left(\frac{\epsilon_0 k T_e}{n_e e^2} \right)^{\frac{1}{2}} \quad (1.1)$$

$$L \gg \lambda_D \quad (1.2)$$

Here, ϵ_0 , k , T_e , n_e , and e are the permittivity of free space, Boltzmann's constant (1.38×10^{-23} J/K), electron temperature, electron density, and electron charge, respectively. Also, L is the dimension of the plasma which must be much greater than the Debye length. The Debye length of any plasma is representative of its polarization and strong charge separation [1]. The Debye length is the radius of the Debye sphere, which is the volume containing the electrons and various other particles. Another condition to be satisfied is that the number of electrons within the sphere must be very large:

$$n_e \lambda_D^3 \gg 1 \quad (1.3)$$

Which results in the average electron distance to be very small compared to the Debye length, λ_D , with the quantity being known as the plasma parameter and defined as:

$$g = 1/(n_e \lambda_D^3) \quad (1.4)$$

Another requirement is the time domain of the plasma:

$$\omega \tau \gg 1 \quad (1.5)$$

where τ is the average time an electron spends between collisions with neutrals and ω is the angular frequency of plasma oscillations [2].

In a plasma, electrons are the primary energy carriers and providers due to the fact that they are the first particles to receive the energy induced. This is because of their very low mass

($m_e = 9.11 \times 10^{-31}$ kg) which also plays a role in their high mobility. After receiving the energy, the collisions with the neutral particles allow them to transmit this energy and result in various processes such as ionization, excitation, and dissociation. These processes rely on the electrons to have the right amount of energy to facilitate the process. Because not every electron will have the same amount of energy, the probability for an electron to have a certain energy to enable a certain process is described as the electron energy distribution function. This distribution function heavily depends on the electric field and gas composition of the system and can usually be defined by the Maxwell-Boltzmann distribution function:

$$f(\varepsilon) = 2\sqrt{\varepsilon/\pi(kT_e)^3} \exp(-\varepsilon/kT_e) \quad (1.6)$$

Here, T_e is the electron temperature and k is the Boltzmann constant. Additionally, the mean electron energy for this distribution is proportional to the electron temperature in the following way:

$$\langle \varepsilon \rangle = \int_0^{\infty} \varepsilon f(\varepsilon) d\varepsilon = \frac{3}{2} T_e \quad (1.7)$$

In the case of an electron containing enough energy to ionize, a positive ion is formed. Relative to electrons, ions are considered to be heavy particles that cannot obtain high energy from the applied electric field the same way electrons do due to their energy exchange with other constituents in the plasma. In non-equilibrium discharges (cold plasma), the mechanism of energy transfers for these positive ions typically yield an energy distribution function similar to the Maxwell-Boltzmann function with the ion temperature (T_i) nearly the same as the neutral gas

temperature (T_0) [1]. The ability for an electron to ionize a neutral atom, molecule, or radical is dependent upon the ionization energy required for that specific atom or molecule to lose the electron. This process requires a high amount of energy and usually dictates the “upper limit” of the energy exchange in the plasma [1].

In addition to positive ions, the formation of negative ions are also possible. They are typically produced through recombination processes or attachment of electrons after being dissociated. Similar to positive ions, they are heavy particles that do not receive energy from the applied EF and have energy distribution functions close to the Maxwell-Boltzmann EEDF. Different atoms, radicals, and molecules each have different electron affinities (EA). Electron affinity is described as the bonding energy between an attaching electron and the subsequent atom or molecule. The higher the electron affinity, the stronger the atom or molecule will want to attach to a free electron. Because of this, halogens and other electronegative particles will have the highest value of electron affinity.

Formations of positive ions through ionization and negative ions through recombination and attachments are examples of the elementary processes that occur in a plasma. Ionization, excitation, and dissociation are examples of inelastic collisions where the electrons transfer kinetic energy gained into the internal degrees of freedom of the atom (translational) and molecules (translational, vibrational, rotational). These processes are governed by the cross sections, mean free path, the interaction frequency reaction rate, and the reaction rate coefficient which depends on the type of process occurring.

To begin with, the cross section of a particle defines the area in which another particle must be within in order for an elementary process to occur. The cross sections heavily depend on the energies of the possible colliding species. For instance, if one of the colliding partners has a

large energy, the cross section can decrease due to the decrease in the probability of having enough time to interact. The cross section of a particle can be visualized as a circle with area π . If another particle travels and passes through the area, then the other particle will interact and go on to begin a certain elementary process. The mean free path between possible colliding partners classifies the distance one particle travels before colliding with another. This relation is defined as:

$$\lambda = \frac{1}{n_B \sigma} \quad (1.8)$$

where n_B is the number density and σ is the cross section of particle “B” (usually a neutral particle). Coupled with the mean free path and its cross section, the colliding partner travels the cylindrical volume $\sigma\lambda$ and the reaction occurs as long as that volume has at least one particle of particle “A” (usually an electron) [1]. The interaction frequency (ν) at this point compensates for the colliding partner’s velocity as well as the cross section at that velocity and is defined as:

$$\nu_A = n_B \int f(\nu) \sigma(\nu) \nu d\nu = \langle \sigma \nu \rangle n_B \quad (1.9)$$

The elementary reaction rate is used to describe the number of elementary processes that take place in unit volume per unit time [1]. To find this reaction rate, the interaction frequency of the colliding partners and their number densities are multiplied together and gives:

$$\omega_{A+B} = \langle \sigma \nu \rangle n_A n_B \quad (1.10)$$

$$k_{A+B} = \int f(v) \sigma(v) v dv = \langle \sigma v \rangle \quad (1.11)$$

The reaction rate coefficient is denoted by k and takes into account the velocity distribution function of the colliding partners as well as the cross sections. Equation (1.11) is calculated for bimolecular reactions, however, to compensate for mononuclear reactions and three-body processes, minor adjustments are made:

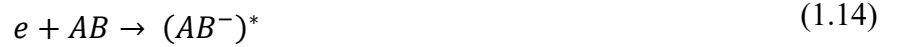
$$\omega_A = k_A n_A \quad (1.12)$$

$$\omega_{A+B+C} = k_{A+B+C} n_A n_B n_C \quad (1.13)$$

Formation of positive ions usually require an electron to have a discrete energy value greater than or equal to the ionization energy, I , in order to knock an electron off the atom or molecule. Be that as it may, that is not the only way to ionize an atom or molecule. One of these ways is referred to as the Penning Ionization Effect. In this circumstance, the electron can enter the cross section of one particle and excite it into a metastable state. The excitation energy of this metastable state can surpass the ionization potential of another particle and the resulting collision can lead to ionization. With this effect, the cross sections can be fairly high ($\sim 10^{-15}$ cm) which allows for a higher probability of the electronically excited metastable state to interact with another particle.

On the other hand, the formation of negative ions also have more than one method of facilitation. One of these processes in particular is known as dissociation. In this instance, the incoming electron is set to collide with a molecule. Molecular vibrations are usually on the scale

of 10^{-14} - 10^{-13} s [1] while the interaction time between the colliding electron and molecule is about 10 to 100 times faster. Due to this large time disparity, the heavy molecules are essentially “frozen” [1] at the time of collision and is only stimulated by the electron impact. This specification is known as the Franck-Condon principle. When the moment of impact arrives, the colliding electron attaches to the molecule and sends it into an intermediate excited state:



This resulting excited state unstable and can lead to one of two possibilities: the excited states reverses to the stable molecule with a free electron ($AB+e$) or the molecule dissociates and the electron attaches to one of the atoms ($A+B^-$ or A^-+B). When the molecule dissociates and the electron is attached, the process is no longer balanced. Because of this, the dissociative attachment process is a resonant reaction which means that the colliding electron must possess an exact amount of energy needed to avoid reversing to the free electron and stable molecule. This is decided by the amount of potential energy harnessed by the molecule after colliding with the electron. If the potential energy of the original molecule (AB) is larger than the intermediate state (AB^-), then it will continue to dissociate and lead to:



The maximum cross section of this process is given by:

$$\sigma_{d.a.}^{max} \approx \sqrt{\frac{m(M_A + M_B)}{M_A M_B}} \quad (1.16)$$

Where m is the mass of the electron and σ_0 is the gas-kinetic cross section. This process is only possible when the electrons have more energy than the difference between the dissociation energy and the molecules electron affinity [1]. Due to its highly resonant nature, it is estimated that the dissociative attachment rate coefficient is proportional to the electron temperature as defined as:

$$k_A(T_e) = \sigma_{d.a.}^{max}(\varepsilon_{max}) \sqrt{\frac{2\varepsilon_{max}}{m} \frac{\Delta \varepsilon}{T_e}} \exp\left(-\frac{\varepsilon_{max}}{T_e}\right) \quad (1.17)$$

In addition to ionization and dissociation, an electron can collide with a neutral atom or molecule and excite it either electronically, vibrationally, or rotationally with the last two only possible in molecules due to the degrees of freedom. In the case of electronic excitation, a particle can be excited into a resonance-excited state where the particle can easily de-excite through spontaneous transitions and photon emissions. On the contrary, an electron can excite a particle into an excited state where this spontaneous radiative transition to the ground state is no longer possible and this is called a metastable excited state. In this mode, they can de-excite through radiation as well as collisions with other plasma components (Penning ionization). Unlike the resonance-excited states, metastables have very long lifetimes that last seconds and even minutes [1]. This allows them to be generated in a discharge and de-excited through a specific collision to produce a specific reaction.

Furthermore, molecules can be excited vibrationally due to the added degrees of freedom. This vibrational excitation is vital due to the fact that most of the energy from the discharge is transferred from the electrons to modes of molecular vibrations [1]. In order to understand these

levels of vibrational excitation, the Morse potential defines the potential curve for diatomic molecules and is mathematically represented as:

$$U(r) = D_0[1 - \exp(-\alpha(r - r_0))]^2 \quad (1.18)$$

Here, r is the distance between the atoms. r_0 , α , and D_0 represent the equilibrium distance between the nuclei in the molecule, the force coefficient of interaction between the nuclei, and the dissociation energy of a diatomic molecule with respect to the minimum energy, respectively. These three variables are also referred to as the Morse parameters. In the case of any type of molecule, the degrees of freedom are not always harmonic. Despite this, the energy of the discrete vibrational levels can still be calculated by:

$$E_v = \hbar\omega \left(v + \frac{1}{2} \right) - \hbar\omega x_e \left(v + \frac{1}{2} \right)^2, x_e = \frac{\hbar\omega}{4D_0} \quad (1.19)$$

To compensate for the anharmonicity of a diatomic molecule, parameter x_e is introduced with a typical value of about .01[1]. Another aspect taken into account is the distance of the vibrational quantum levels. For a molecule that oscillates harmonically, the distance between the levels are equal, but this is not the case with the vibrational quantum of the anharmonic oscillator. As the vibrational quantum level increases, the energy distance decreases and this change is represented by:

$$\Delta E_v = E_{v+1} - E_v = \hbar\omega - 2 \hbar\omega x_e(v + 1) \quad (1.20)$$

Due to this constant energy decrease as the vibrational quantum number increases, the last two vibrational levels have the smallest energy difference.

The rotation energy of a diatomic molecule does not suffer from the complexities of harmonic and anharmonic and can be found from the Schrödinger equation as a function of its rotational quantum number:

$$E_r = \frac{\hbar}{2I} J(J + 1) = BJ(J + 1) \quad (1.21)$$

$$I = [M_1 M_2 / (M_1 + M_2)] r_0^2 \quad (1.22)$$

Where B is the rotational constant and I is the momentum of inertia of the diatomic molecule and factoring in the two masses of the molecule. These values are heavily dependent upon r_0 which is the distance between nuclei during molecule vibration. With this relation, it is clear that the constant B decreases as the vibrational quantum number increases:

$$B = B_e - \alpha_e \left(v + \frac{1}{2} \right) \quad (1.23)$$

For this relation, B_e defines the zero vibrational level and constant α_e describes the influence of molecular vibration on the momentum of inertia and rotational constant, B .

What has been discussed helps to understand the elementary processes of charged species and the processes of excited molecules in the plasma, however it does not help to explain how a

plasma is produced. As mentioned earlier, various forms of power can be used to generate it (AC, DC [pulsed], RF) and in these cases, they provide the breakdown voltage necessary to produce a plasma through an applied electric field. When the electric field is sufficiently high enough, the electrons gain more energy from the applied EF than they lose through collisions with the neutral particles. This causes them to accelerate and produce the electron avalanche needed to breakdown the gas. The avalanche can more accurately described as a multiplication of electrons per unit length of the applied electric field, which is known as the Townsend breakdown mechanism. The ionization coefficient in this mechanism is denoted by α , and is related to the direct electron impact ionization coefficient by:

$$\alpha = \frac{v_i}{v_d} = \frac{1}{k_i} \left(\frac{E}{n_0} \right) n_0 = \frac{1}{\mu_e} \frac{k_i(E/n_0)}{E/n_0} \quad (1.24)$$

Where v_d is the electron drift velocity, v_i is the ionization frequency and μ_e is the electron mobility. Because this electron mobility is inversely proportional to the pressure in the system, the Townsend coefficient is adjusted to become parameter α/p . Moreover, due to the nature of the Townsend breakdown mechanism, another parameter is factored in and it is called the secondary electron emission coefficient, γ , which is the probability of a secondary electron being generated when a positive ion impacts the cathode. In the Townsend breakdown, each primary electron (electron to start the avalanche) produces $\exp(\alpha d)-1$ positive ions in the gap. As these positive ions are forming, they move towards the cathode and eliminate $\gamma[\exp(\alpha d)-1]$ electrons from the cathode [1]. This γ depends on the type of material, type of gas and ion energy.

However, different circumstances require different applied EFs to initiate the breakdown of the gas. In 1889, Friedrich Paschen established Paschen's Law which is an equation that provides the breakdown voltage for a gas between two electrodes as a function of pressure (in Torr) and gap distance (in cm) and is defined as:

$$V = \frac{B(pd)}{C + \ln(pd)} \quad (1.25)$$

Where C equals:

$$C = \ln A - \ln \ln[(1/\gamma) + 1] \quad (1.26)$$

In this relation, A is defined as saturation ionization of the gas while parameter B is related to the excitation and ionization energies.

When this breakdown voltage is met, the non-conducting working gas is now conductive. The strong primary avalanche then forms a thin plasma channel that is described as a “streamer” [1]. The direction of the streamer is dependent upon the discharge gap. For example, if the discharge gap is small, then streamer forms only when the primary avalanche reaches the anode and is known as a cathode directed streamer. The streamer first begins at the anode because the electric field will be the highest due to the concentration of positive charges and this results in a fast propagation towards the cathode. Typical values of plasma densities (maximum electron concentration) at the head of the streamer is about 10^{12} - 10^{13} cm^{-3} [1].

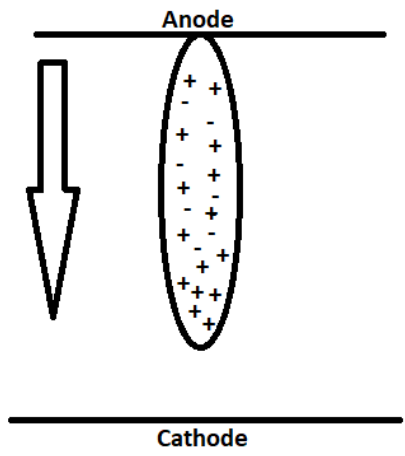


Figure 1. Illustration of cathode-directed streamer. Ref. Adam Zandani

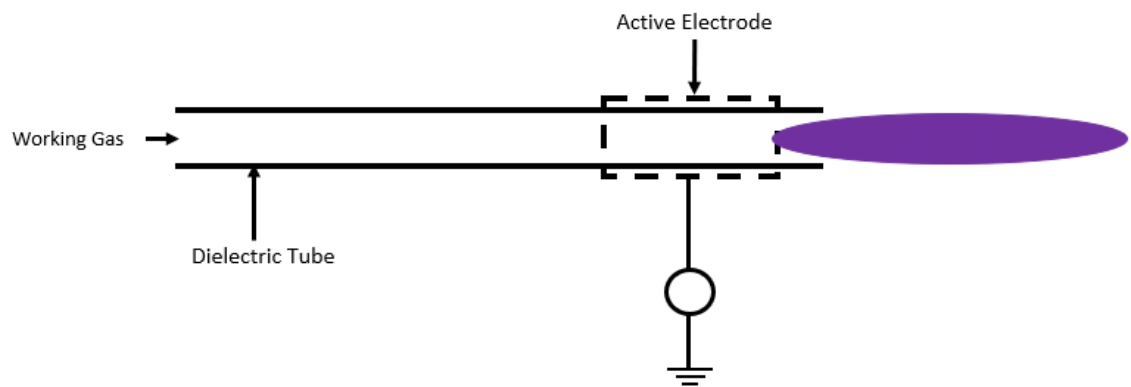
CHAPTER 2: DBD & LITERATURE REVIEW

DBD directly means Dielectric Barrier Discharge. The barrier usually consists of two electrodes separated by a dielectric. In some cases, the dielectric between the electrode gap can be the carrier gas while in other instances it can be an insulating material such as ceramic, glass, or a form of polymer. When a high electric field is applied across the electrodes, a discharge can occur. Hence, constituting the name Dielectric Barrier Discharge. Although this method is a common tactic in generating atmospheric pressure plasma, there is not only one way to configure it. In fact, there are four ways: dielectric-free electrode jets (DFE), single electrode jets, dielectric barrier discharge-like jets and, dielectric barrier discharge-based jets (DBD).

To begin with, a dielectric free electrode jet is just as the name describes. It is free of a dielectric and uses two electrodes in which a high voltage electrode is placed within an electrode in the form of a tube. This tube electrode is then grounded and an RF power source allows for the discharge to occur. However, due to the fact it does not contain a dielectric, the power coupled into the plasma is relatively high compared to other methods. This high power that is delivered to the plasma results in gas temperatures higher than room temperature.

Single electrode jets can be constructed in one of two ways, either with a dielectric tube on the outside of a high voltage electrode or just with a single high voltage electrode. When placed inside of the dielectric tube, the tube only acts as carrier of whatever working gas is used. As with any other form of DBD plasma, it can be generated with a wide host of power systems such as AC, DC (pulsed), or RF, but this construction is prone to arcing. To combat this, an RC (resistor-capacitor) circuit is usually coupled into the system in order to control exactly how much of the applied voltage and current makes it to the discharge. A DBD-like jet is built similarly to the single electrode jet, but differs with the addition of a grounded electrode.

In this work, the DBD-based jet is of primary concern. In this configuration, a high voltage electrode is placed in series with a dielectric tube with the working gas usually a noble gas (He, or Ar) and results in a discharge of an atmospheric pressure plasma jet which operates with an electron temperature of 1-2 eV [10]. It can also be built with either only the high voltage electrode in series or also with a grounded electrode in series. It should be noted that in the instance of only one electrode, the discharge that occurs is not as strong as in a double electrode setup. The benefit of using a dielectric in these configurations is that it is significant to the non-thermal property of the plasma. As the electric field is applied to the electrode to allow discharge, charge builds up on the dielectric material. This creates an electrical potential which limits the amount of applied current that makes it into the discharge which results in a plasma with a low power density [2]. This limitation allows the jet to be developed while only using several watts of power [2]. The dielectric also serves a way avoid arcing due to its insulating properties. The reason noble gases are used as the working gas is because of its ability to be excited into a metastable state and allowing for breakdown through collisions with these metastables and primary electrons provided by the applied electric field or through Penning Ionization. This type of breakdown is known as the Townsend breakdown which is described in the previous chapter.



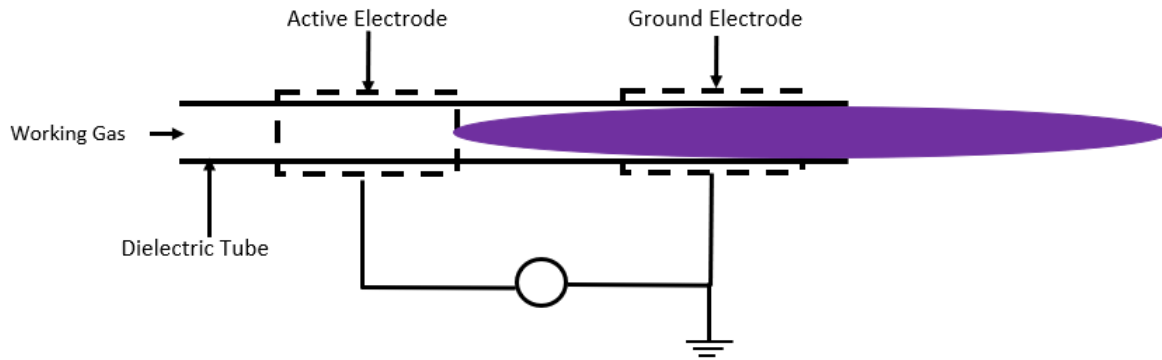


Figure 2. Schematic of single electrode and double electrode DBD based jet. Ref. Adam Zandani

Both the single and double electrode design has been studied by Jiang *et al.* [3] to understand its effect on the plasma generation and characteristics. The jet length, optical intensities, discharge current, and propagation velocities were examined as a function of changing design, gas flow rates, and voltage. The method of generation used is an AC power supply with a constant output of 17 kHz with voltage ranging from 4 kV to 12 kV with helium (99.999% purity) as the working gas. The dielectric used here is a quartz capillary tube and placed in series with aluminum electrodes that are 2 cm apart in the double electrode configuration. The active electrode remains at 1 cm from the dielectric tip throughout the study. The optical intensities were observed by placing two photoelectron multiplier tubes orthogonal to the jet axis at 25 mm away from the effluent which also provides information on the propagation velocity by recording the photoelectron emission through a time instance. In the case of studying the discharge current, a 300 Ω load resistor is placed on the active electrode or on the ground electrode, depending on the design, then connected to high voltage passive probe to obtain the waveform and record it through an oscilloscope. It was observed that as gas flow rate increased from 50 L/min to 200 L/min, the jet length increased.

This trend was also observed as the peak-to-peak voltage was increased; however, it was seen that at a necessarily high voltage, the discharge extends further than the ground electrode. When the voltage gets to that point, the ground electrode can no longer compensate this high polarization which “results in an overfall of charges” [3]. In this circumstance, the applied voltage must surpass ~8 kV in order to sustain a discharge. This gives insight into how a discharge is able to form in a single electrode design. Due to the absence of a ground electrode, the circuit is completed by the drift of charge carriers in the working gas and acts as a virtual ground [3]. Furthermore, this means that the active electrode is the anode while the virtual ground (gas) is the cathode. When the discharge occurs, it is propelled into the ambient air (downstream) and upstream through the tube by the flow of the gas making the jet formation a cathode-directed streamer. It is mentioned that with a ground electrode, the streamer makes a conducting channel which categorizes it as a streamer-triggered glow discharge [3].

In addition to this study, other investigations of the single electrode design have been performed such as the spectroscopic study of an atmospheric plasma jet conducted by Zhu *et al.* [4]. Here, the jet was propelled into both ambient air as well as a glass bottle purged with helium to understand how it interacts with the air once it leaves the dielectric tube. A copper electrode is placed 4 cm away from the glass tube and being driven by an AC power source at 52 kHz and around 4 kV [4]. To obtain spectroscopic readings, an EMCCD (electron multiplying charge coupled device) is placed perpendicular to the jet axis. It was observed that the emission spectrum in the ambient air was predominately comprised of excited N_2 ($C^3\Pi_u-B^3\Pi_g$), ionized N_2 , metastable He atoms, Oxygen and OH particles. On the other hand, when emission spectrum was taken of the jet in the helium filled tube, the helium metastable species were much more prevalent than any others. This is because the N_2 , OH, and O lines are only strongly emitted due

to the plasma's interaction with the air. N₂ and OH lines were still present in this case due to the N₂ and H₂O molecules on the surface of the glass walls and possible impurities in the gas feed lines [4].

When it comes to spectroscopy readings, recognizing the distance away from the light source, how much light is being collected, and where along the effluent readings are being taken are vital to understanding the information provided by the emission intensities of various species. With this in mind, Ilik *et al.* [5] conducted a study in which the optical behavior of a helium jet is of concern. It should be noted that although this paper is focused on a single electrode jet driven by AC power, the design utilized by Ilik and co-author use an axial pin electrode and an external ring electrode design [2]. Despite this, the similarity between the single electrode and this design is that they are both types of a DBD-based configuration. To continue, a spectrometer is coupled with a CCD to study the emission intensities as flow rate changes. The jet is powered by an AC power supply with a voltage of 18 kV and a frequency of 15 kHz. The helium gas flow rates were varied from 1 L/min to 5 L/min in increments of 1 L/min. It was observed that as gas flow rate increased, Oxygen species, OH, and ionized N₂ molecules increased while excited N₂ reached a peak value at around 3 L/min. According to the authors, this is due to the increasing ionization of N₂ molecules. As gas flow rate increases, N₂ becomes increasingly ionized by the increased flow of helium metastables that allow for the Penning Ionization of the molecule.

Just as important as the chemistry of the atmospheric pressure jets, is the electrical parameters and information provided. Typical electrical characteristics are usually the applied voltage, current, and frequency coming from the power supply to the electrode(s). The applied voltage and frequency is usually provided through the use of a high voltage passive probe, while the applied current is provided through an inductive coil or a high voltage load resistor when

available (double electrode system, second high voltage probe) which are all then connected back to an oscilloscope to be digitally stored. One massive advantage in using a double electrode configuration is the ability to obtain the discharge current and a QV analysis (Lissajous figure) of the plasma reactor by relatively easy circuit adjustments. That analysis allows for one to figure out exactly how much power is coupled into the plasma and allows some correlation between power consumed by the reactor and the emission intensities of the various species.

Arguably one of the most important aspects of an atmospheric pressure cold plasma jet is its gas temperature. The temperature is around room temperature which makes it ideal for a whole host of applications and implementations. Because of this, techniques for obtaining values of the gas temperature have been employed. Depending on the level of excitation in the air plasmas, either the OH radical, the excited N₂ ($C^3\Pi_u-B^3\Pi_g$) molecule, the ionized N₂, NO or O₂ can be used. Also, due to the nonequilibrium nature of these plasmas, it was determined that the overall gas temperature is best estimated by the rotational temperatures. In this paper, Laux *et al.* [7] uses the technique of a program called SpecAir. In this program, the spectra of the selected molecule is imported and the program uses theoretical values in order to best fit the experimental spectra. Through functions such as the slit function, the program is able to take into account (through input of the user) the grating, center wavelength, FWHM (full-width half maximum) and slit width of the spectrometer used in an attempt to best match the experimental parameters. After specifying all of these conditions, the program fits a theoretical spectrum with the measured in order to provide a very good estimation of not only the rotational temperatures, but also the electronic, translational, and vibrational temperatures depending on user need and resolution.

CHAPTER 3: EXPERIMENTAL SETUP AND METHOD

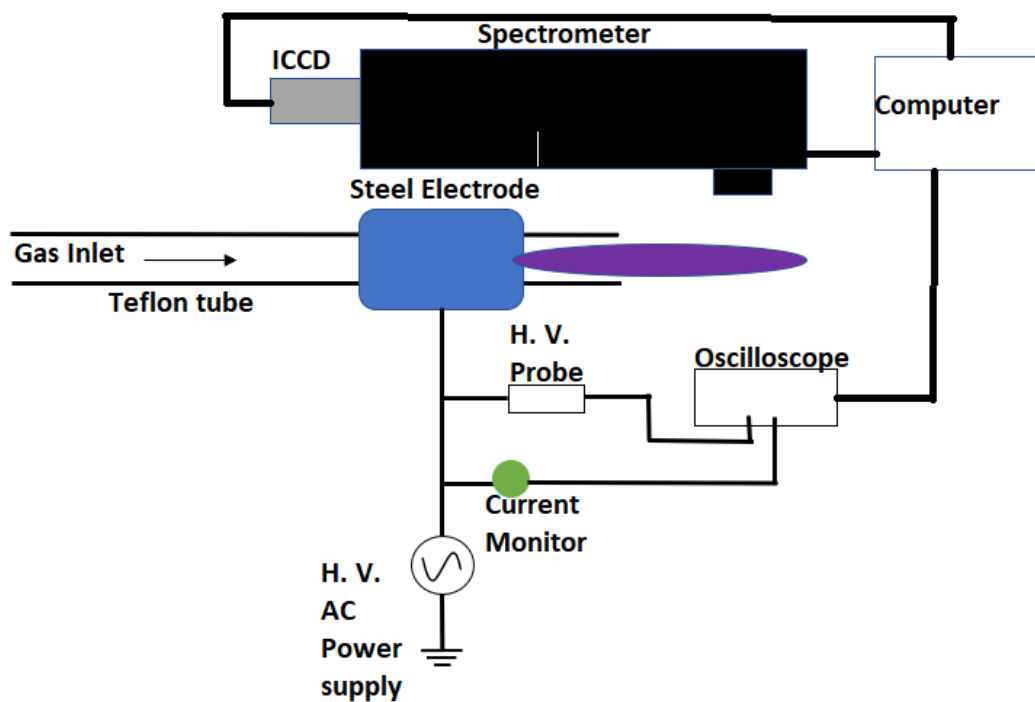


Figure 3. Schematic of experimental setup.

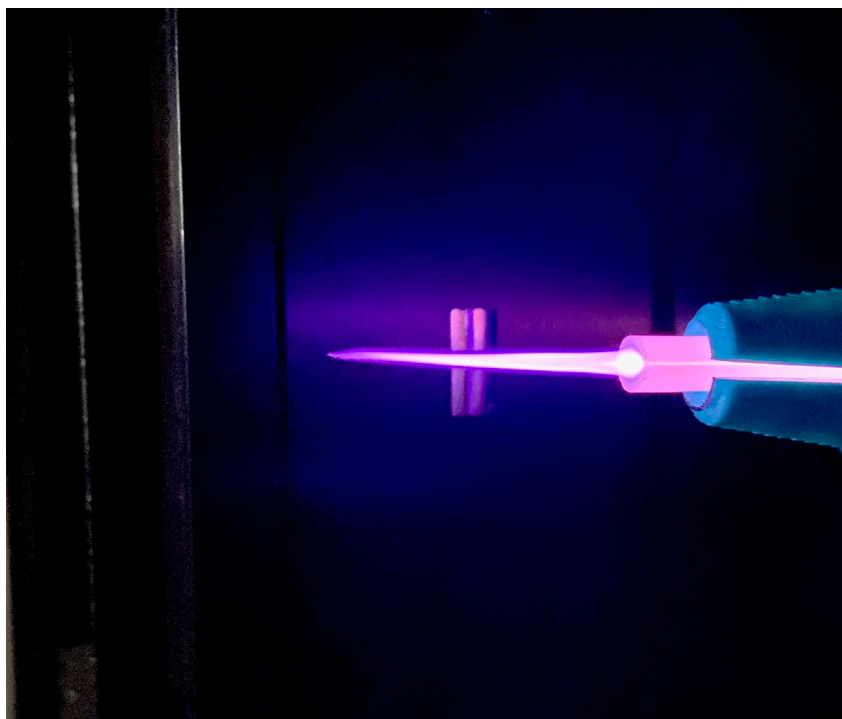


Figure 4. Photo of jet during experiment. Taken by Adam Zandani.

The plasma jet in this study is a single electrode DBD-based configuration and is schematically shown in figure 3. High purity helium (99.999%) is fed through the Teflon dielectric tube with an inner diameter of 4.4 mm, an outer diameter of 6.4 mm (.25 in), wall thickness of 1 mm, and length of 15.3 cm. This tube is placed in series with a 1 inch long steel electrode with an inner diameter of 6.5 mm, outer diameter of 1 cm, and wall thickness of 2.5 mm. Both the dielectric and electrode are placed in a 3D printed holder, with the electrode 47 mm away from the Teflon tip. The electrode was then connected to a high voltage alternating current power supply (Amazing1 PVM/DDR plasma driver) which has a maximum peak-to-peak output of 30 kV and 50 mA. To obtain the values of applied voltage and current, a high voltage passive probe (Tektronix P6015A 10 ft) with a bandwidth of 75 MHz and a wide band current monitor (Pearson Model 6585) both took readings along the high voltage cable coming from the power supply. These resulting waveforms and values were obtained using a Tektronix MSO 4054 mixed signal oscilloscope with a sampling rate of 50 mega-samples per second with a bandwidth of 500 MHz.

To understand the species produced by this jet, emission intensities from 300 nm to 800 nm were measured using optical emission spectroscopy (OES) with a .75-meter Princeton Instruments Acton SP2750 spectrometer coupled with a PI-MAX 3 1024i ICCD camera. Emitted light from the plasma entered the spectrometer slit (100 μm) and is split with a 300 grooves/mm (Blazed 500 nm) grating in order to resolve the resulting peaks. For these measurements, the effluent was 3 cm away from the slit and readings were taken after 20 minutes of operation to confirm stable readings. The camera was operated with a gate width of 2 seconds and averaged over 20 accumulations to ensure consistency among the data. The spectrometer wavelength and

intensity were calibrated through Princeton Instruments Intellical system and spectral data was obtained through use of Princeton Instruments LightField software.

This experiment varied operating parameters such as applied voltage, frequency, gas flow rate, and distance along the jet axis to understand specie production and how each operating condition relates to their production. Voltage was varied from 8 kV to 12 kV in increments of 2 kV, frequency was varied from 26 kHz to 30 kHz in increments of 2 kHz, gas flow rates were varied from 2.5 L/min to 7.5 L/min in increments of 2.5 L/min, and distance along the axis was varied from 0 cm to 3 cm in increments of 1.5 cm. Gas temperature was analyzed through SpecAir software using the N₂ second positive system (315 nm) to see how the non-thermal properties of the plasma were affected as power coupling and other operating conditions were varied. For this measurement, greater resolution of the rotational peak is desired, so a much higher dispersion grating is used (2400 grooves/mm Blazed Holographic-UV). Also, electrical measurements such as peak-to-peak values and RMS values of both voltage and current were taken during each measurement to correlate applied power and estimate the power consumed by the jet while producing the resulting emission intensities.

CHAPTER 4: RESULTS AND DISCUSSION

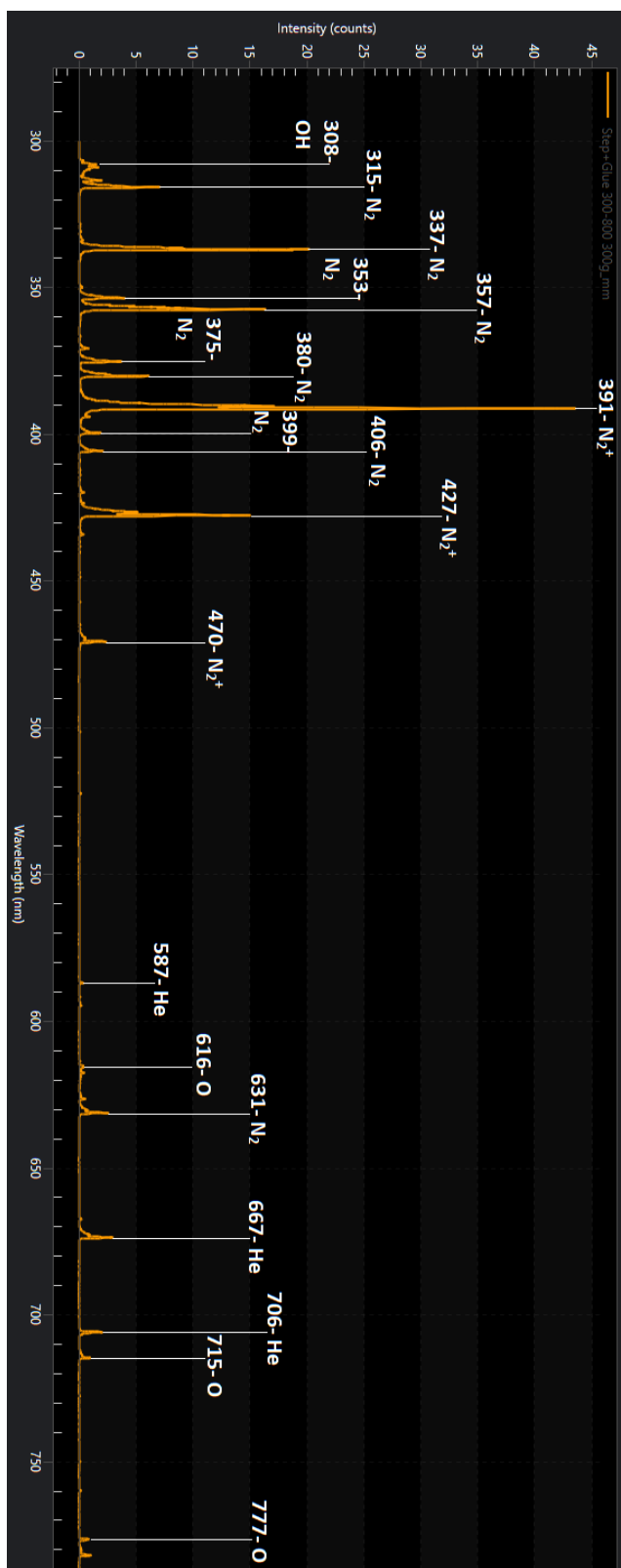


Figure 5. Typical optical emission spectrum.
Ref. Adam Zandani

4.1- Species Production

A general optical emission spectrum recorded by the ICCD is shown in figure 5 along with the corresponding chemical species related to the peaks. The raw data is obtained through the LightField software and then normalized to better show the relevant changes with respect to each variable. For a broadband view of the entire spectra, a 300 grooves/mm (Blazed 500nm) grating is used coupled with an ICCD gate width of 2 seconds to allow sufficient light to accumulate on the microchannel plate (MCP). Just as important as light collection, is understanding how the camera accumulates signal. When the camera is powered on, it will naturally begin to accumulate “dark charge” regardless of the status of the photocathode, which can severely alter concentration counts between measurements. To limit this thermally induced phenomenon, the internal temperature of the camera is operated at -20° C. Furthermore, the camera’s ability to employ cleaning cycles are also utilized. Cleaning cycles continuously remove any signal gathered until the camera begins data acquisition. The amount of cleaning cycles can be specified by the user depending on the circumstances, however for this case, the camera was set for 128 cleaning cycles before acquisition to limit the dark charge accumulation as well as a background subtraction each use. In accordance with many other studies concerning helium appjs [4] [5] [14] [16-17], the species generated agree with what was observed. A complete and extensive list of all species generated in this jet is found in Table 1 and contains corresponding wavelengths, specific band transitions and photon emission energy.

Table 1- List of species generated

λ (nm) (approximate)	Species	Band Transition	Emitted Photon ε
308	OH (A-X)	(0,0)	4.02 eV
315	N ₂ (Second Positive System)	(1,0)	3.93 eV
337	N ₂ (Second Positive System)	(0,0)	3.69 eV
353	N ₂ (Second Positive System)	(1,2)	3.51 eV
357	N ₂ (Second Positive System)	(0,1)	3.47 eV
371	N ₂ (Second Positive System)	(2,4)	3.34 eV
375	N ₂ (Second Positive System)	(1,3)	3.31 eV
380	N ₂ (Second Positive System)	(0,2)	3.26 eV
391	N ₂ (First Negative System)	(0,0)	3.17 eV
399	N ₂ (Second Positive System)	(1,4)	3.11 eV
406	N ₂ (Second Positive System)	(0,3)	3.06 eV
420	N ₂ (Second Positive System)	(2,6)	3.01 eV
427	N ₂ (First Negative System)	(0,1)	2.9 eV
434	N ₂ (Second Positive System)	(0,4)	2.86 eV
447	He	(4d ³ -2p ³)	2.77 eV
457	N ₂ (Second Positive System)	(1,6)	2.71 eV
470	N ₂ (First Negative System)	(0,2)	2.63 eV
486	H(β)		2.55 eV
492	He	(4d ¹ -2p ¹)	2.52 eV
502	He	(3p ¹ -2s ¹)	2.47 eV
522	N ₂ (First Negative System)	(0,3)	2.37 eV
587	He	(3d ³ -2p ³)	2.11 eV

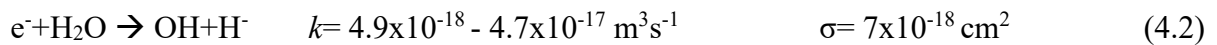
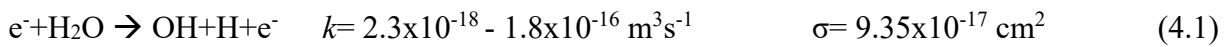
616	Oxygen Triplet	(4d ⁵ -3p ⁵)	2.01 eV
631	N ₂ (First Positive System)	(10,7)	1.96 eV
656	H(α)		1.89 eV
667	He	(3d ¹ -2p ¹)	1.86 eV
674	N ₂	Infrared	1.84 eV
		Afterglow	
706	He	(3s ³ -2p ³)	1.75 eV
715	Oxygen Triplet	(3p ¹ -3s ¹)	1.73 eV
727	He	(3s ¹ -2p ¹)	1.71 eV
777	Oxygen Triplet	(3s-2p)	1.59 eV

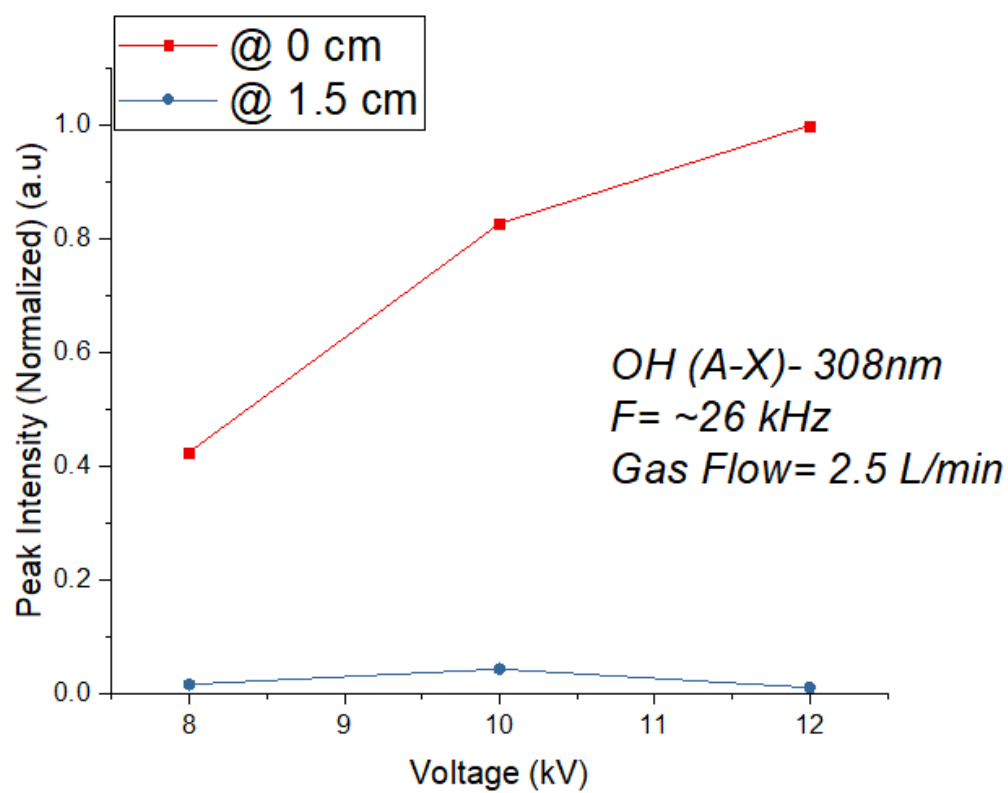
4.1.1- Hydroxyl radical

The hydroxyl radical, OH ($A^2\Sigma-X^2\Pi$), is an oxidizing agent and is a specie that has gained the attention of researchers across all of the sciences such as biology, chemistry, and physics. This is due to its effectiveness and wide range of vital capabilities such as water purification, energy storage, and pollutant removal [8]. Although it is a stable molecule, meaning it is electrically neutral, it is highly reactive as well as very short lived. However, it is this high reactivity which gives this molecule the consequent interest. This high reactivity is caused by its unstable electron configuration in which the orbital shell is not full, leading to a need to take an electron through reactive processes or share an electron through combination with other atoms or molecules. This is evident in its ability to purify water and rid the atmosphere of pollutants such as greenhouse gases such as methane (CH₄) and ozone (O₃). By being an oxidizing agent, its tendency to react with these types of molecules cause it to break apart various bonds through

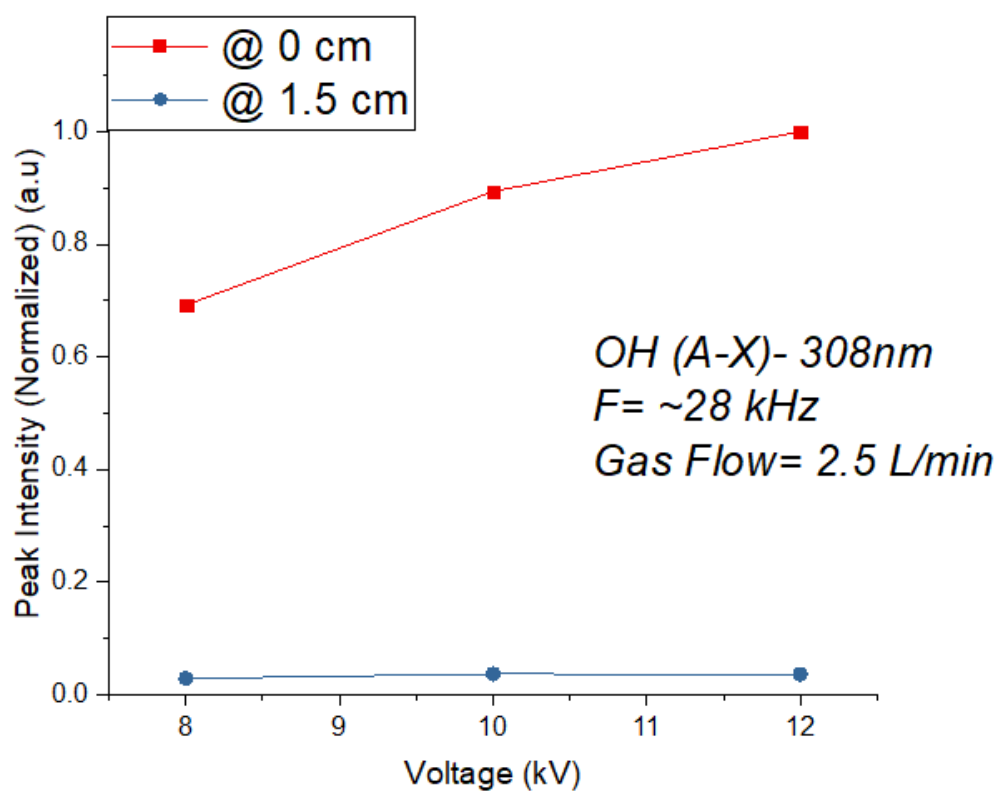
reactive processes in search of an electron. Overall, this high reactivity results in an electron affinity of 1.8 eV.

This molecule is formed in multiple ways depending on the application and environment, but in this system, it is facilitated through electron impact dissociation and/or electron dissociative attachment of water (H₂O) molecule that is present in the ambient air and possibly in the gas lines as an impurity. To dissociate the H₂O molecule, the energy for the incident electron must be ~9.1 eV [10] while for dissociative attachment, the electron energy required is 6.5 eV [1]. This disparity in electron energy dictates the reaction which will occur. When the electron has enough energy (9.5 eV), it is able to dissociate the water molecule through an elastic collision and remain as a free electron in the system. However, when it has a value less than that (6.5 eV), it is able to provide dissociation, but not able to perform an elastic collision by attaching to the free hydrogen which has a relatively weak electron affinity of .75 eV [1]. The reaction process, rate constants, and cross sections for the electron impact with H₂O is given by [1] [9] [10]:





(a)



(b)

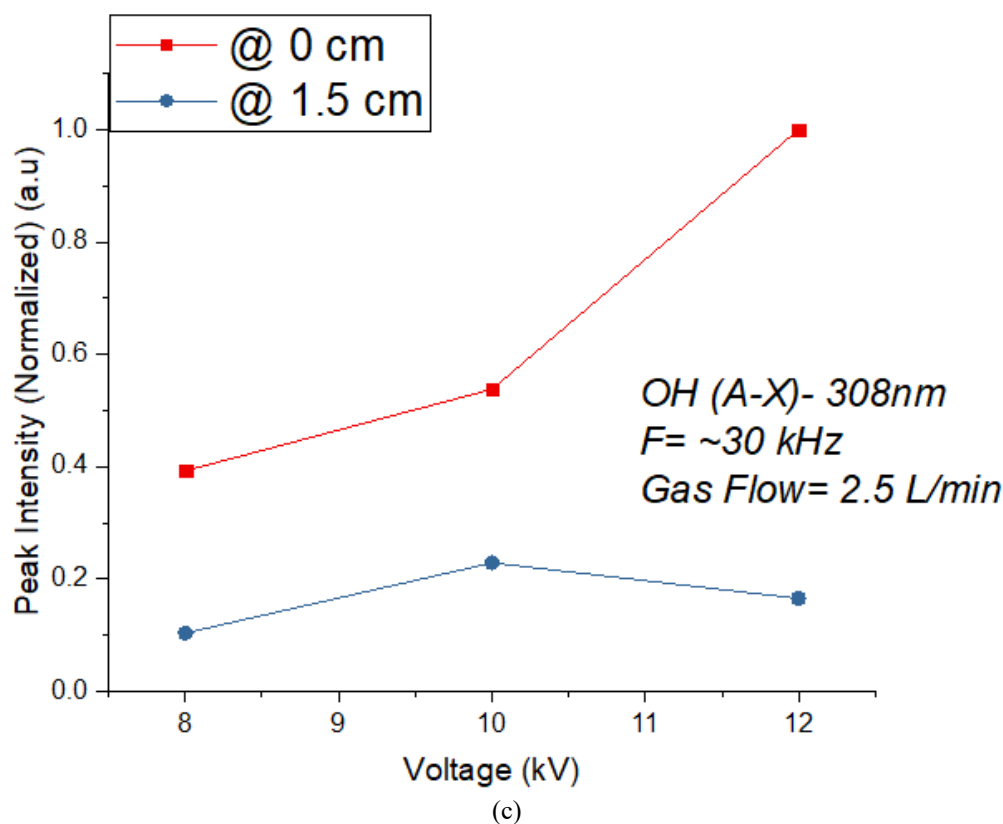
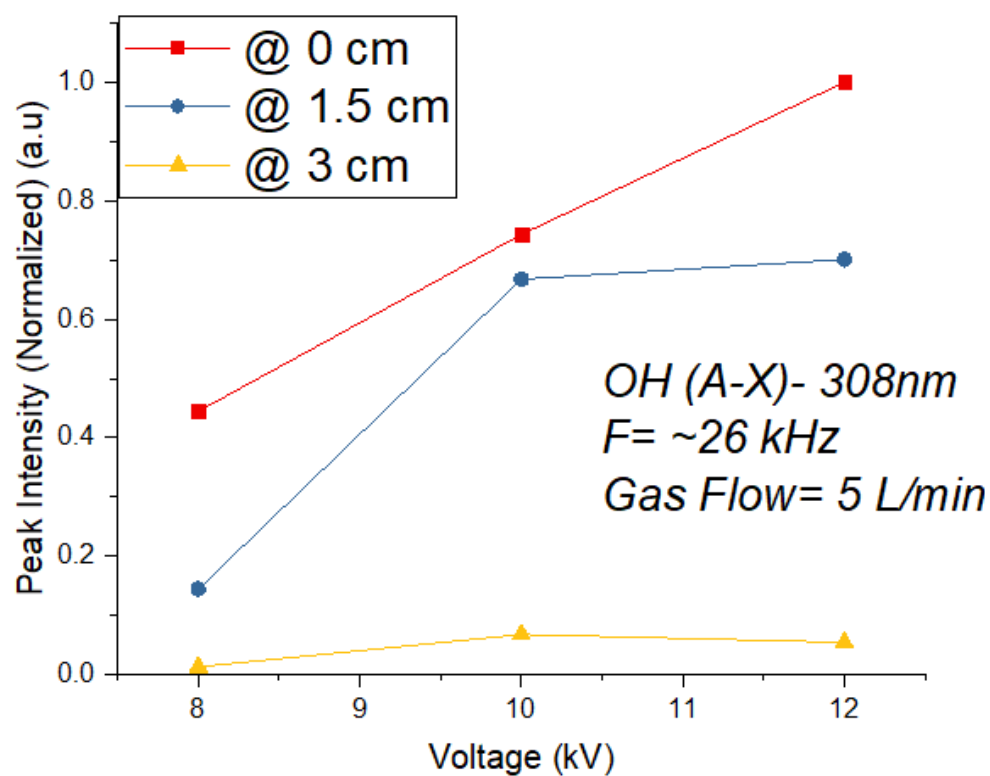
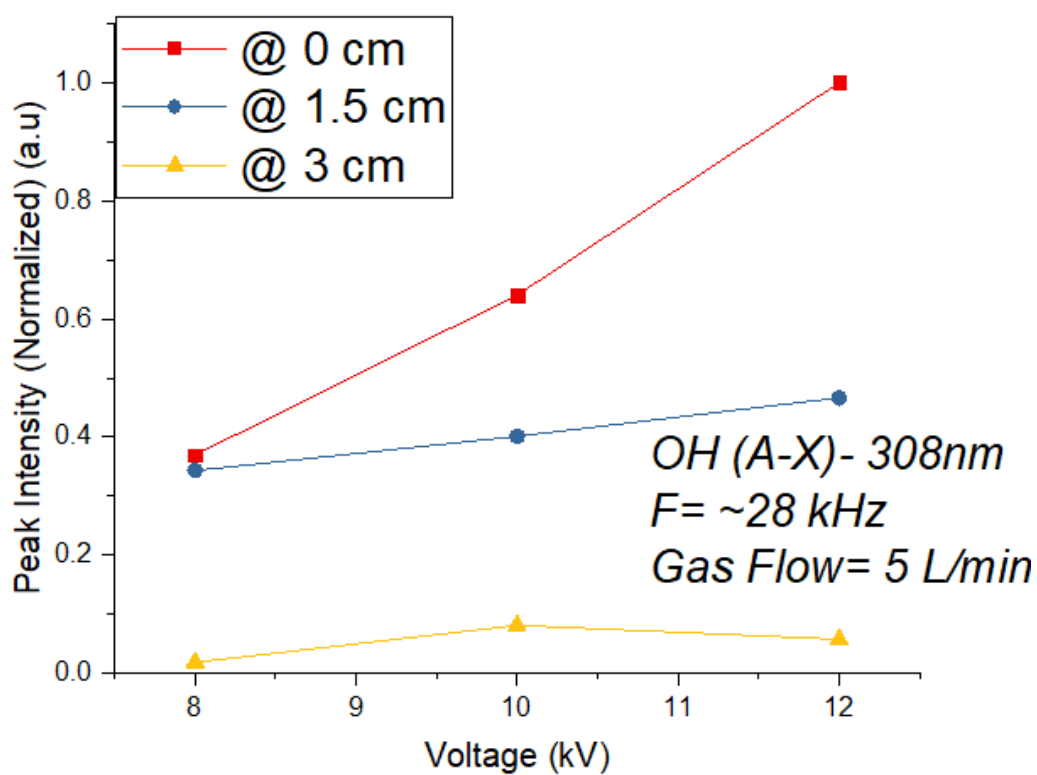


Figure 6. Dependence of OH at (a) 26 kHz, (b) 28 kHz, (c) 30 kHz, on voltage and distance at gas flow rate 2.5 L/min.

To begin, the hydroxyl radical was first analyzed as a function of changing voltage from 8 kV to 12 kV in 2 kV increments and distance every 1.5 cm at different frequencies. In figure 6, it is clear that as voltage increases, the emission intensity of the radical increases. When applied voltage increases, the amount of power and energy going into the system increases, which also increases the electron density within the effluent. This electron density increase is beneficial due to the fact that the OH radical is primarily facilitated through electron interaction with H_2O to either perform dissociation or dissociative attachment. In the case of 2.5 L/min, the jet length only extended to about 1.75 cm, so only two distance readings were able to be taken. But for 5 L/min and 7.5 L/min, all readings were able to be obtained as the jet lengths were about 3 cm and 5 cm, respectively.



(a)



(b)

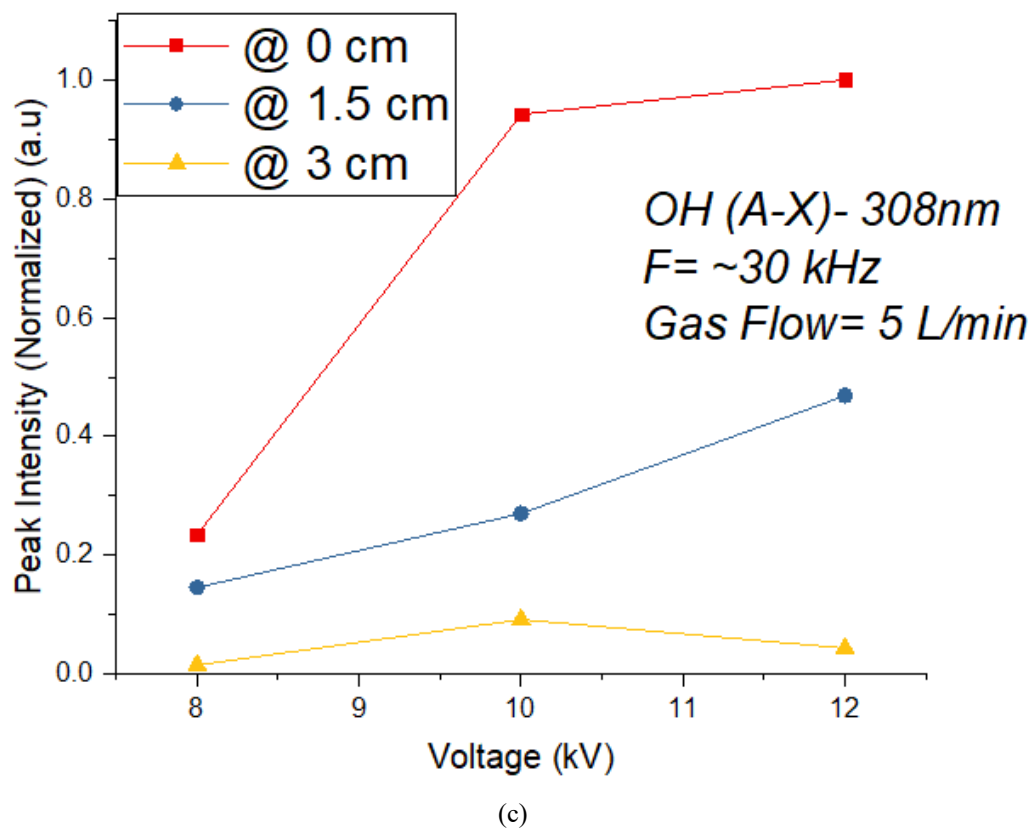
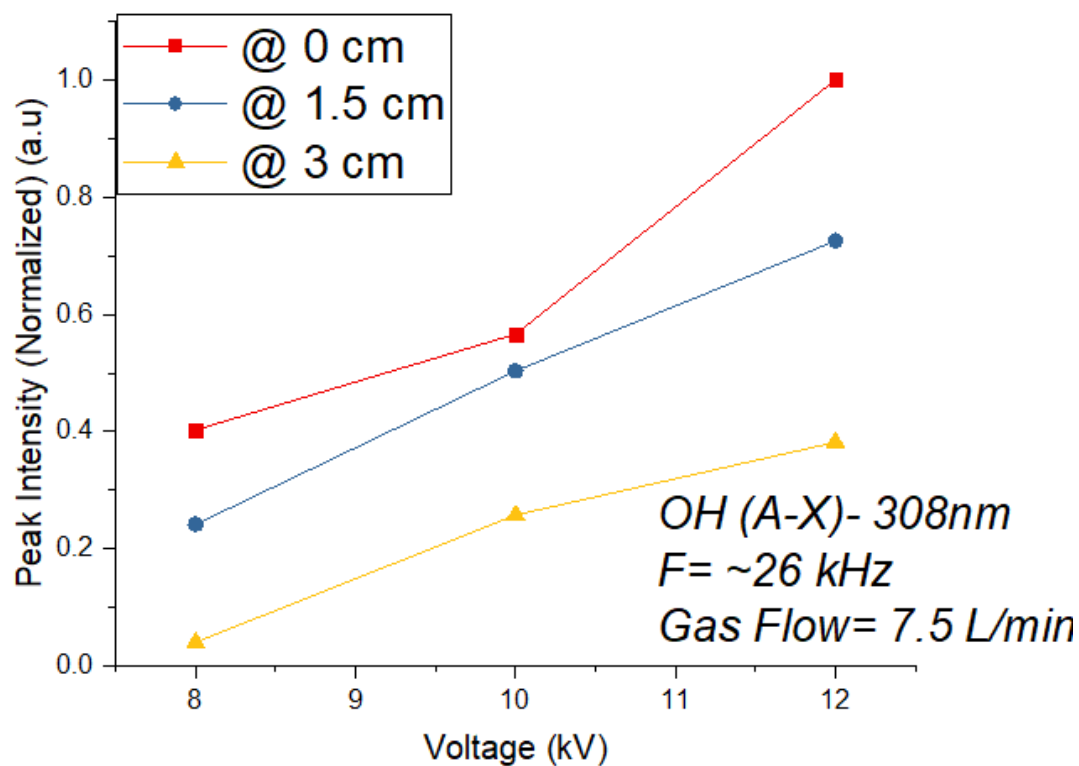
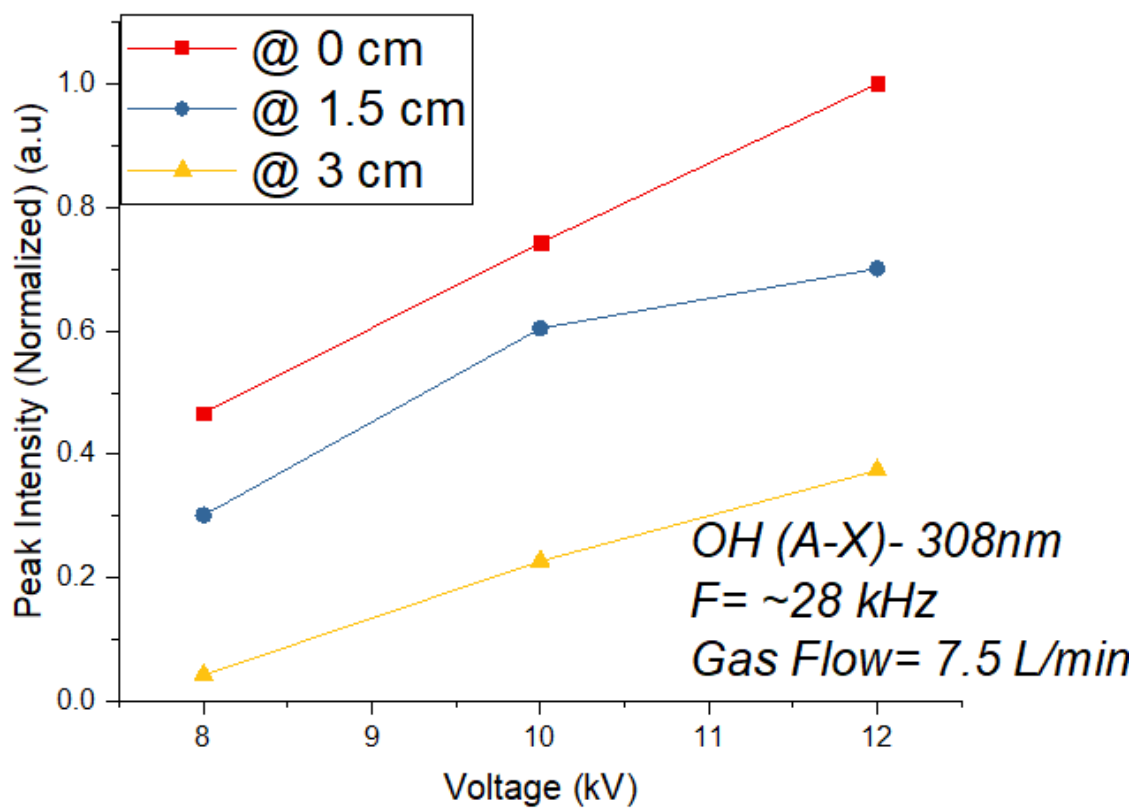


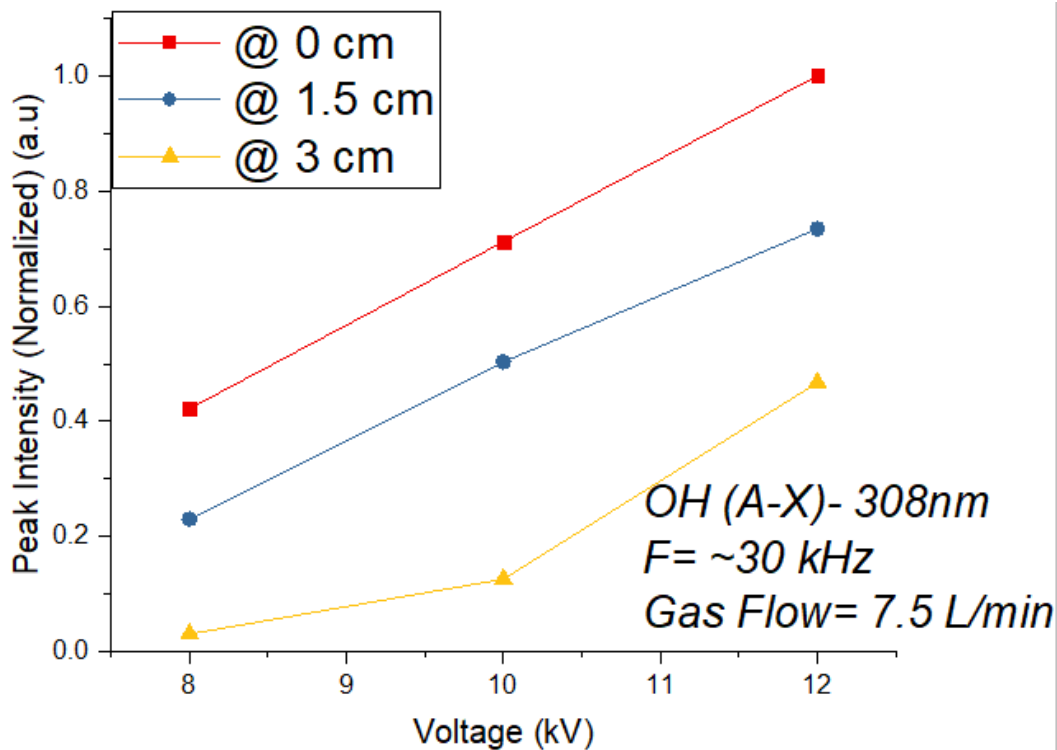
Figure 7. Dependence of OH at (a) 26 kHz, (b) 28 kHz, (c) 30 kHz, on voltage and distance at gas flow rate 5 L/min.



(a)



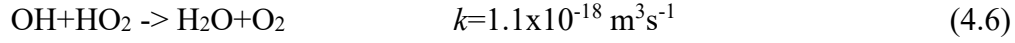
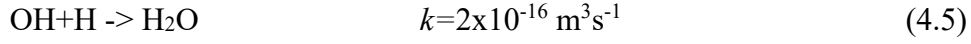
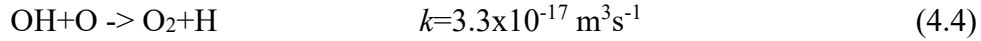
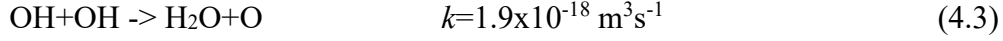
(b)



(c)

Figure 8. Dependence of OH at (a) 26 kHz, (b) 28 kHz, (c) 30 kHz, on voltage and distance at gas flow rate 7.5 L/min.

This trend of increasing voltage leading to an increase in emission intensity is evident through different flow rates as well as different frequencies as shown in figure 7 and 8. However, it is also evident that as distance from the dielectric tip increases, there is a decrease in overall intensity and production. This change is a result of the effluent leaving the tube and interacting with ambient air. As mentioned earlier, the high reactivity of this specie causes it to be very short-lived and effectively destroyed as it interacts with the ambient air. The main mechanisms for this result are due to the quenching and recombination processes that occur with air constituents as well as a decrease in electron density along the length of the plasma. The mechanisms responsible for this behavior are provided by [9] [11] [12] [32]:



These reactions signify the importance of electron density and applied power in the production of the OH radical. In other studies, the hydroxyl radical has shown to be heavily reliant upon the gas temperature ($T_g \sim 300 \text{ K}$ in non-thermal jets), electron temperature ($T_e \sim 1\text{-}2 \text{ eV}$), ionization degree of the plasma system ($10^{-5}\text{-}10^{-4}$), electron and particle density ($n_e \sim 10^{20}\text{-}10^{21} \text{ m}^{-3}$, $n_0 = 2.55 \times 10^{19} \text{ cm}^{-3}$) and gas composition as well as any admixtures (Helium- 99.999%) [10] [13]. Another observation is the favorable effect of increased gas flow rate on the concentration of OH produced throughout the effluent. In figures 6-8, the intensity readings at the end of the jet lengths increase relative to the highest concentration as a function of increasing flow rate. This is also displayed in figure 9, which looks at the effect of the gas flow rate at the same distance along the axis and same frequency from the power supply.

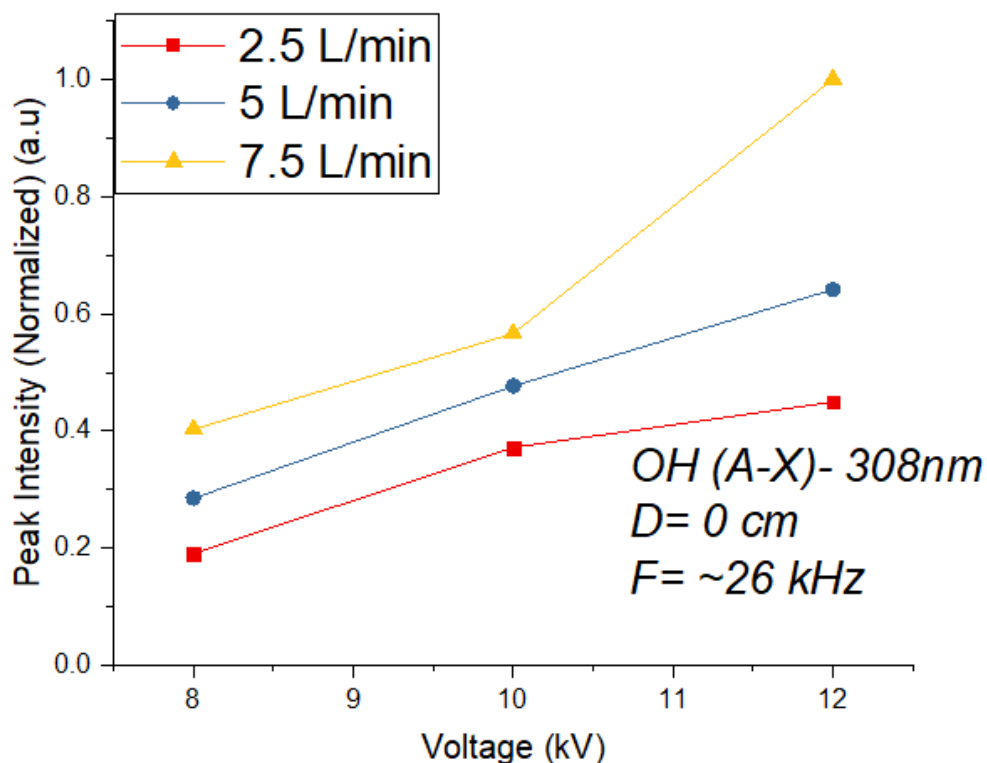


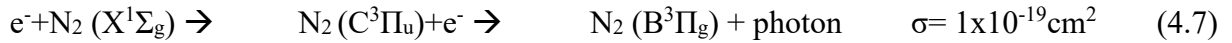
Figure 9. Dependence of OH on gas flow rate at a frequency of 26 kHz.

As gas flow rate increases from 2.5 L/min to 7.5 L/min, the gas residency time decreases from .054 s to .025 s. Here, gas residency time just defines how long the helium gas stays in the tube before being propelled out into the environment. The shorter the gas residency time, the faster the gas velocity. This increase in gas velocity limits the interaction of the surrounding air by exiting the tube with more force, hence shifting a lot of that ambient air away from the tube exit. The higher velocity also allows for it to live a much longer lifetime along the distance of the effluent by a combination of pushing it further and limiting the amount of air it comes into contact with. Overall, these results agree with those seen by Gott *et al.* [14] and Ilik *et al.* [5].

4.1.2- N₂ (Second Positive System)

The N₂ second positive system (C³Π_u-B³Π_g) is a vibrationally excited electronic state that can be facilitated either through direct impact with an electron. This particular molecule along with the ionized version of it, which will be discussed later, dominates the optical emission spectrum of this helium jet. That is due to the plethora of N₂ in the atmosphere and consequently, in the surrounding air. This system is known to appear most readily in discharges containing nitrogen or air as seen in figure 5 and Table 1 and also instances in nature such as the Aurora Borealis (Northern Lights) which is an example of a cold plasma phenomenon.

Before the discharge, the N₂ molecule is in its vibrational ground state which is denoted by X¹Σ_g. When the discharge occurs and the electrons begin to collide with the N₂ in the ambient air, it is then excited one of its electronic states which is denoted by C³Π_u. Depending on the amount of energy transferred in these collisions, the N₂(C³Π_u) can be excited into various vibrational levels. As with excited species, which do not have the ability to go into a metastable state, the N₂(C³Π_u) decays at a rate of 1.33x10⁷ s⁻¹[23] [24], into a vibrational level of a lower electronic state B³Π_g, and releases that energy in the form of photon emission and with a radiative lifetime of 6 x 10⁻⁶ s [1]. This occurrence is known as the second positive system of N₂. The process, energy associated, reaction rate, and cross section are given by [15] [18] [22]:



$$11.1 \text{ eV} \quad 7.4 \text{ eV} \quad k = 2.7 \times 10^7 \text{ cm s} \quad (4.8)$$

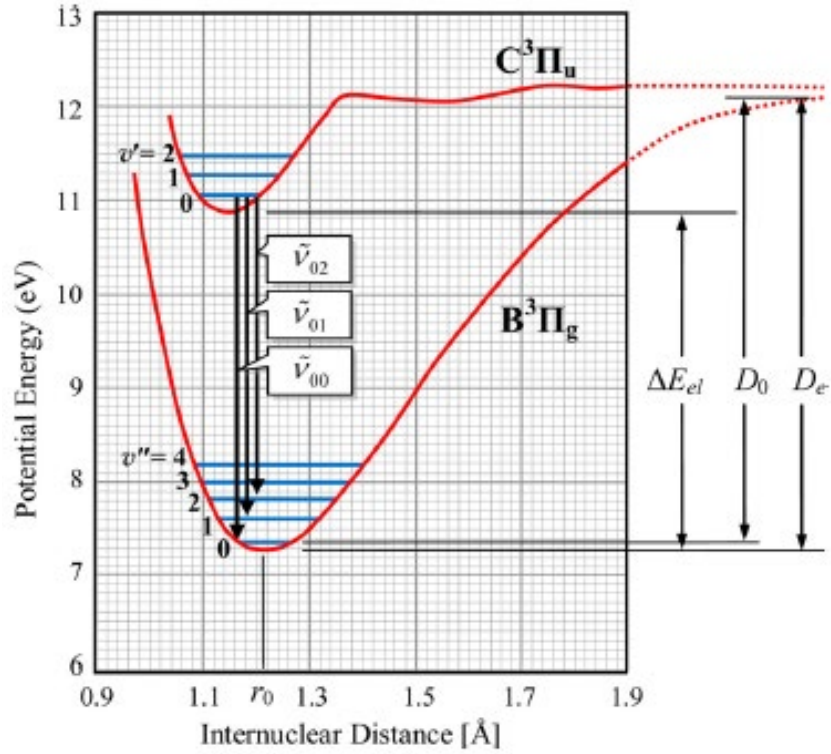


Figure 10. Anharmonic potential energy curves for this particular N₂ system. Ref. 18, 20.

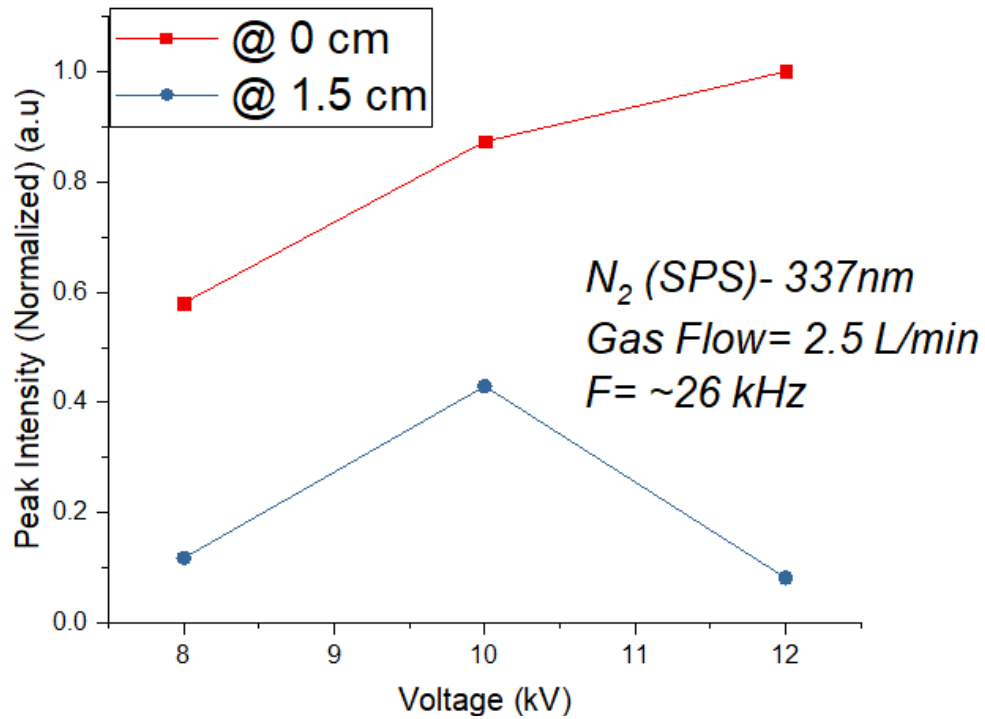
The information provided in 4.7 and 4.8 is only representative of the ground state (0,0) of this system. The plasma employed here generates various different vibrational levels of this band as shown in table 1, which each have different energies and electron impact cross sections associated with them and is given in table 2 [15] [20] [27]:

Table 2- Optical emission cross sections and vibrational energy levels for the N₂ (C³Π_u-B³Π_g)

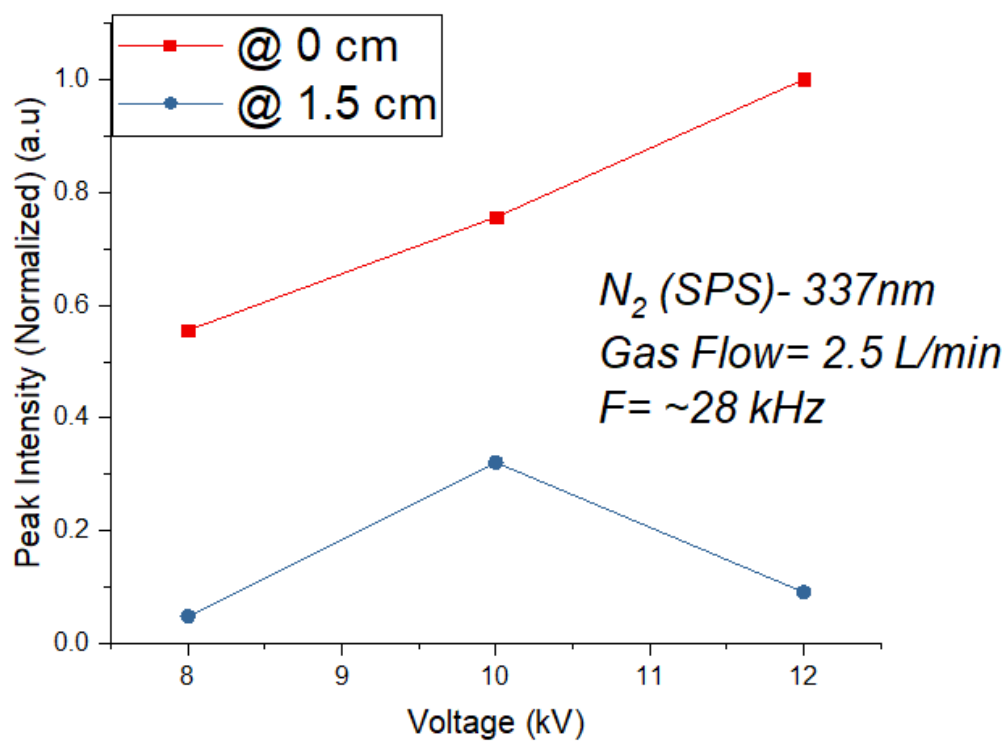
Transition (v', v'')	E _i (eV)	E _f (eV)	σ (10 ⁻¹⁸ cm ²)
(1,0)	~11.3	~7.4	7.03 (±1.2)
(1,2)	~11.3	~7.8	3.16 (±.63)
(0,1)	~11.1	~7.6	6.87 (±1.17)
(1,3)	~11.3	~8	3.02 (±.51)

(0,2)	~11.1	~7.8	2.73 ($\pm.46$)
(1,4)	~11.3	~8.2	1.12 ($\pm.23$)
(0,3)	~11.1	~8	.88 ($\pm.18$)
(3,7)	~11.7	~8.7	.13 ($\pm.023$)
(2,6)	~11.5	~8.5	.21 ($\pm.041$)
(0,4)	~11.1	~8.2	.23 ($\pm.050$)
(1,6)	~11.3	~8.5	.15 ($\pm.031$)

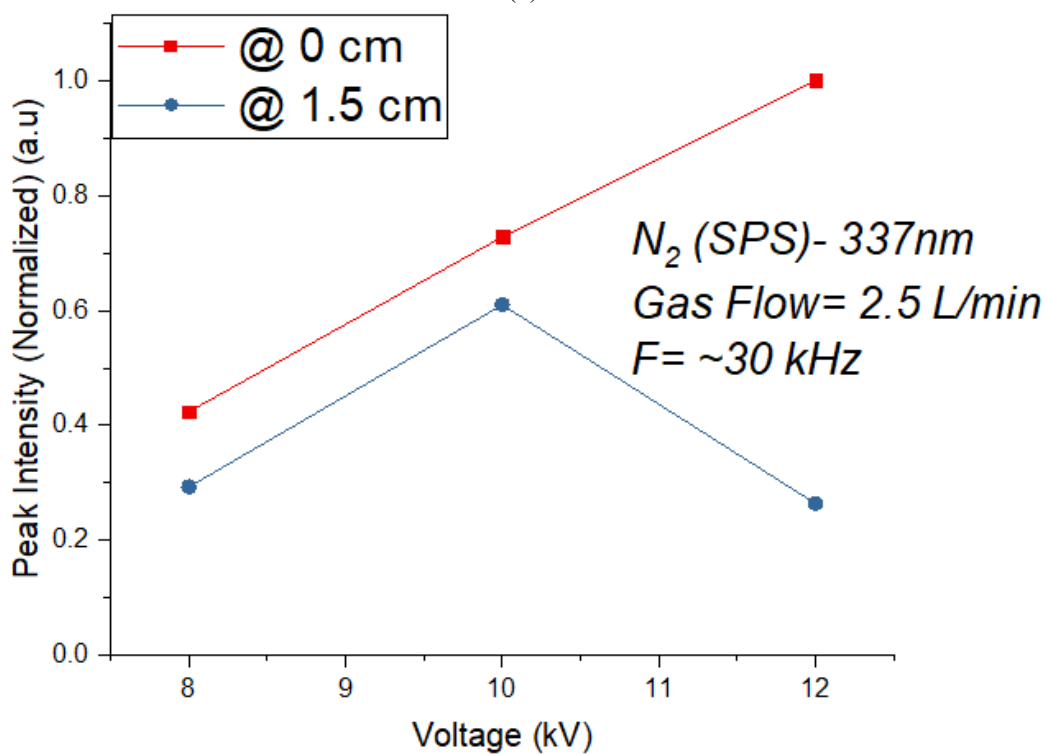
Figure 10 details the potential energy curve for the N_2 second positive system and shows the different vibrational levels within the electronic states. With this information, the various vibrational band transitions can be understood along with the excited energy at electron/metastable impact, energy after decay, and photon emission energy as is quantified in table 2.



(a)



(b)



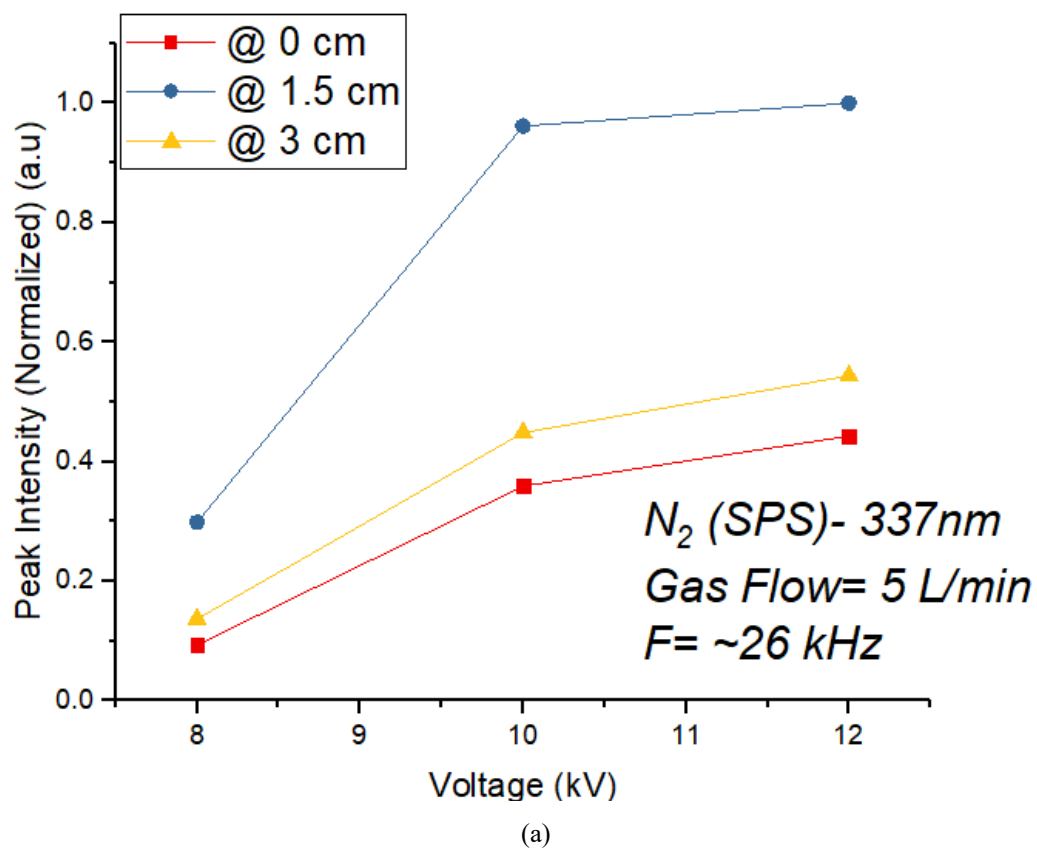
(c)

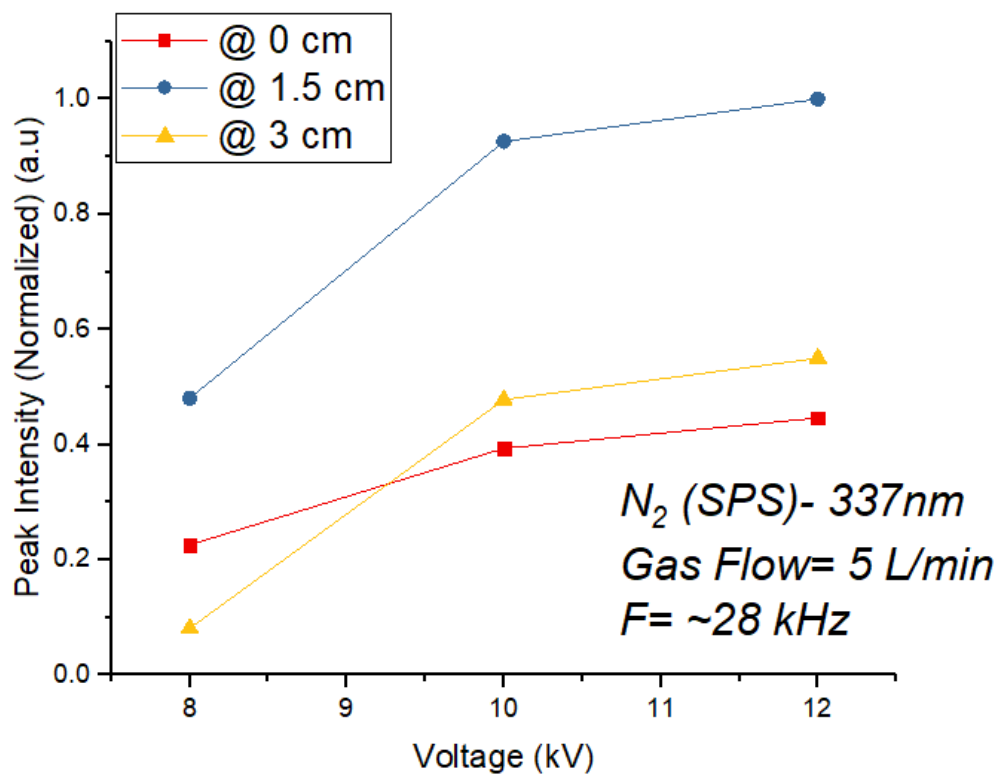
Figure 11. Dependence of N_2 ($C^3\Pi_u-B^3\Pi_g$) at (a) 26 kHz, (b) 28 kHz, (c) 30 kHz, on voltage and distance at gas flow rate 2.5 L/min.

Figure 11 shows the effect of increasing voltage on the emission intensity of this vibrationally excited system. It is observed that as voltage increases, intensity increases as well. Adding more voltage into the system results in added power input into the system and this leads to a higher electron density within the discharge. For this second positive system, the vibrationally ground state of N_2 must gain at least 11.032 eV of energy through electron collisions in order to be excited into the $C^3\Pi_u$ electronic state. A higher electron density and power input allow for more electrons to be generated and gain a high enough energy from the applied electric field in order to facilitate this process. On the other hand, at 2.5 L/min, the jet length only extended to about 1.75 cm. A measurement at 1.5 cm along the jet axis effectively means it is a measurement at the end of the jet, where the electron density will be the lowest. Therefore, the effect of distance on intensity can not be confirmed without the measurements from a gas flow rate of 5 L/min and 7.5 L/min under the same circumstances.

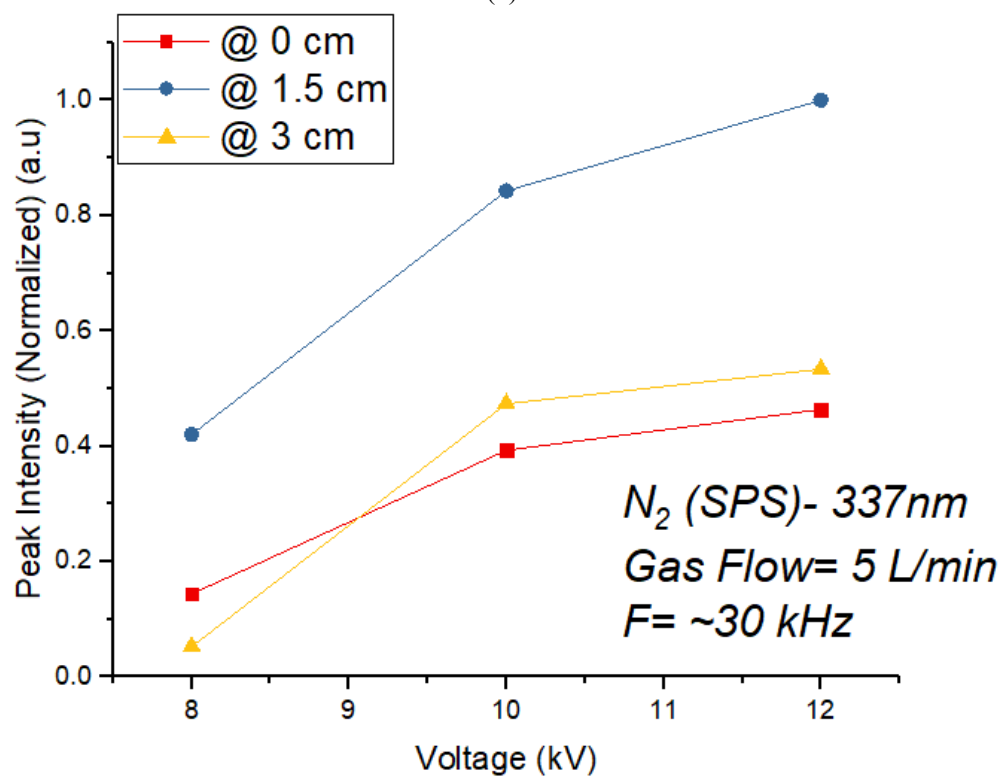
It should also be noted that for all species operated at 12 kV, 2.5 L/min, at a distance of 1.5 cm from the jet, the emission intensity suffers a decline relative to other voltages at that same distance which is portrayed in figure 11. During experiments, it was observed that when voltage was increased from 10 kV to 12 kV, the jet length actually shortened by a few tenths of a centimeter. This occurrence is isolated to this voltage parameter and this flow rate. In the single electrode system, the cathode is essentially the flow of the working gas and the jet length is dictated by the void of macroscopic neutrality by the presence of electrons within the medium. It is postulated that when the voltage increases to this point, the increased electron density become primarily concentrated inside of the tube coupled with the low gas flow rate not being able to push these charge carriers out of the tube and/or not being able to efficiently compensate the polarization as a virtual ground. The latter supposition can be explored further through applied

voltage, current, and total circuit measurement comparisons at different flow rates and same frequencies to see the extent of the difference of gas flow rate alone on electrical characteristics, which will be discussed in the next section.



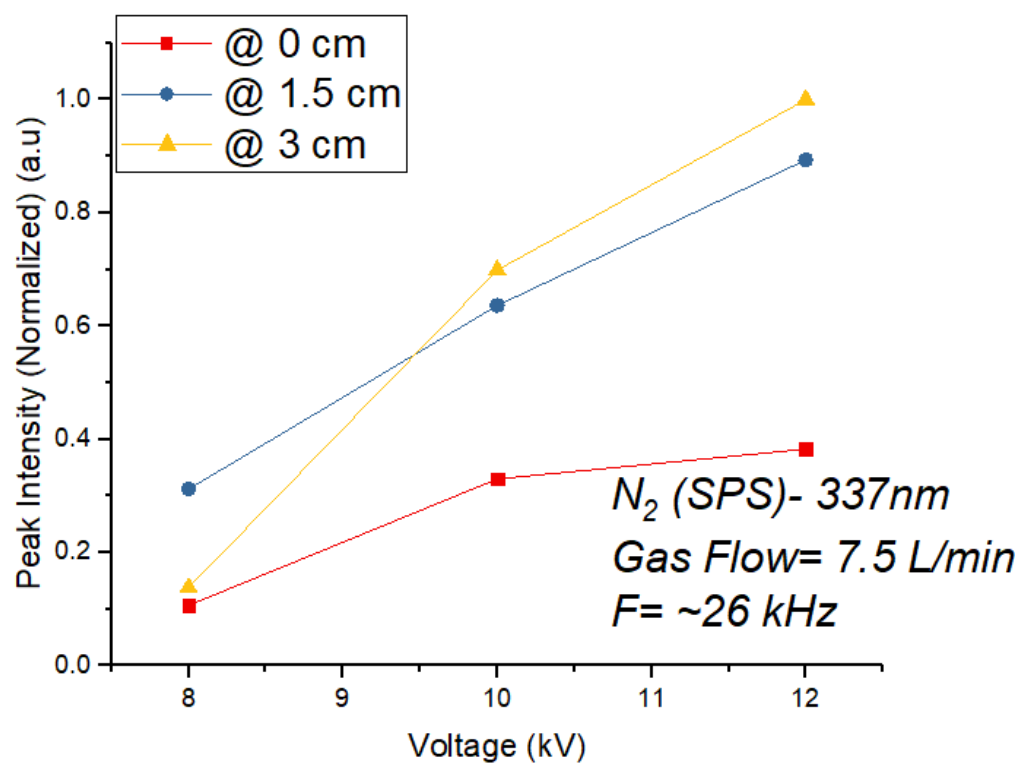


(b)

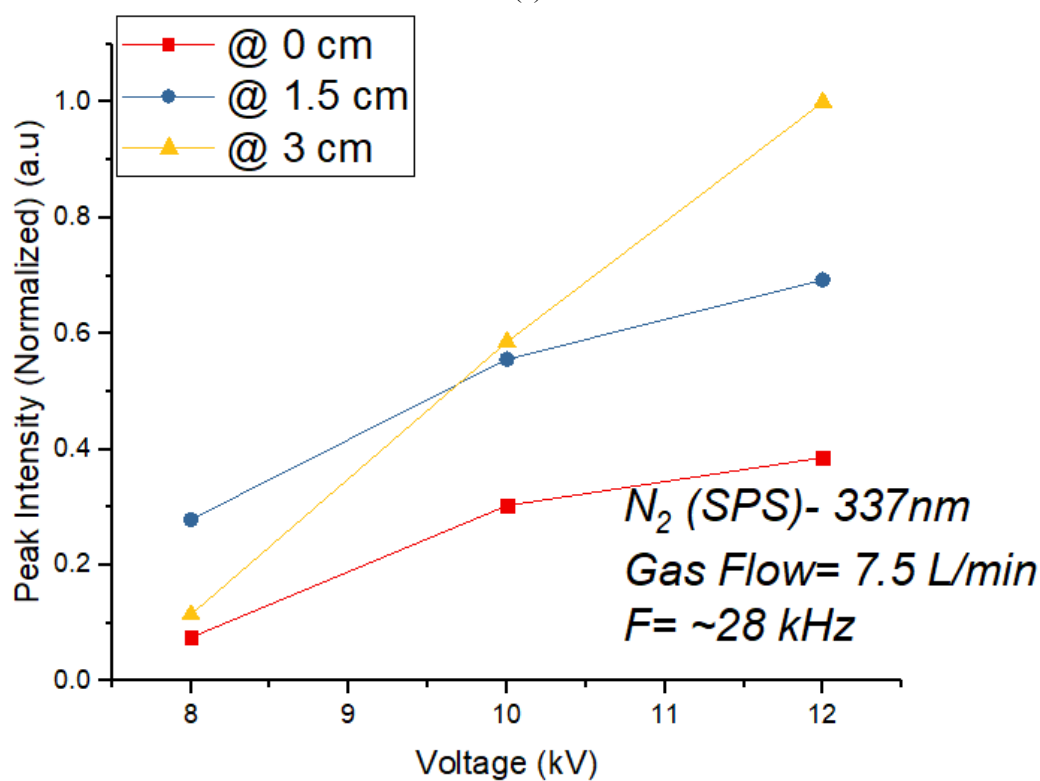


(c)

Figure 12. Dependence of N_2 ($C^3\Pi_u-B^3\Pi_g$) at (a) 26 kHz, (b) 28 kHz, (c) 30 kHz, on voltage and distance at gas flow rate 5 L/min.



(a)



(b)

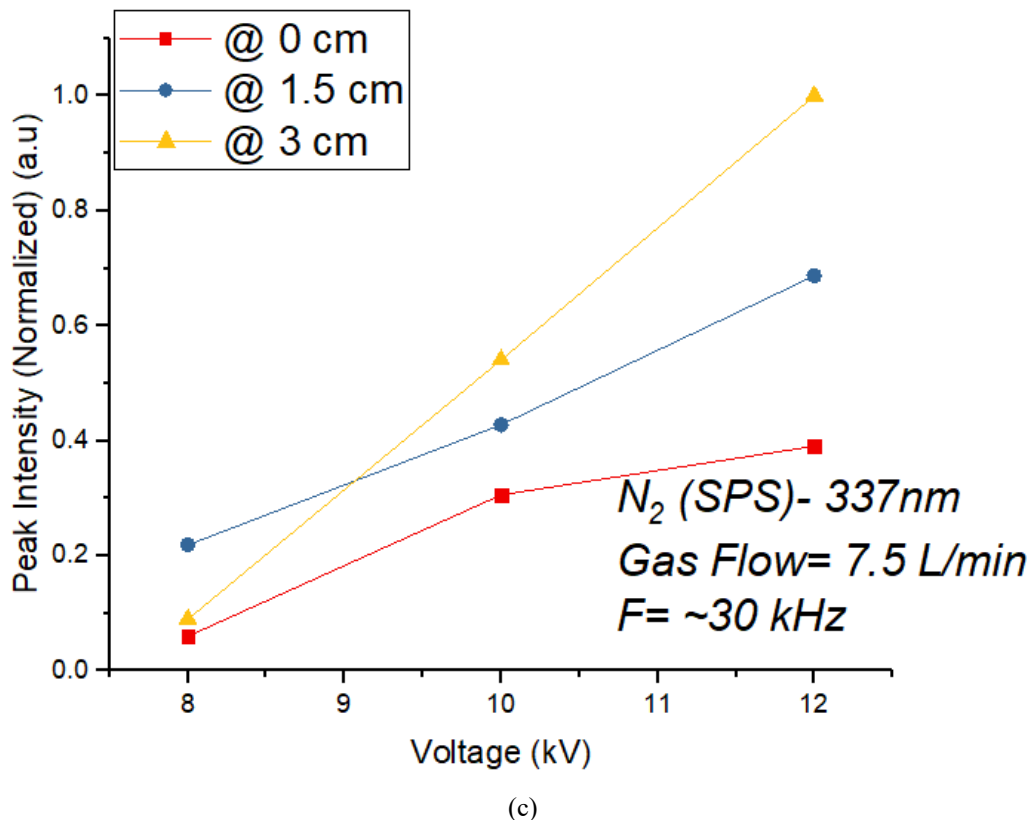


Figure 13. Dependence of N_2 ($C^3\Pi_u-B^3\Pi_g$) at (a) 26 kHz, (b) 28 kHz, (c) 30 kHz, on voltage and distance at gas flow rate 7.5 L/min.

Figure 12 and 13 both display the intensity of the second positive system as a function of voltage and distance at 5 L/min and 7.5 L/min gas flow rate, respectively. It also provides a better understanding on the effect of the distance from the tube exit, which looks at the effect of air interaction on the specie in question. At both of these flow rates, the trend in the effect of increased voltage holds true. But at 5 L/min, it is observed that the N_2 (SPS) reaches its peak intensity value at 1.5 cm from the tube exit, while it continues to rise and reach its peak at 3 cm from the tube exit at a gas flow rate of 7.5 L/min. This excited molecule is produced through a combination of interaction of the plasma with the surrounding air and reliance on free electrons to provide that excitation energy. In both of these situations, it is clear that the intensity increases as measurements are taken further down the effluent. This is due to the fact that at this point,

other species such as OH and other oxidants concentrations heavily decline as a function of distance away from the tube exit due to various quenching and recombination processes that occur as a result of reactivity. Despite this, the intensity of the second positive system decreases going from 1.5 cm to 3 cm at 5 L/min when this distance change only means more interaction with the air which should actually increase the emission. In the case of 5 L/min, the jet length reached 3 cm, which means the reading was taken at the tip of the jet where the resulting electron density would be the least. As established before, this N_2 second positive system relies on the presence of high energy electrons in order to allow for excitation to occur. At 7.5 L/min, it continues to increase in accordance with the voltage and distance. This is because at this flow rate, the jet length was measured to be 5 cm, which means there would be a much higher electron density at this point compared to 5 L/min.

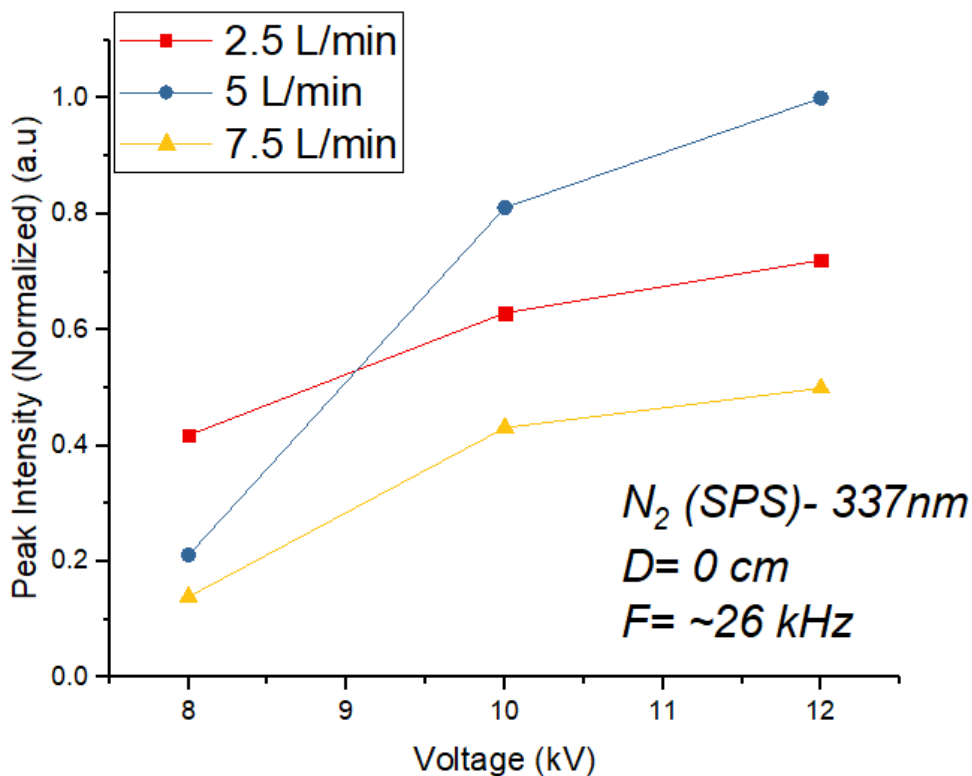


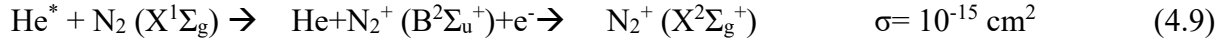
Figure 9. Dependence of N_2 ($C^3\Pi_u-B^3\Pi_g$) on gas flow rate at a frequency of 26 kHz.

The effect of gas flow rate on the emission intensity of N_2 ($C^3\Pi_u-B^3\Pi_g$) is portrayed in figure 14 and indicates that it reaches its peak value in accordance with increasing voltage and at a gas flow rate of 5 L/min. At 2.5 L/min, the gas flow is weak, displacing the least amount of air, which results in the most interaction between the plasma and the surrounding air. The gas flow is responsible for the carrying the charged particles and at low velocity, it is not able to allow maximum interaction with the N_2 in the surrounding air. At 5 L/min, more air is displaced, however, more charged particles are able to be carried throughout the effluent to cause those collisions with the molecules. At 7.5 L/min, the air displaced is at a maximum meaning the air interaction is at its minimum although the charged particles are able to be carried the furthest. These results are in agreement with a number of studies concerning optical emission spectroscopy positioned along the jet axis such as [5] [14] [17] [21]. Typical losses of this excited state come from quenching effects with air molecules such as the two most abundant: N_2 and O_2 . The quenching rates by these two molecules are in the range of 10^{-11} - 10^{-10} $cm^3 s^{-1}$ [23] [24].

4.1.3- N_2^+ First Negative System

The N_2^+ first negative system ($B^2\Sigma_u^+ - X^2\Sigma_g^+$) is an ionized N_2 molecule that is primarily facilitated through collisions with helium metastables through a process called Penning Ionization. Similar to the second positive system, it dominates the emission spectrum of this jet and also begins as a vibrationally ground N_2 ($X^1\Sigma_g$) molecule in the ambient air until discharge occurs. Once discharge occurs the helium atoms in the working gas are excited into a metastable state and begin to collide with the N_2 molecules. The collision results in ionization of the molecule as well as exciting it into an electronic state, denoted by $B^2\Sigma_u^+$. Due to the instability at these excited states, the N_2^+ ($B^2\Sigma_u^+$) molecule decays at a rate of $1.21 \times 10^7 s^{-1}$ [23] [24] to the

$X^2\Sigma_g^+$ electronic state with a radiative lifetime of 6.5×10^{-8} s and releases the energy loss as an emitted photon. The ionization process, energy level associated throughout the process, cross section, and reaction rate are given by [15] [20] [22] [24]:

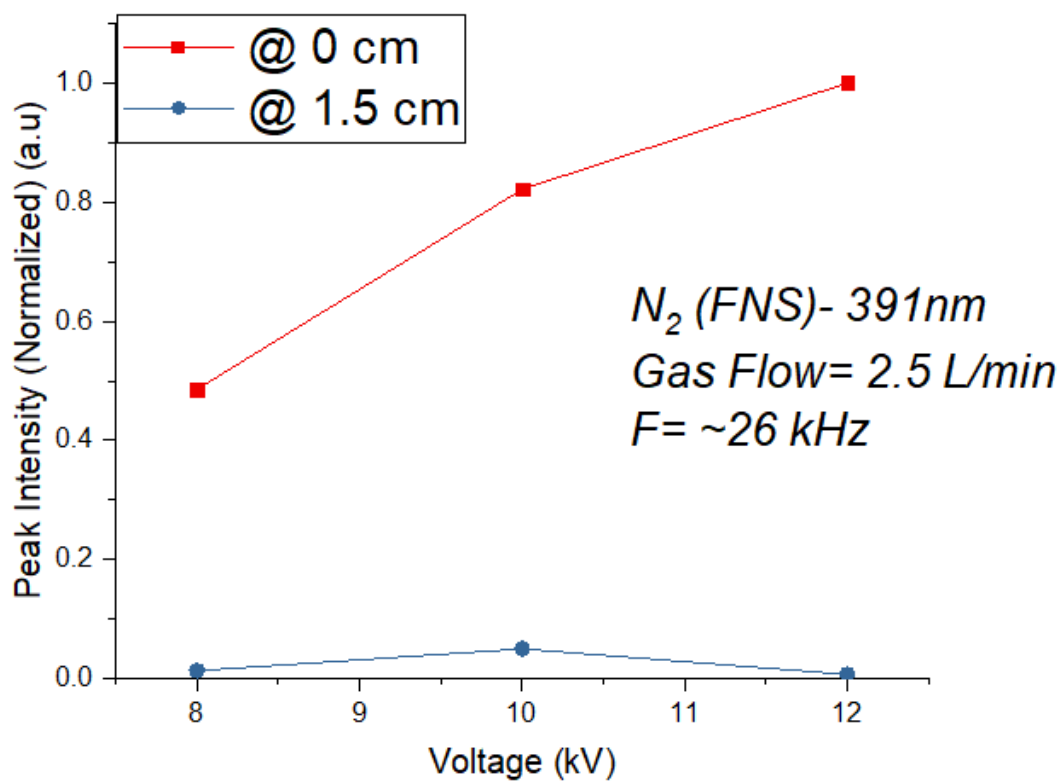


$$18.7 \text{ eV} \quad 15.6 \text{ eV} \quad k = 7 \times 10^{-11} \text{ cm}^3 \text{ s}^{-1} \quad (4.10)$$

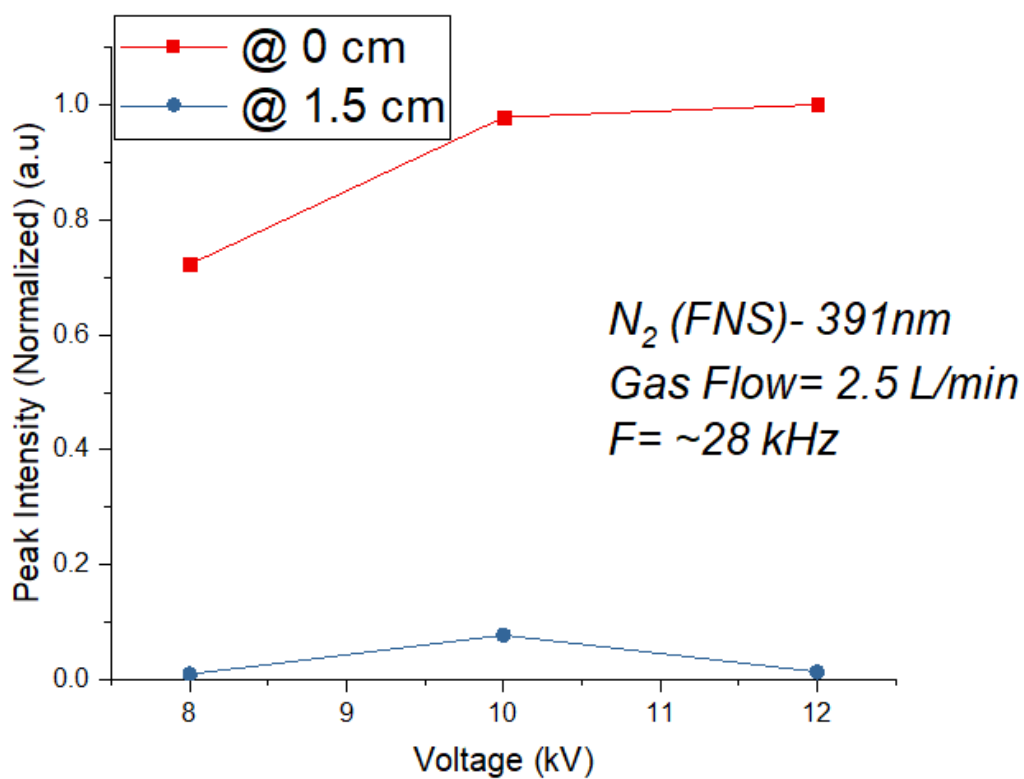
As was the case previously, this information (4.9 & 4.10) is only indicative of the ground state of the first negative system which is not the only vibrational excitation band produced here. The different energies associated with these transitions are given in table 3 [20]:

Table 3- Vibrational energy levels for the $\text{N}_2 (B^2\Sigma_u^+ - X^2\Sigma_g^+)$

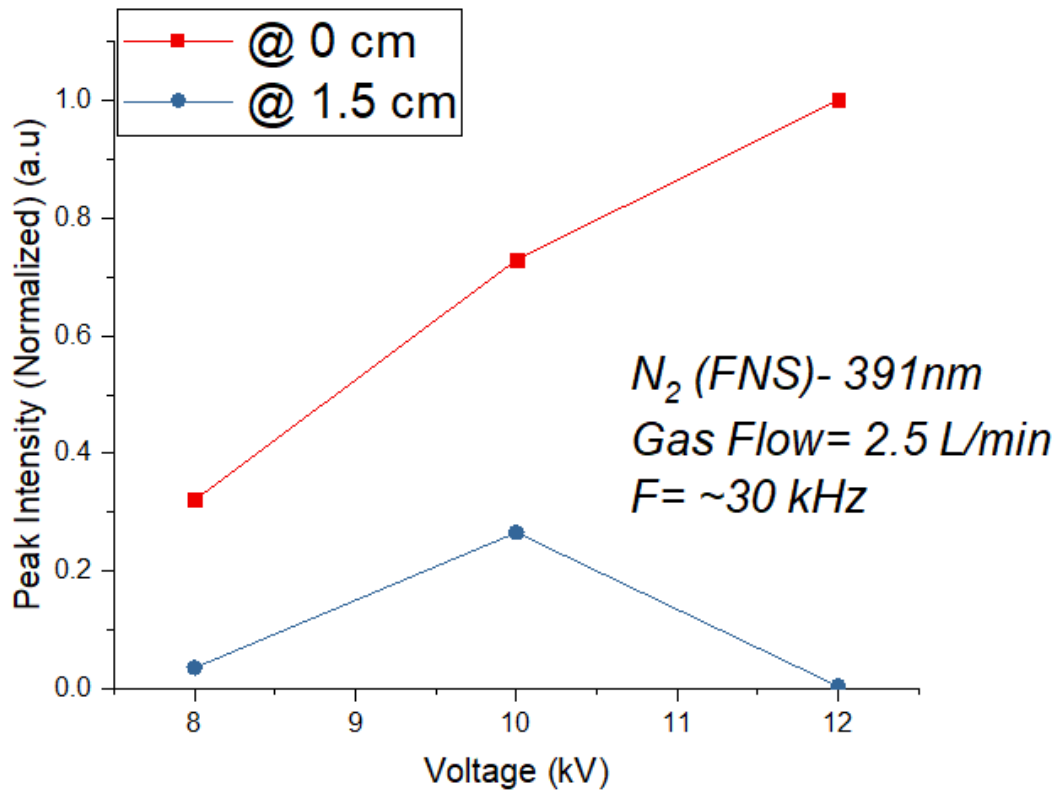
Transition (v', v'')	E_i (eV)	E_f (eV)
(0,1)	~18.7	~15.8
(0,2)	~18.7	~16.1
(0,3)	~18.7	~16.3



(a)



(b)

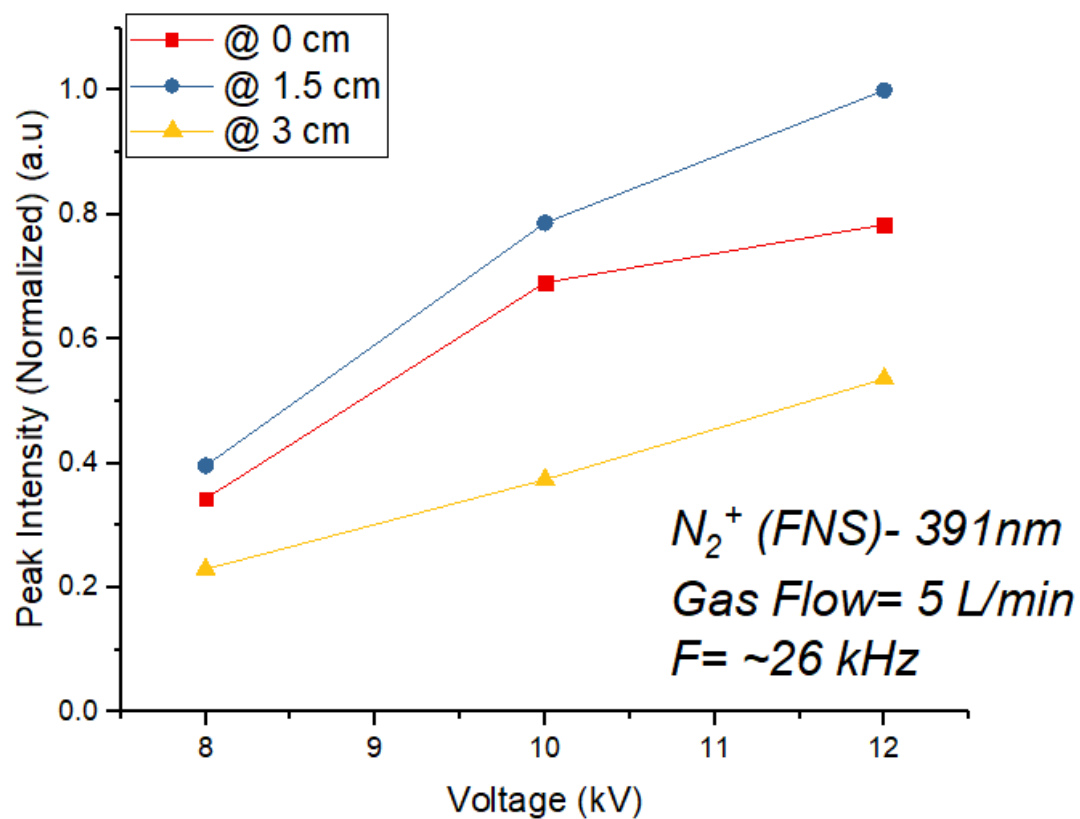


(c)

Figure 15. Dependence of N_2^+ ($B^2\Sigma_u^+ - X^2\Sigma_g^+$) at (a) 26 kHz, (b) 28 kHz, (c) 30 kHz, on voltage and distance at gas flow rate 2.5 L/min.

In figure 15, the effect of increased voltage on the first negative system shows to be a favorable one. The increased electron density and power going into the system increase the concentration of this specific band although its method of production does not directly contain the use of electrons. N_2 first negative system has an ionization energy of 18.7 eV which is essentially not attainable in non-thermal atmospheric pressure plasma jets through direct electron impact. This is because the low power delivered to the plasma coupled with the charge accumulation on the dielectric do not allow for electrons to reach such high energies. Typical non-thermal appjs have a mean electron energy of only several eV. Despite this, this molecule is able to be ionized by metastable helium atoms only when the energy level of the metastable surpasses the ionization energy needed. The helium atoms in the working gas receive these

energies through collisions with the free electrons. This increase in voltage leads to an increase in number density and energy of the electrons, which impart that energy to the helium atoms in the working gas, which then de-excite through Penning Ionization with the nitrogen molecules [22].



(a)

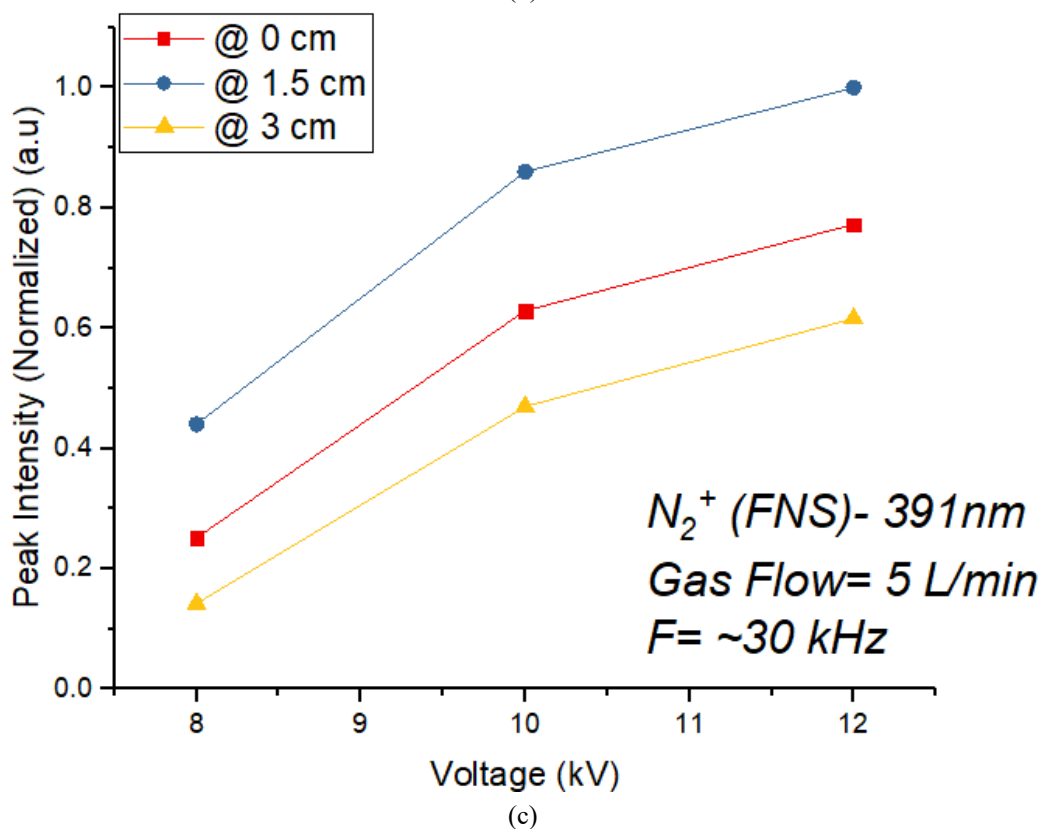
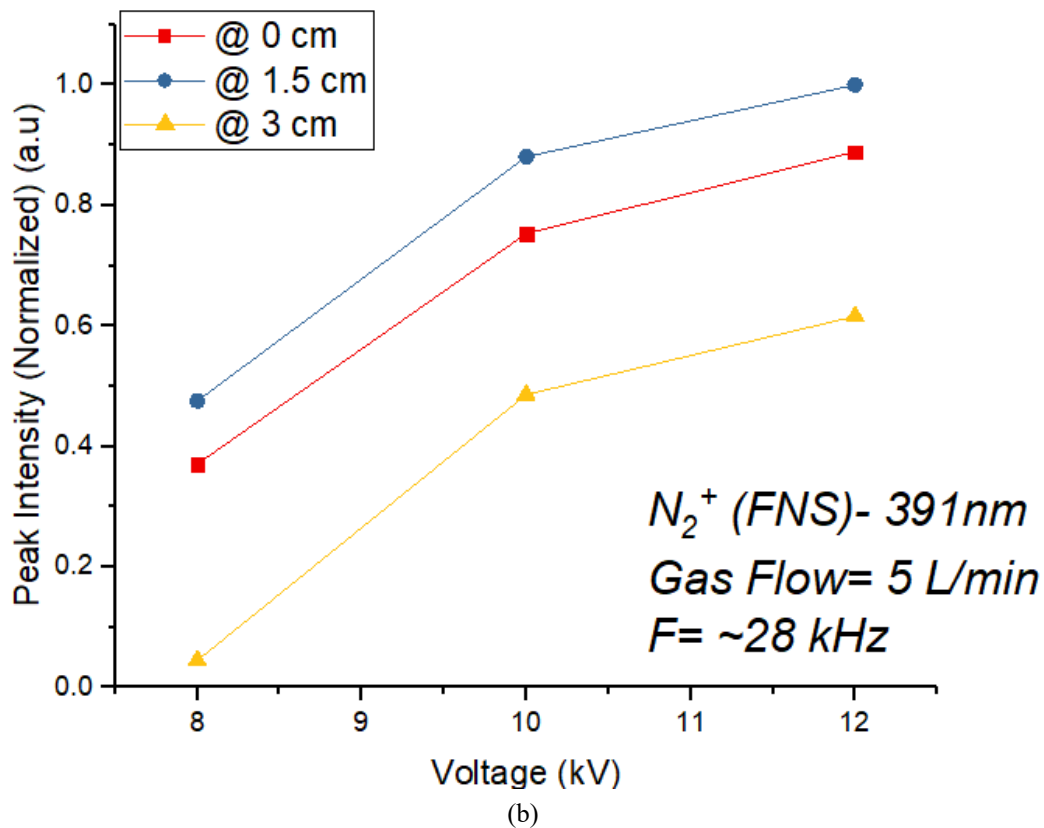
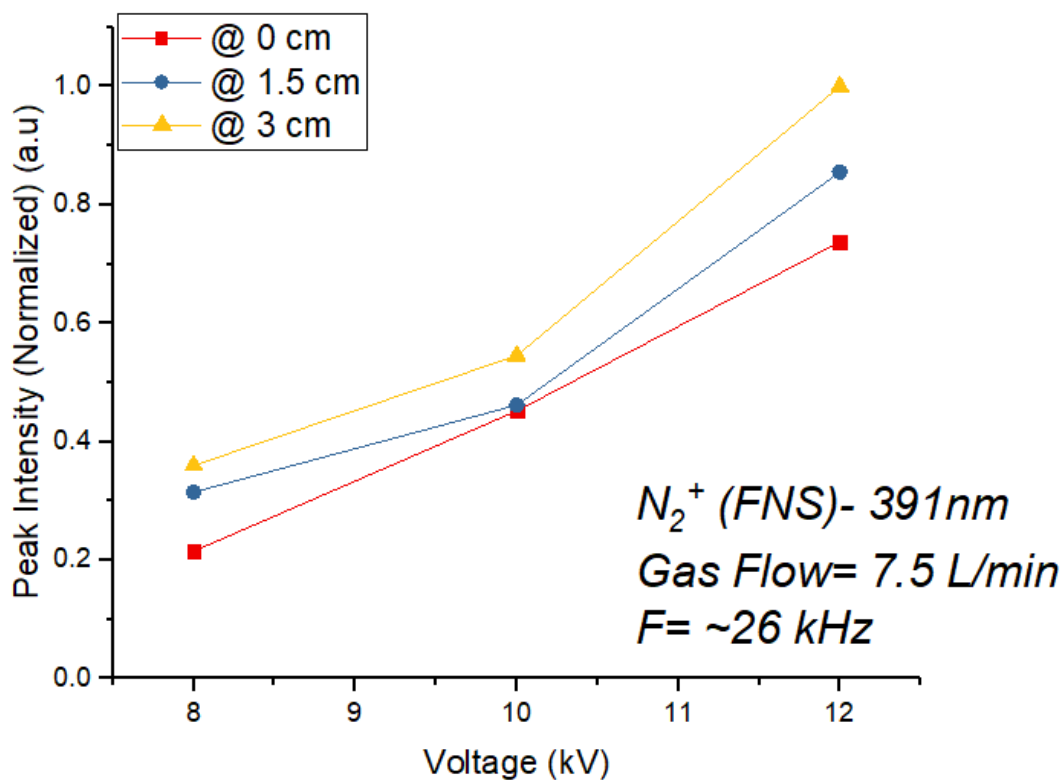
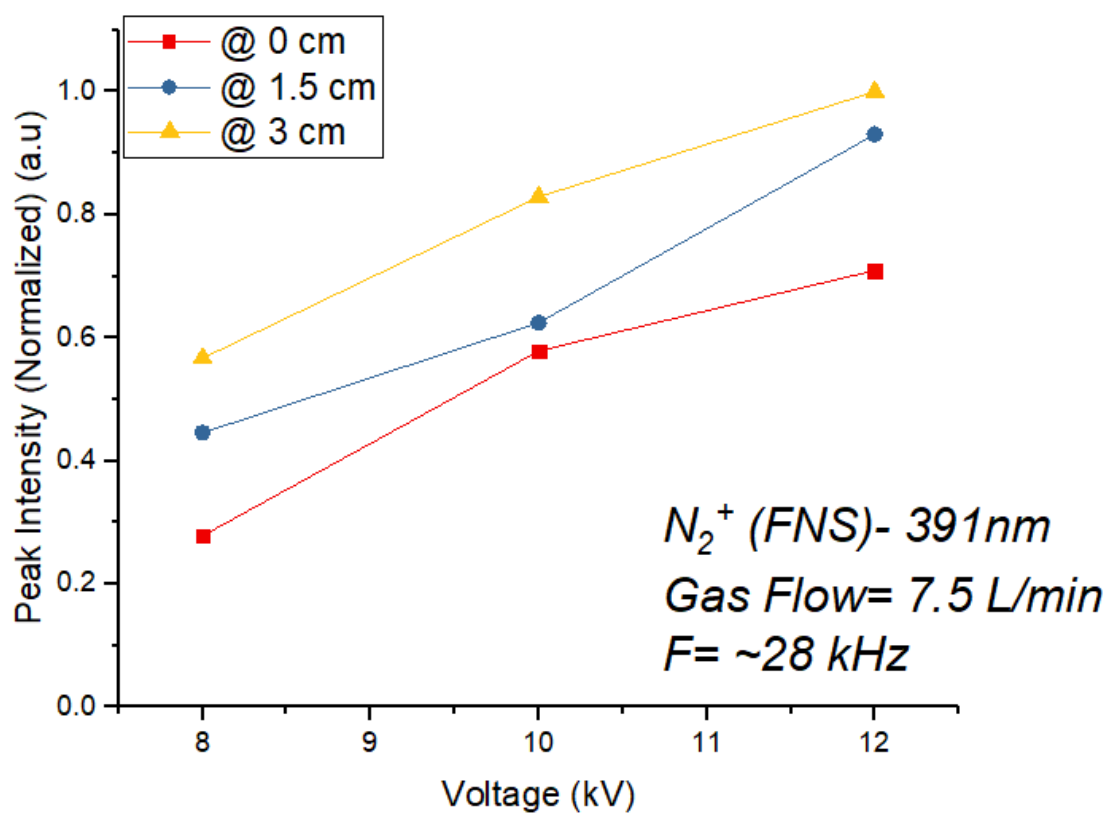


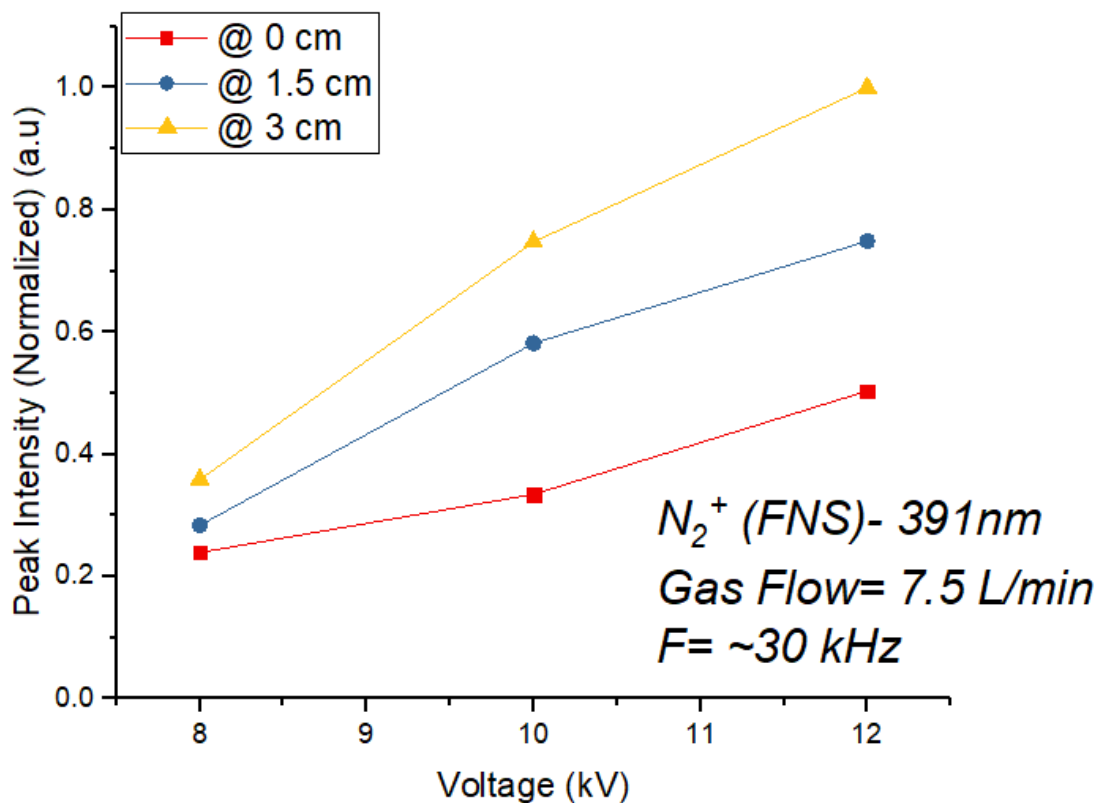
Figure 16. Dependence of N_2^+ ($B^2\Sigma_u^+ - X^2\Sigma_g^+$) at (a) 26 kHz, (b) 28 kHz, (c) 30 kHz, on voltage and distance at gas flow rate 5 L/min.



(a)



(b)



(c)
Figure 17. Dependence of N_2^+ ($B^2\Sigma_u^+ - X^2\Sigma_g^+$) at (a) 26 kHz, (b) 28 kHz, (c) 30 kHz, on voltage and distance at gas flow rate 7.5 L/min.

Figure 16 and 17 allow for the analysis of the effect of air interaction to be investigated on the production of this first negative system. The observations here are very similar to that of the second positive system because they are the same molecule and rely on the same circumstance in order to be excited or ionized: plasma interaction with the air. Here, the first negative system reaches its peak at 1.5 cm with the helium flow rate at 5 L/min. The reason for this is the same as mentioned in the case of the second positive system. The reading at 3 cm along the jet axis with a flow rate of 5 L/min corresponds to the point of the jet with the lowest number density of electrons. These electrons are vital to the production of the first negative system in that it provides the energy necessary to get the helium atoms into that metastable state so they may impart that energy to the nitrogen molecule and perform Penning Ionization. The

similarities continue as in the case of gas flow rate 7.5 L/min, it reaches its peak further along the effluent due to the high number of free electrons at that point.

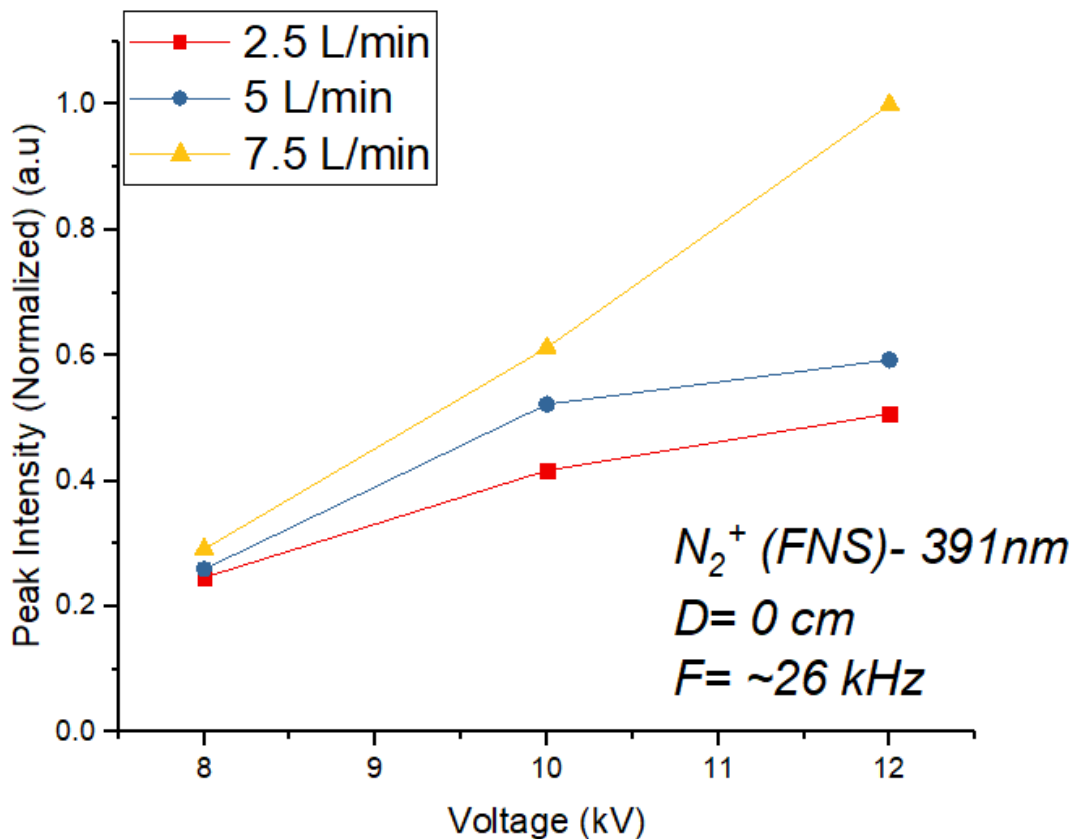


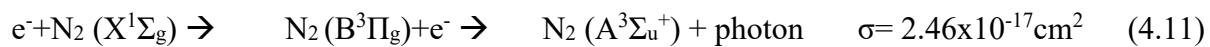
Figure 18. Dependence of N_2^+ ($B^2\Sigma_u^+ - X^2\Sigma_g^+$) on gas flow rate at a frequency of 26 kHz.

In order to gauge the significance of gas flow rate, figure 18 presents the data at the same distance from the tube exit and same frequency, while plotting the different flow rates. It is evident that the N_2 first negative system increases in accordance to voltage as well as flow rate. This is because of the importance of the presence of metastable helium atoms to the facilitation of the ionization. As mentioned previously, due to the non-thermal nature of the plasma it is extremely unlikely to produce this reaction through electron impact ionization. This heavy dependency upon the presence and flow of helium also contributes to the reason why the N_2 second positive system reaches its peak at 5 L/min. As flow rate increases, more helium atoms are flowed through the system meaning this increased number of helium atoms will gain energy

from the free electrons which are those same free electrons which facilitate the electron impact excitation needed to generate those vibrationally excited N₂ molecules [5]. Losses of this ionized specie come from quenching molecules that are most commonly found in air which are N₂ and O₂. The rates of these losses are very similar to that of the second positive system, $10^{-11} - 10^{-10}$ cm³ s⁻¹. These reported results are in agreement with similar studies done [5] [21].

4.1.4- N₂ First Positive System

The N₂ first positive system ($B^3\Pi_g - A^3\Sigma_u^+$) is a vibrationally excited electronic state that is produced through a seemingly complicated process. As discussed in subsection 4.1.2, the method for generating N₂ second positive ($C^3\Pi_u - B^3\Pi_g$) consists of an electron colliding with the vibrationally ground N₂ molecule in the ambient air and exciting it into the $C^3\Pi_u$ electronic state. Naturally, the excited state then decays into the $B^3\Pi_g$ electronic state with the energy difference being released as a photon. In the case of the first positive system, it is excited into the $B^3\Pi_g$ state and then decays into the metastable $A^3\Sigma_u^+$ electronic state. The specific band observed in this discharge is identified as the (10,7) transition at approximately 631 nm. In a study conducted by Manalis *et al.* [26], the vibrational distributions of this system in a helium afterglow were investigated to understand its production. It was observed that there was a large population of N₂ molecules in the tenth vibrational level (9.3 eV) [20], which was “unusual” [26]. This large population was found to be a result collision-induced level crossing with the $B^3\Sigma$ electronic state, which is very close in potential energy as shown in figure 19. This collisional level crossing is made possible by the overlap of the turning points of the curves [26]. The reaction process, energy associated with the transitions, and relevant cross sections are given by [15] [20]:



$$9.3 \text{ eV} \qquad 7.35 \text{ eV} \qquad (4.12)$$

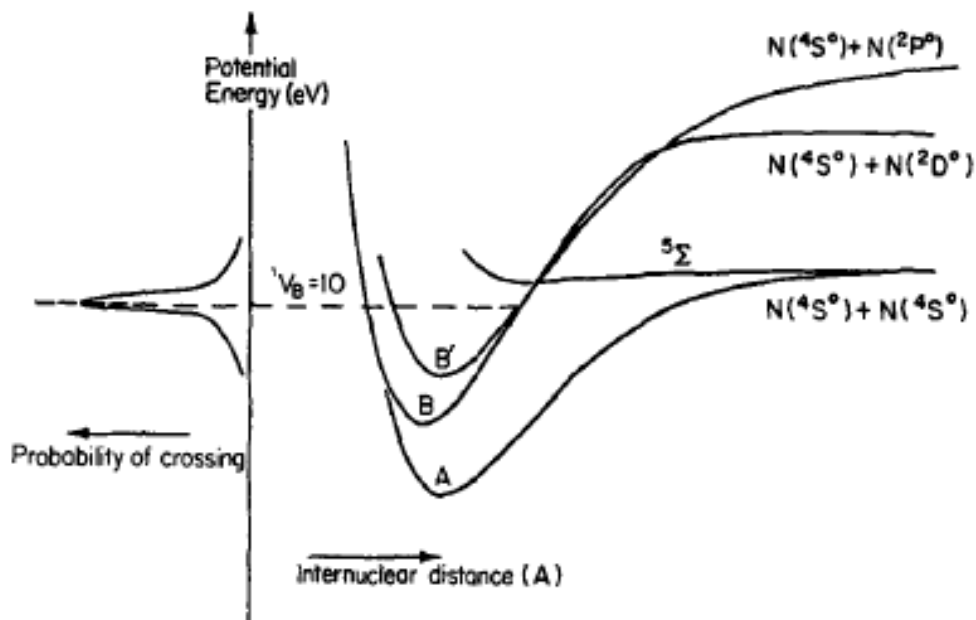
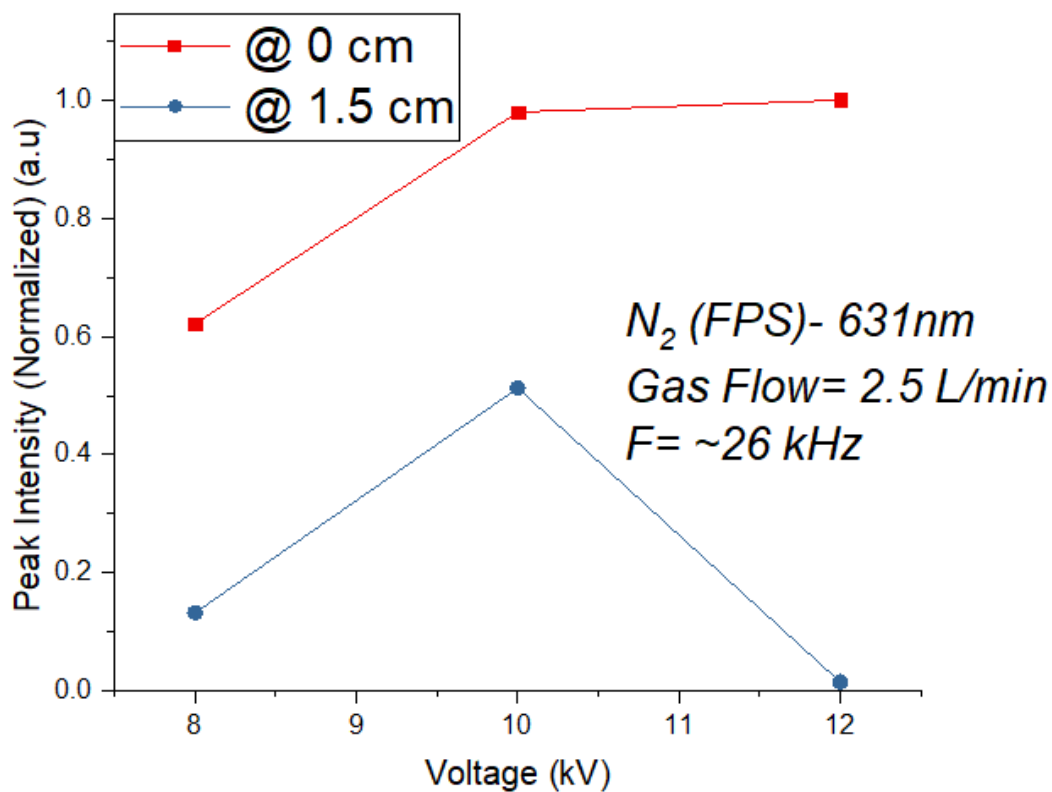


Figure 19. Potential energy level curve showing the level crossing at the observed vibrational level. Ref. 26.



(a)

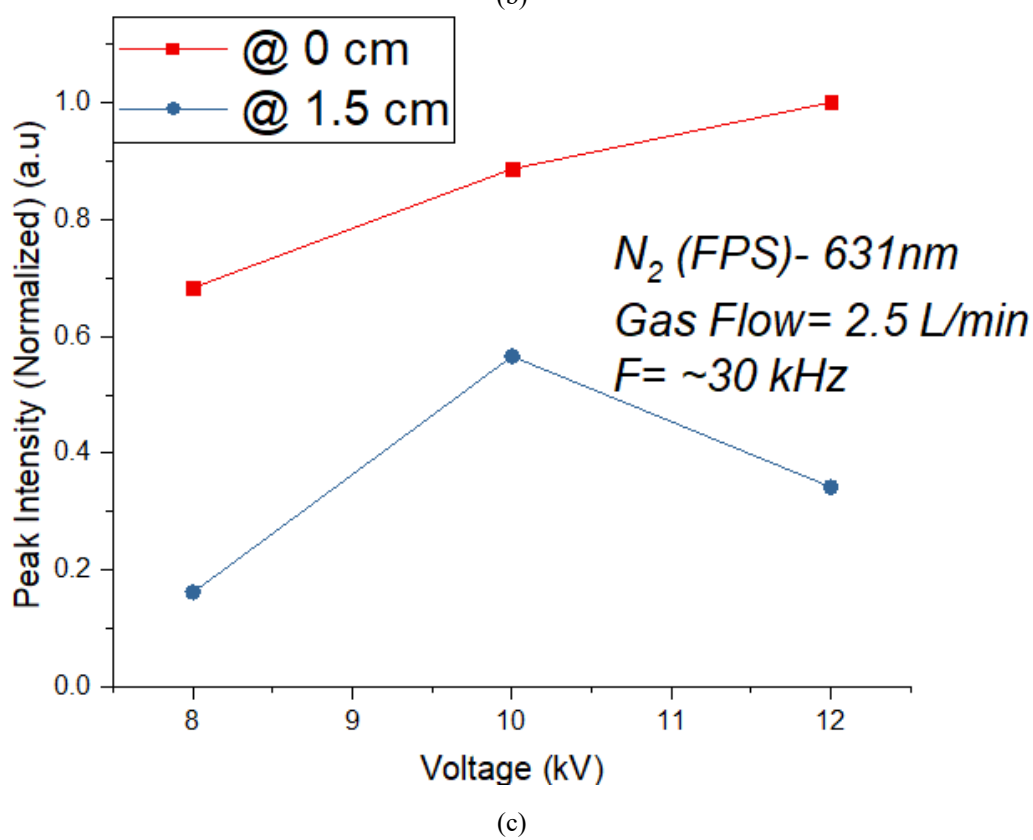
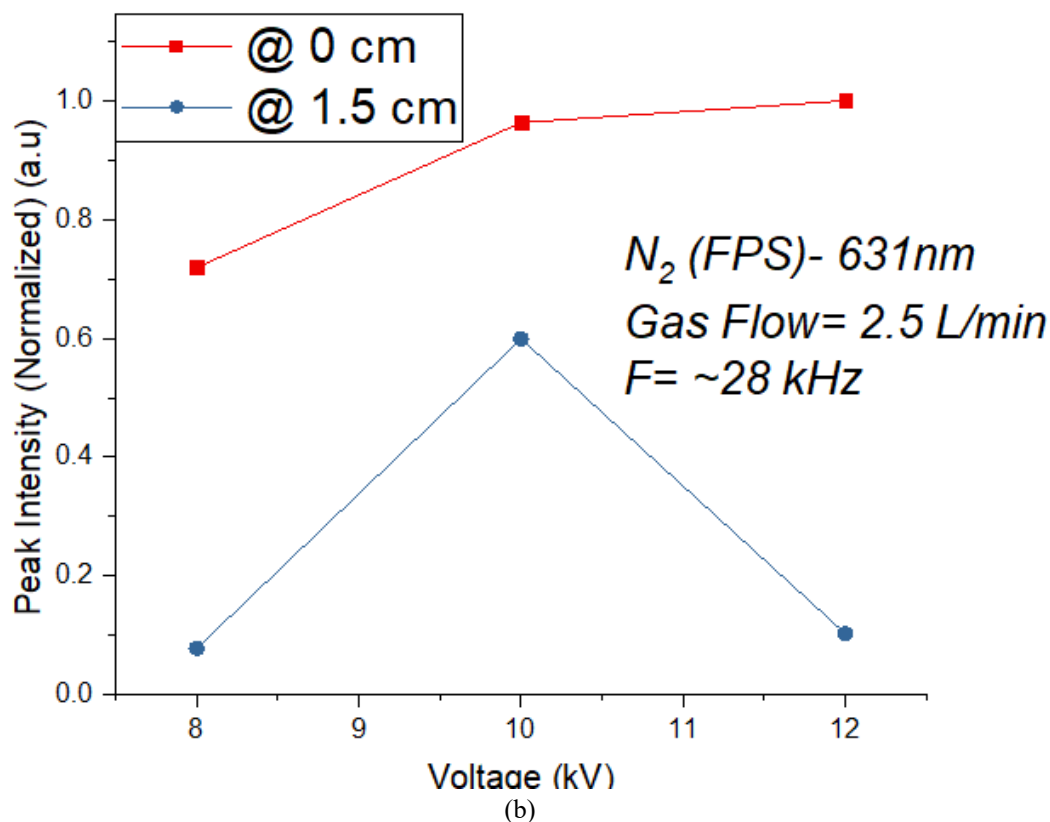
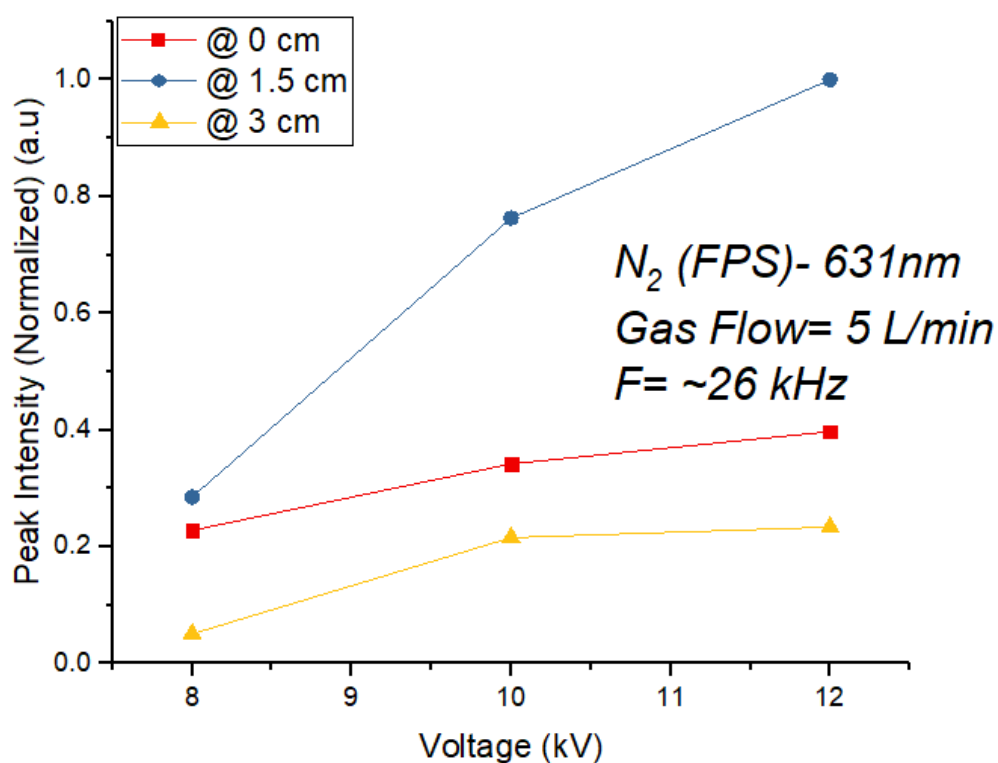


Figure 20. Dependence of N_2 ($B^3\Pi_g - A^3\Sigma_u^+$) at (a) 26 kHz, (b) 28 kHz, (c) 30 kHz, on voltage and distance at gas flow rate 2.5 L/min.

As is the case in figure 20, an increase in voltage results in an increase of emission intensity of this molecule. This transition of N_2 is reliant upon the energy gained by the free electrons from the applied electric field in order to facilitate the excitation and subsequent decay into metastable state. The added voltage generates more electrons and high energy variants, which is favorable to cause the emission of this state.



(a)

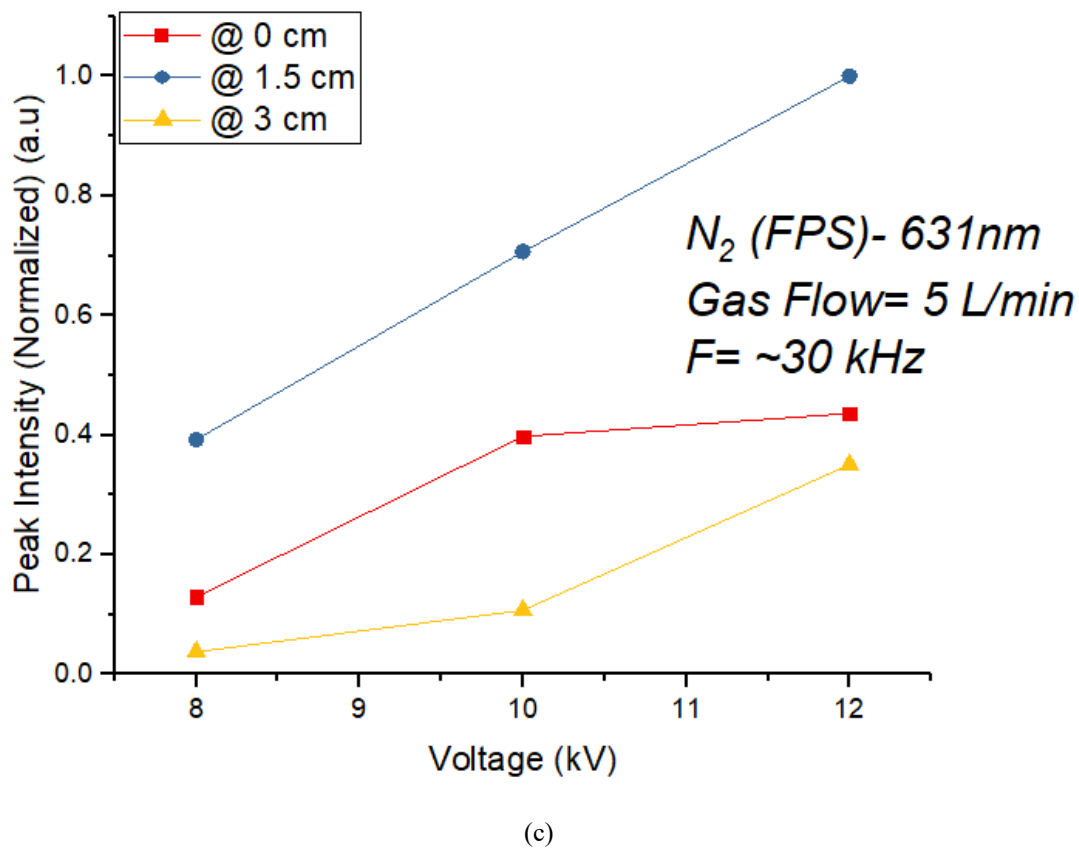
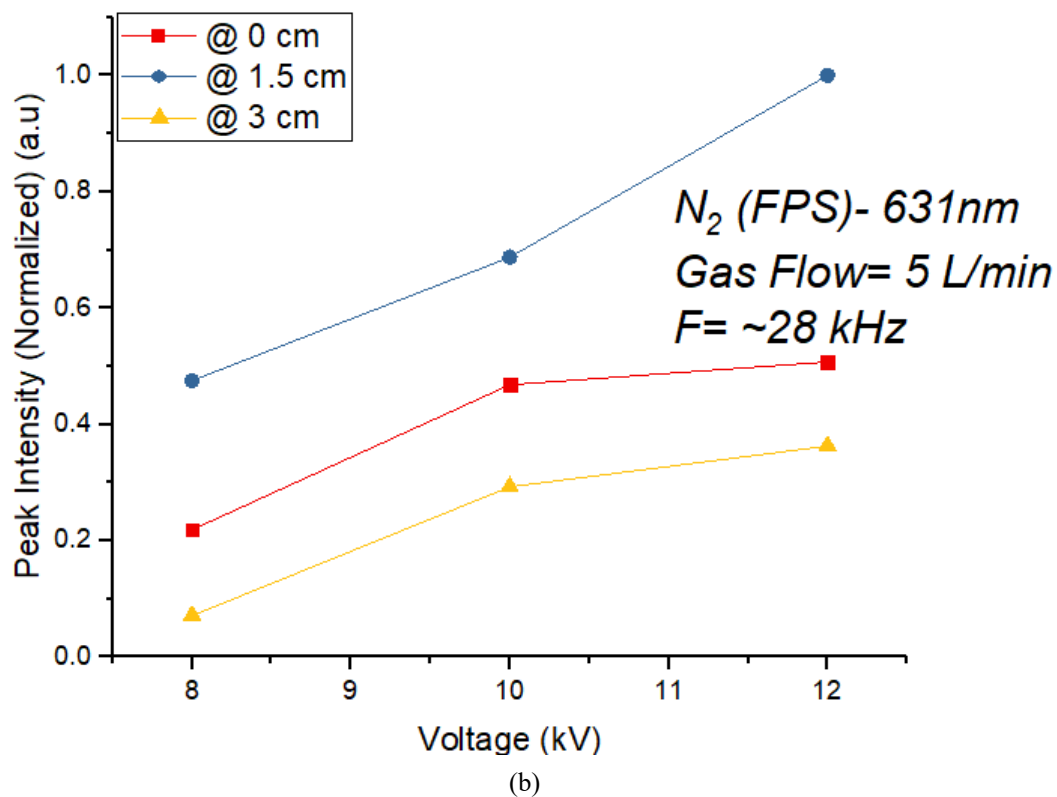
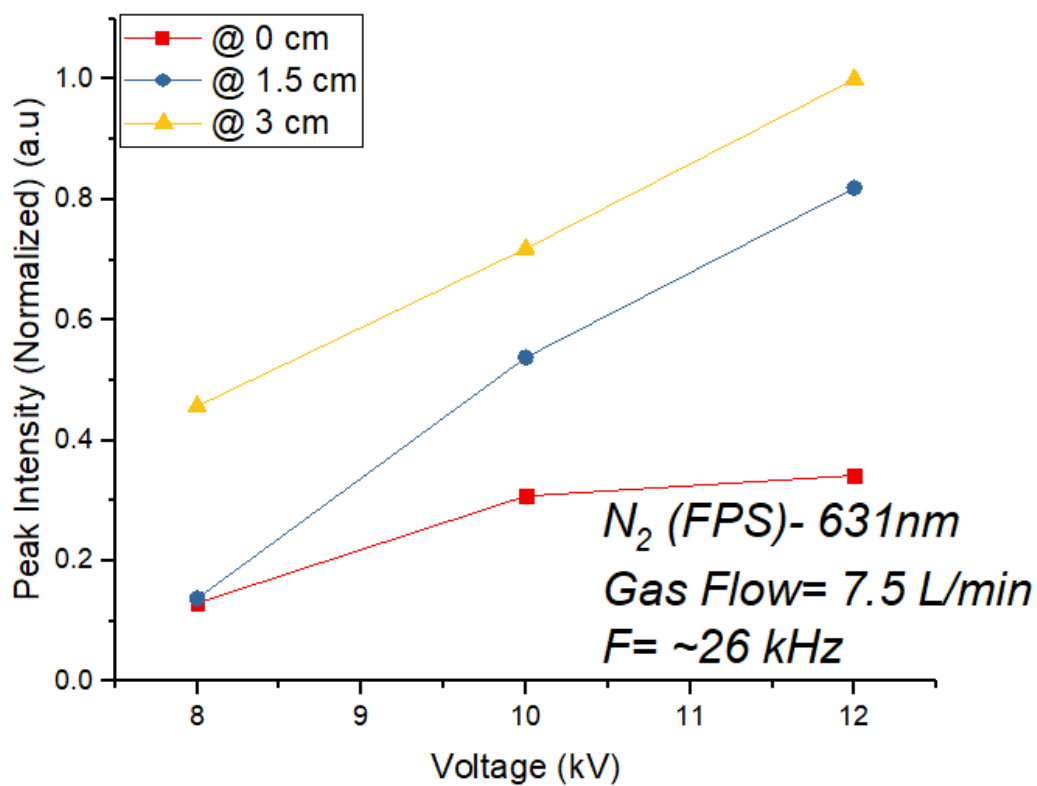
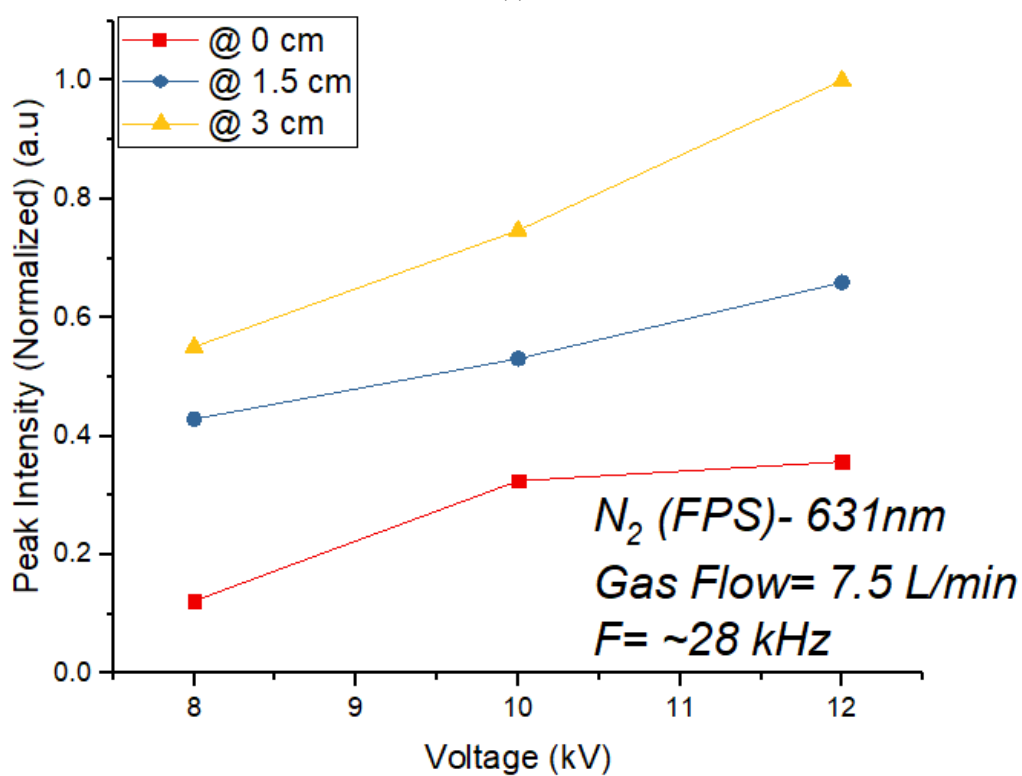


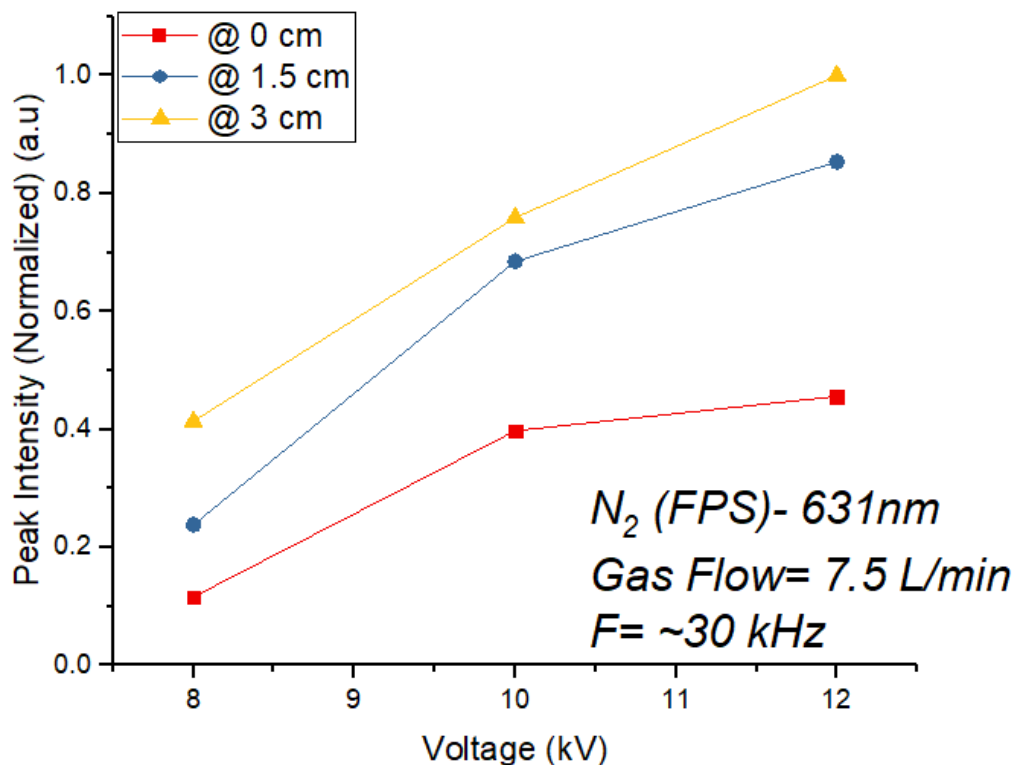
Figure 21. Dependence of N_2 ($B^3\Pi_g - A^3\Sigma_u^+$) at (a) 26 kHz, (b) 28 kHz, (c) 30 kHz, on voltage and distance at gas flow rate 5 L/min.



(a)



(b)



(c)
Figure 22. Dependence of N_2 ($B^3\Pi_g - A^3\Sigma_u^+$) at (a) 26 kHz, (b) 28 kHz, (c) 30 kHz, on voltage and distance at gas flow rate 7.5 L/min.

In figures 20-22, it is clear that regardless of frequency or flow rate, the trend of intensity proportional to applied voltage holds true. In figures 21 and 22, the effect of air interaction with the plasma is investigated at these different flow rates and frequencies. It is observed that the effect of these parameters on the behavior of its emission intensity is very similar to that of the second positive system. In like manner, the first positive system reaches its peak value at a distance of 1.5 cm at 5 L/min, while continuing to increase along the effluent when flow rate increases to 7.5 L/min. For 5 L/min, 0 cm away from the tube exit refers to a point where electron density is highest (relative to further away from tube exit) and plasma interaction with the air is the least. At 3 cm away, this represents a point where number density is the least while air interaction is the highest. 1.5 cm away represents the median between these two parameters which are very significant to the production of both the first and second positive systems. At 7.5

L/min, the conditions mentioned are no different for air interaction and electron density, however, this increase in flow rate does change these facts. Due to the increased jet length from 3 cm to ~5 cm, the disparity between number densities are not as pronounced. This is evident in both the first and second positive systems as the concentration continues to increase from 1.5 cm to 3 cm.

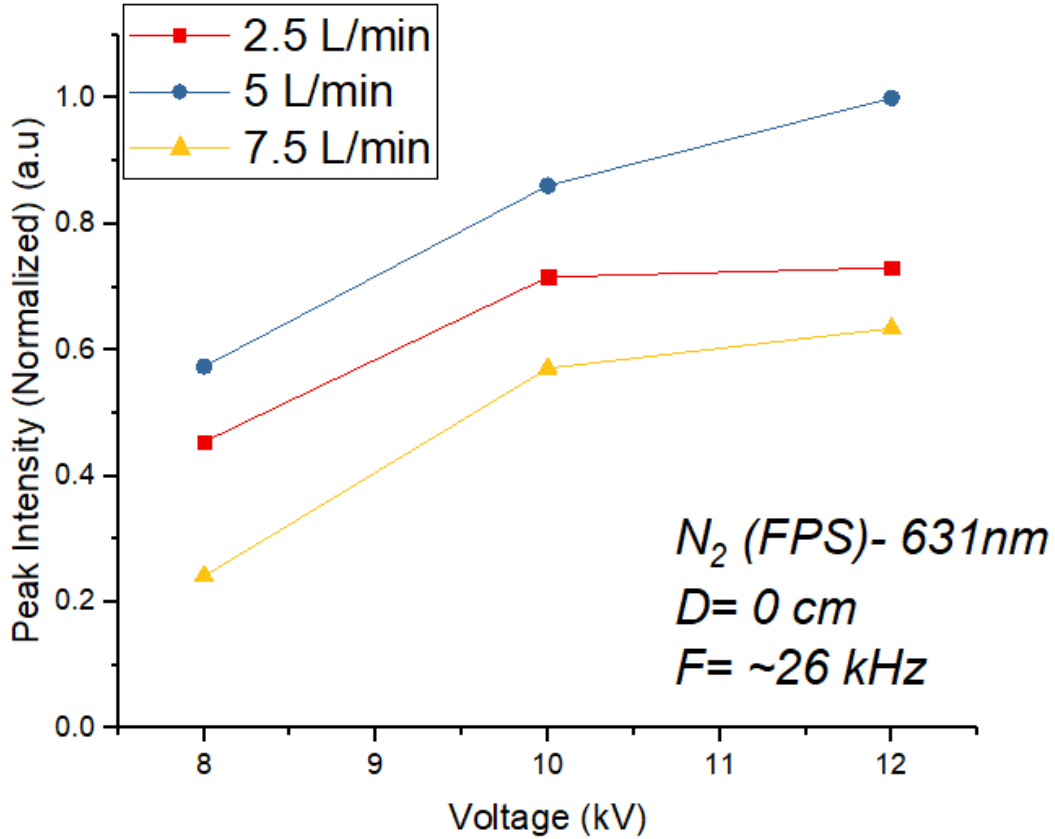


Figure 23. Dependence of $N_2 (B^3\Pi_g - A^3\Sigma_u^+)$ on gas flow rate at a frequency of 26 kHz

The effect of helium flow rate on this system is shown in figure 23 and yields the same findings as was observed with the second positive system. A flow rate of 5 L/min was most favorable in the role of producing this system while a flow rate of 7.5 L/min had the least favorable effect. This is due to the higher flow of charge particles into the surrounding air, which

is the main generation mechanism for the vibrationally excited N₂ molecules. 7.5 L/min was observed to have an adverse effect on this generation mechanism due to the increased ionization of N₂ by helium metastables at this flow rate which was observed and discussed in subsection 4.1.3.

4.1.5- Helium Metastable

The helium metastable is an electronically excited atom that is produced as a result of electron impact. Helium atoms are introduced through its flow as the working gas and gains energy through collisions with the electrons applied through the electric field. Similar to other species that obtain its energy through electron impact collisions, it is excited into a particular electronic state depending on the energy acquired. However, unlike most other atoms or molecules that are excited, it does not decay to its ground state, but to a “stable” electronically excited state and de-excites through collisions with other particles, as is the case with the ionization of N₂ in this system. This ionization only occurs when the energy level of the metastable atom exceeds the ionization energy of the molecule in question. It is considered to be stable due to its very long lifetime where it can remain for seconds and even minutes. For context, radiative lifetimes of typically excited atoms or molecules is usually between the range of 10⁻⁶ s to 10⁻¹⁰ s. For the helium metastable states observed in this plasma, the excitation process is given below, while the electronic state energy levels, emission transition probabilities (A_{ki}), and corresponding electron impact cross sections are given in table 4 [22] [24] [28-31]:

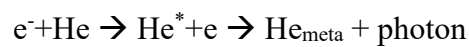
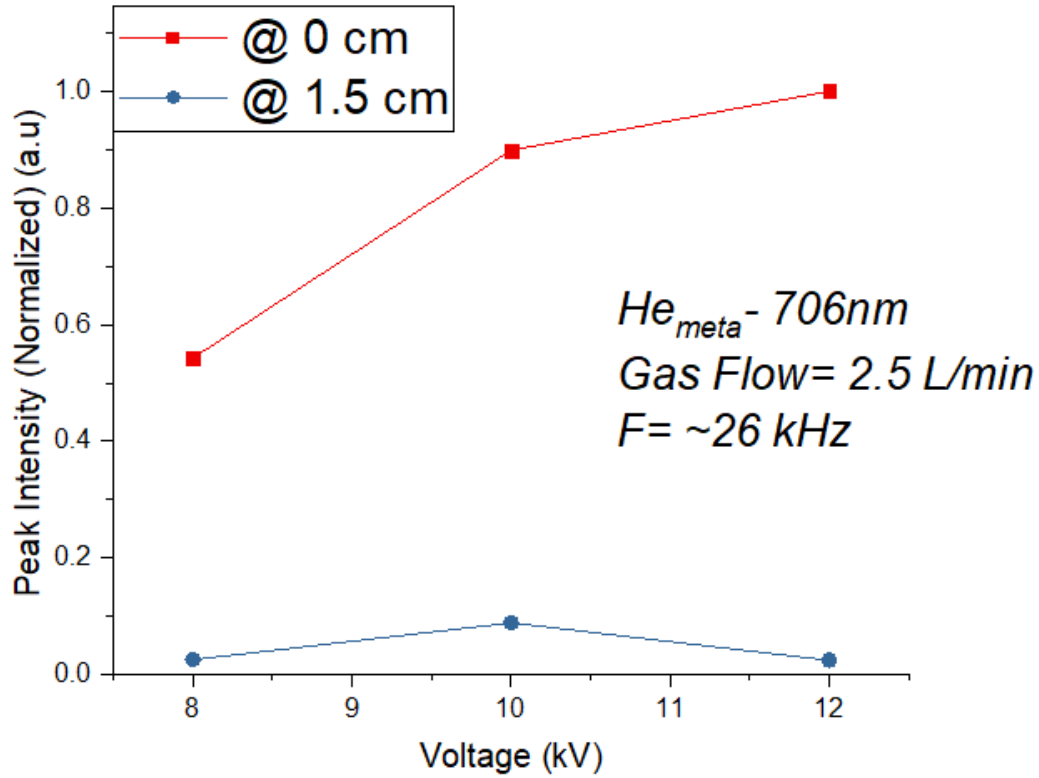
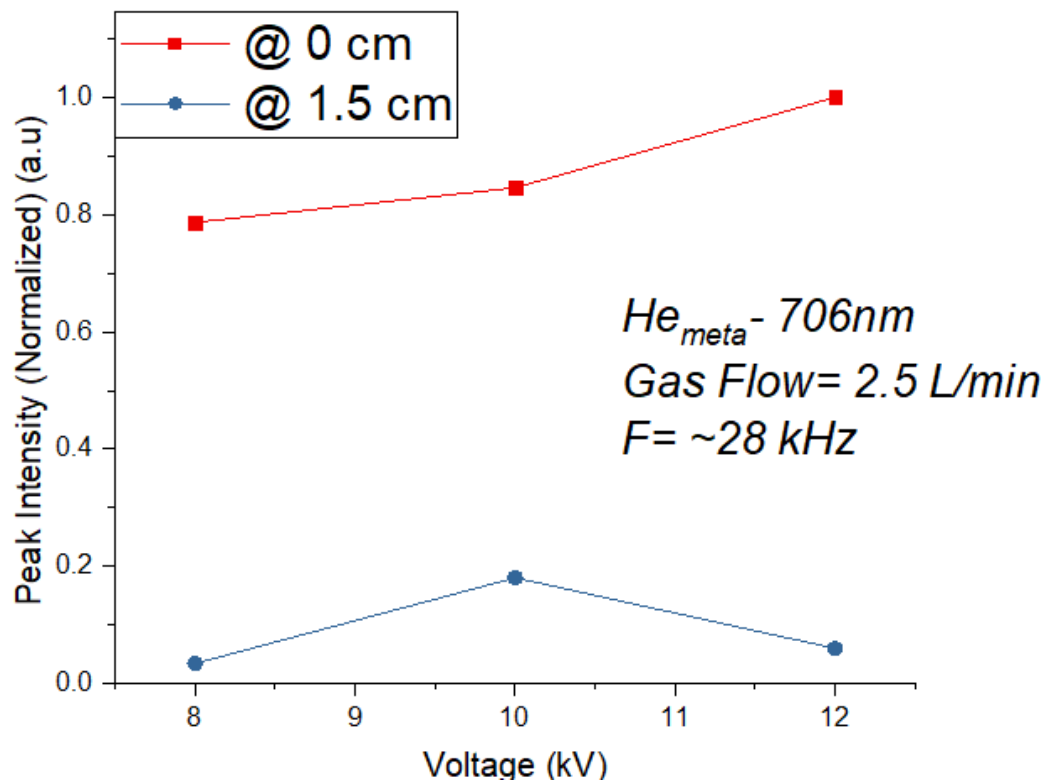


Table 4- Electron Impact cross sections and transition probability for Metastable Helium

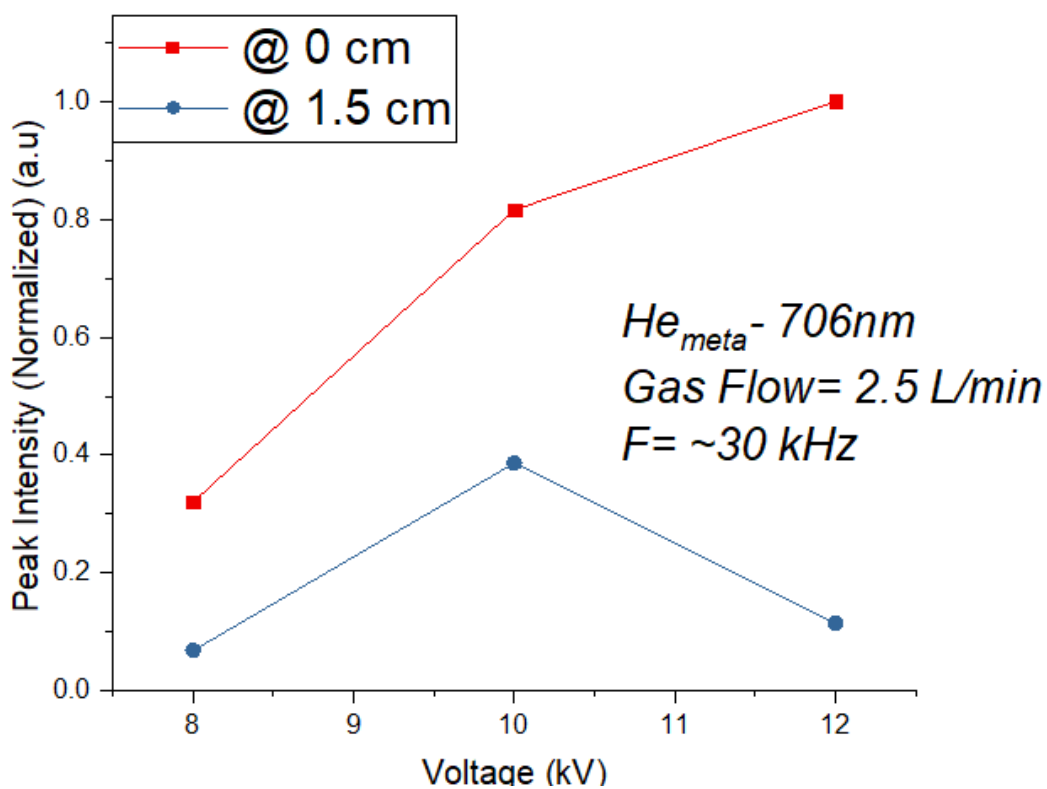
Transition	E_i (eV)	E_f (eV)	σ (cm ²)	A_{ki} (s ⁻¹)
4d ³ -2p ³	23.7	20.96	$\sim 10^{-18}$	3.77×10^8
4d ¹ -2p ¹	23.74	21.2	$\sim 10^{-18}$	1.01×10^8
3p ¹ -2s ¹	23.1	20.6	$\sim 10^{-18}$	4.01×10^7
3d ³ -2p ³	23.07	20.96	$\sim 10^{-18}$	1.06×10^9
3d ¹ -2p ¹	23.07	21.2	$\sim 10^{-18}$	3.19×10^8
3s ¹ -2p ¹	22.92	21.2	$\sim 10^{-18}$	1.83×10^7
3s ³ -2p ³	22.7	20.96	$\sim 10^{-18}$	8.3×10^7



(a)



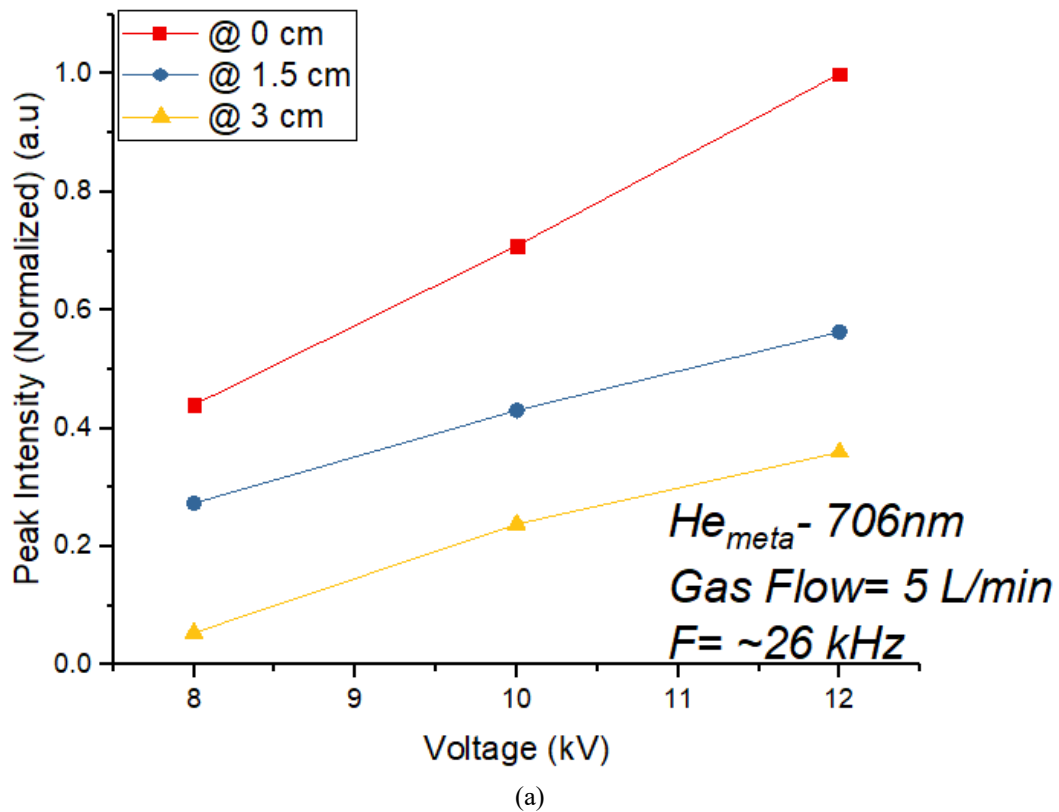
(b)



(c)

Figure 24. Dependence of metastable helium at (a) 26 kHz, (b) 28 kHz, (c) 30 kHz, on voltage and distance at gas flow rate 2.5 L/min.

As shown in figure 24, regardless of frequency, an increase in voltage results in an increase in emission intensity of the helium metastable. This is due to its production mechanism which relies on the availability of high energy electrons required for excitement. Increasing power delivered to the reactor generates more electrons and more high energy variants which benefits the generation of these metastables.



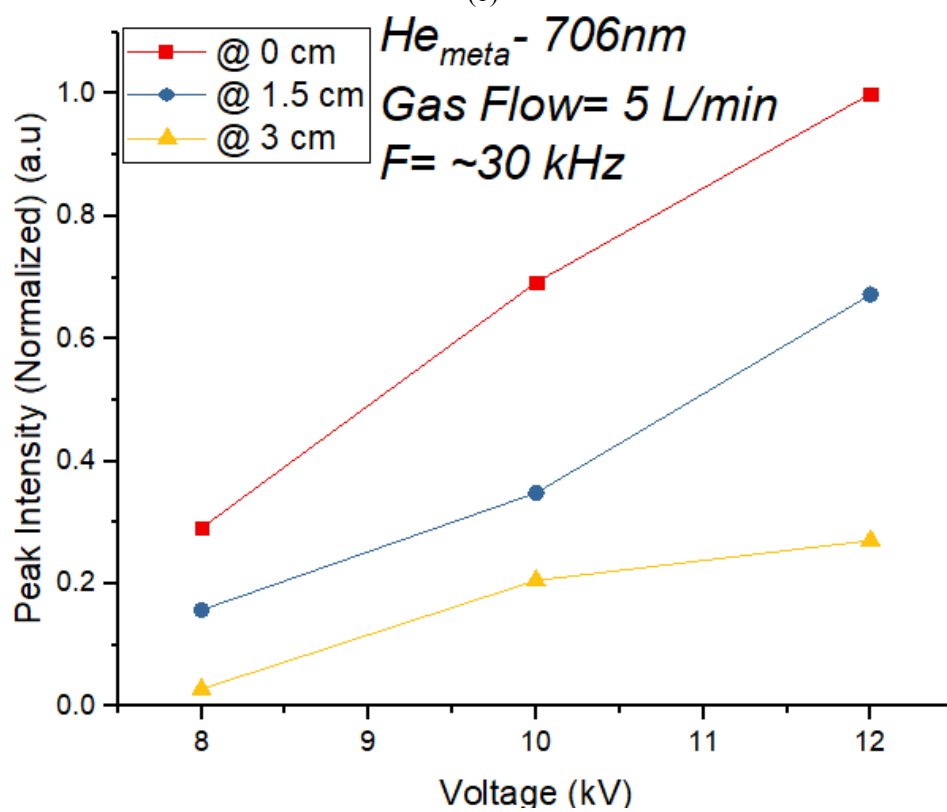
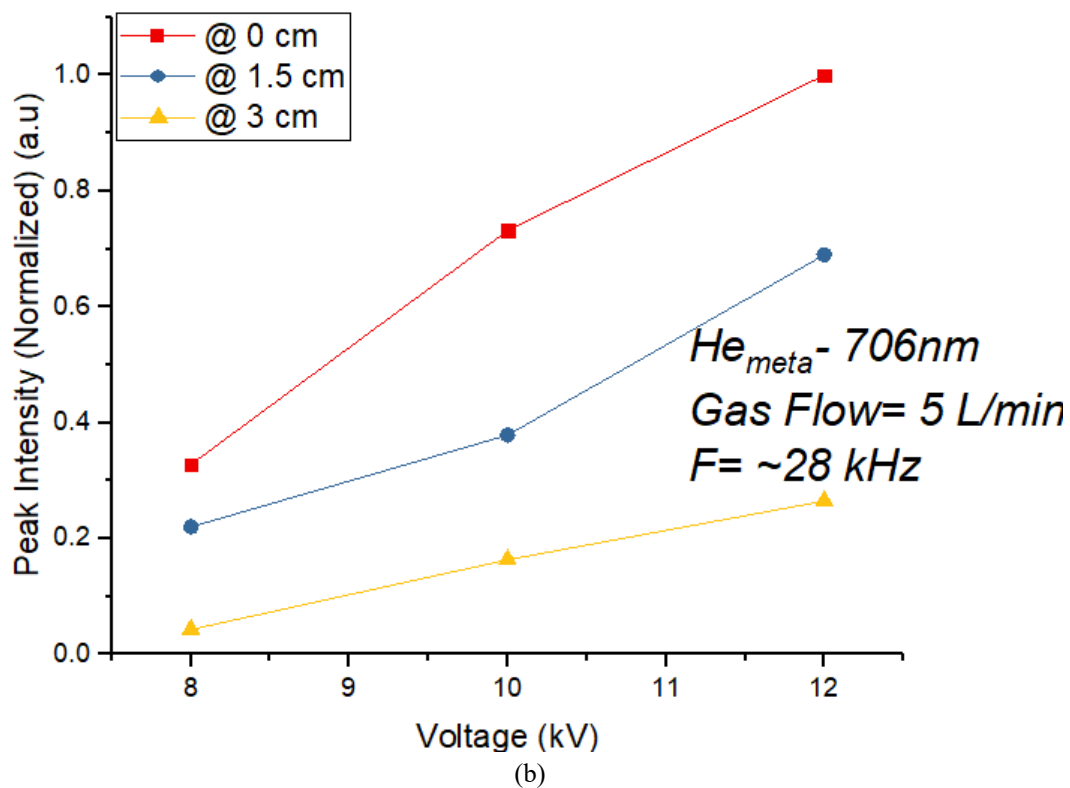
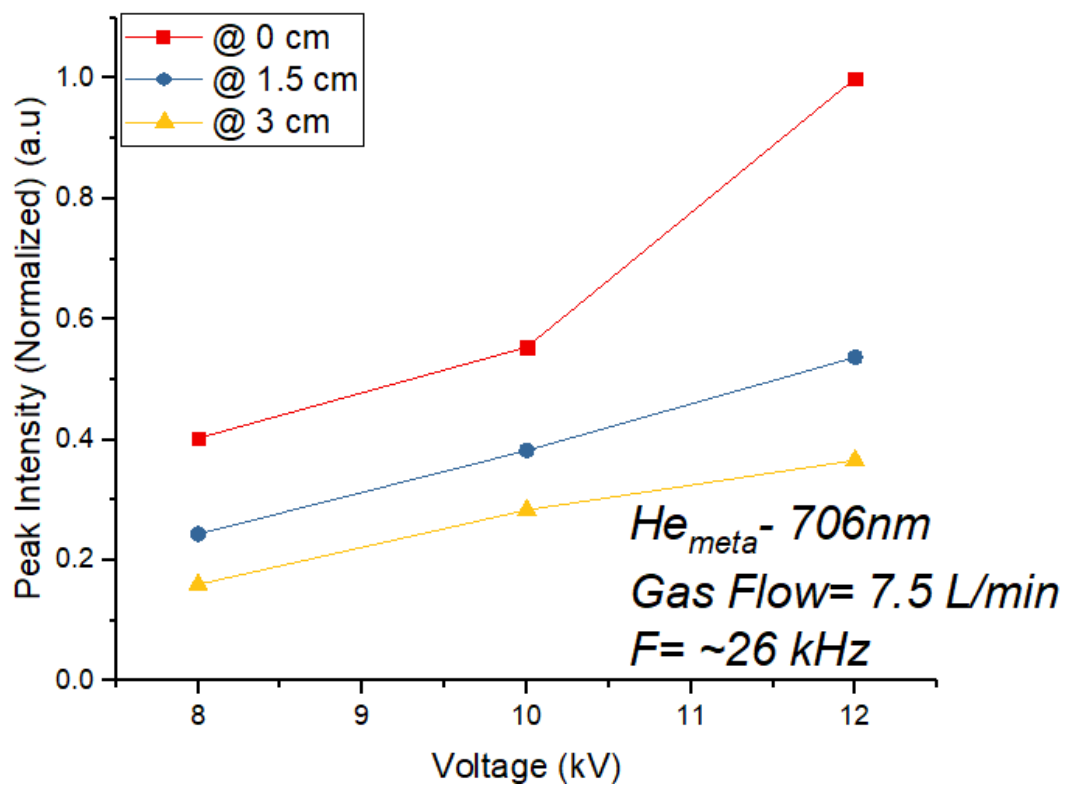
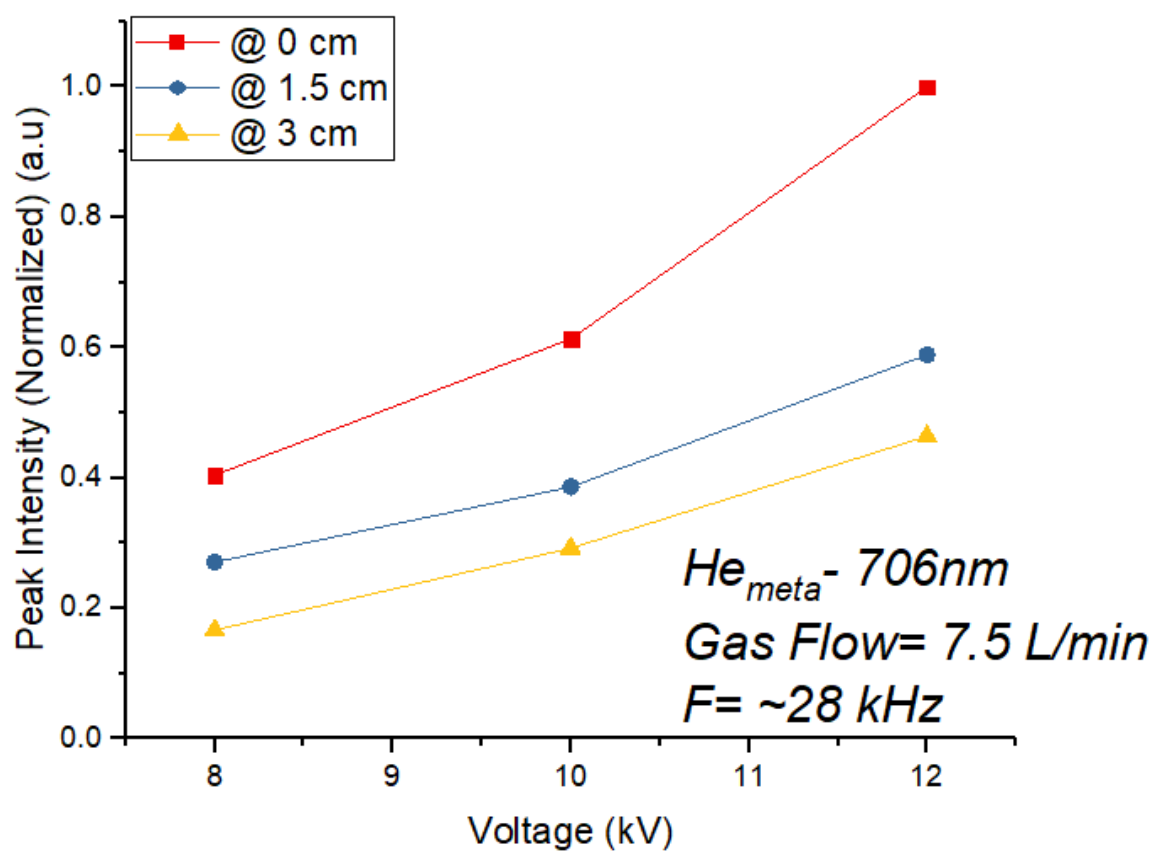


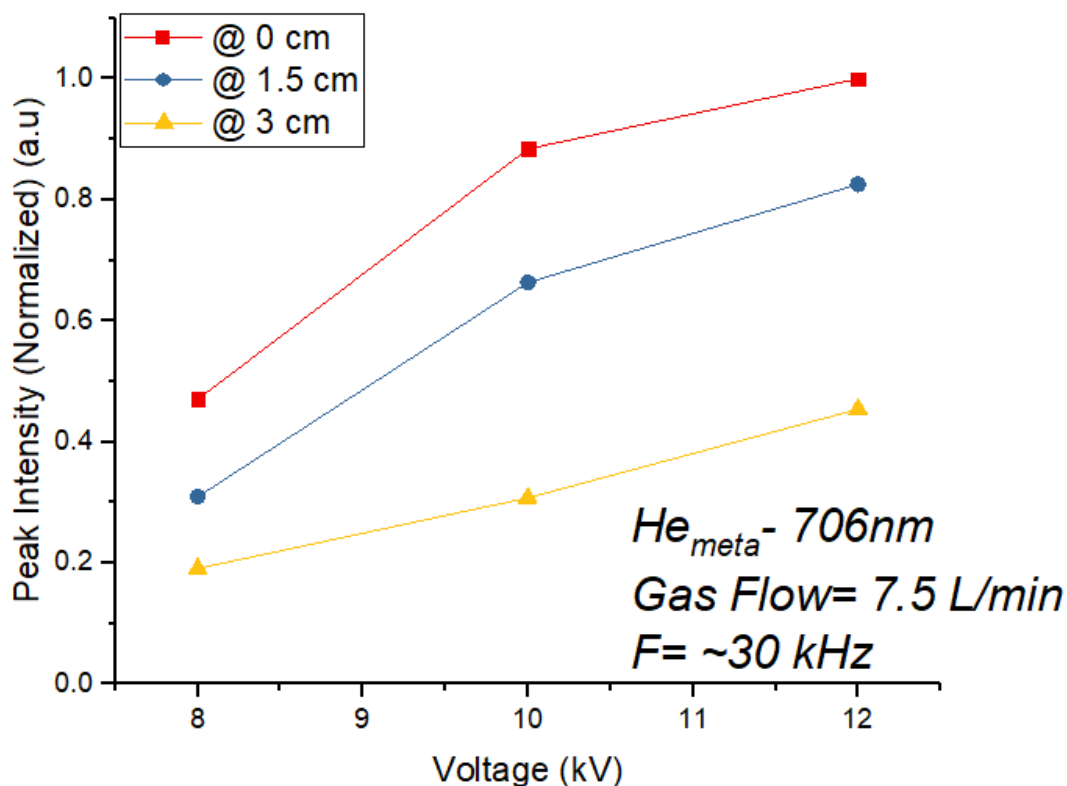
Figure 25. Dependence of metastable helium at (a) 26 kHz, (b) 28 kHz, (c) 30 kHz, on voltage and distance at gas flow rate 5 L/min.



(a)



(b)



(c)

Figure 26. Dependence of metastable helium at (a) 26 kHz, (b) 28 kHz, (c) 30 kHz, on voltage and distance at gas flow rate 7.5 L/min.

Despite different flows of helium and applied frequencies, voltage increase always results in an increase of specie concentration. However, figures 25 and 26 indicate a decrease in the concentration of these metastable atoms as it gets further from the tube exit regardless of frequency and flow rate. In the plasma, the helium atoms gain the energy during the discharge and is propelled outward into the ambient air where it interacts with molecules such as N_2 and O_2 . This increased interaction leads to more opportunities to collide with these molecules and result in de-excitation in ways such as Penning Ionization and dissociation. This process is precisely how the N_2^+ first negative system is generated. This observation is supported by the data in figures 16 and 17 that show an increase in emission intensity of the first negative system as the plasma is increasingly exposed to air. This decrease also provides an explanation of the

main loss mechanisms of this specie. Provided that metastable states have long radiative lifetimes, the only other forms of de-excitement are ionization and excitation of the air molecules. For this reason, the rate at which there is a loss due to N_2 is essentially equal to reaction rate at which Penning Ionization occurs as is defined in 4.9 and 4.10.

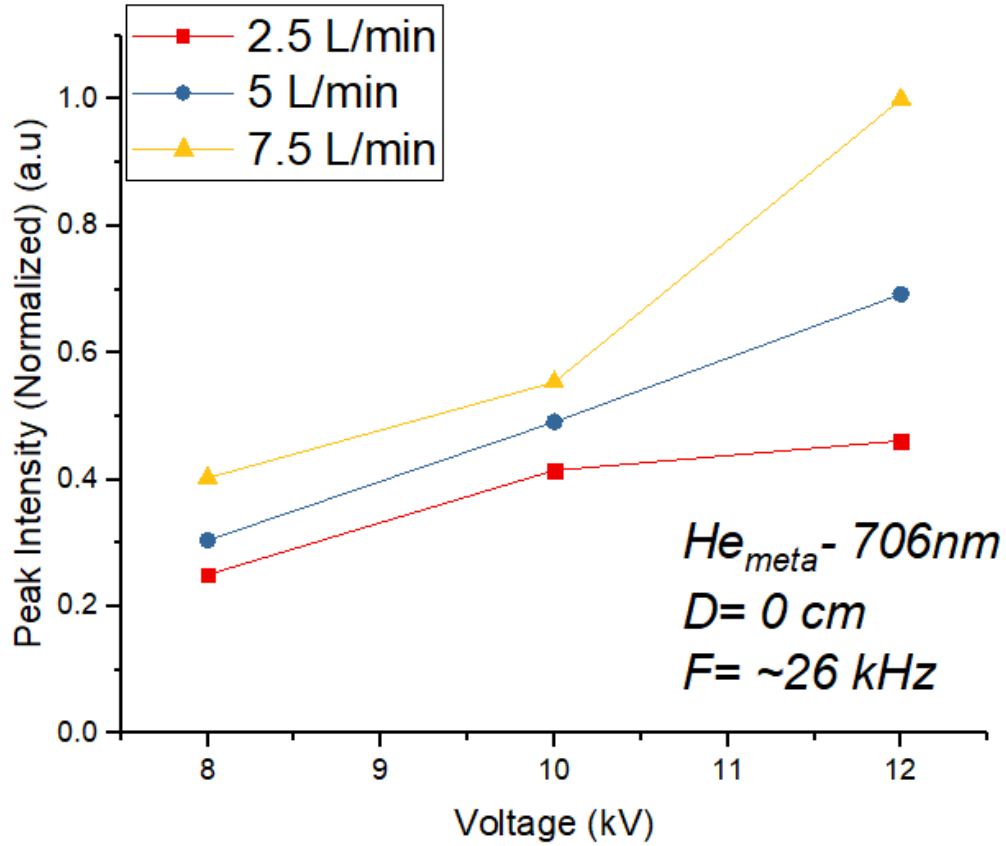


Figure 27. Dependence of the helium metastable on gas flow rate at a frequency of 26 kHz.

When gas flow rate was increased, the emission of the metastable helium saw a similar increase as shown in figure 27. Increasing flow rate increases the amount of the atoms flowing through the discharge zone within the dielectric tube. This allows more of these atoms to capture the energy through electron collisions, directly leading to an increase in the amount of helium atoms that gain enough energy to conduct the excitation process. Under this circumstance, more excited helium atoms would have to lead to more ionization. Figure 18 explores this correlation

and shows that the emission of N_2^+ first negative system increases as flow rate increases. The ionization here is only able to be facilitated by metastable helium making the findings agree with one another. These results also agree with studies done which examine the correlation between this operating parameter and specie production such as [5] [17] [21] [29] as long as the flow remains laminar.

4.1.6- Atomic Oxygen

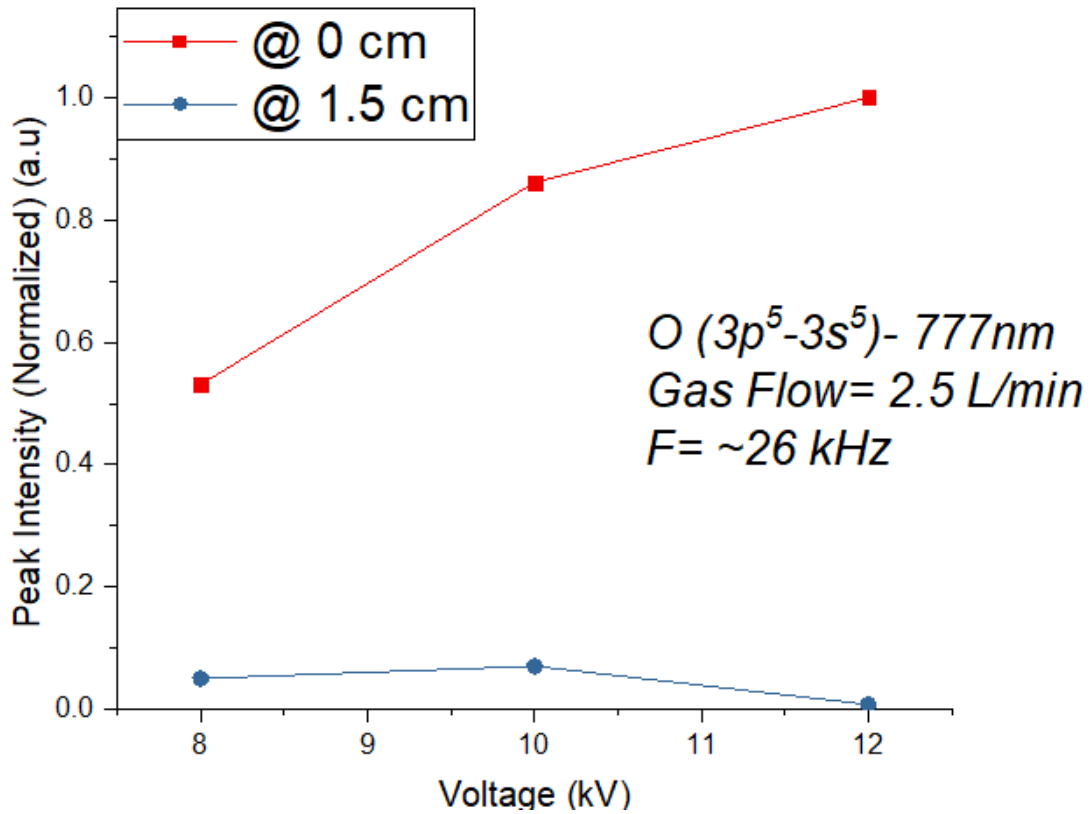
Atomic oxygen is best known for its strong oxidizing ability which makes it particularly useful for applications such as etching and bacterial decontamination. Similar to the hydroxyl radical (4.1.1), it is electrically neutral but highly reactive due to its unstable electron configuration. It is the second most electronegative element (electron affinity= 1.5 eV), which means it is very attracted to electrons and other molecules or atoms in an attempt to close its electron orbital shells. In this plasma, atomic oxygen triplet bands is produced through a combination of both electron impact dissociation excitation with O_2 in the ambient air, and Penning-type collisions with helium metastables with O_2 as reported by Xiong *et al.* [34]. Its facilitation begins as an O_2 molecule, but when collisions occur with either the electron or helium metastable, the bond between the oxygen atoms are broken and results in dissociation which only requires about 5.2 eV of energy [24]. The bands observed in this system contain more energy than the 5.2 eV required for dissociation and leads to excitation of the atomic oxygen to an electronic state depending on the amount of energy imparted. As with any excited state, the instability causes it to decay into another electronic state and release that energy difference in the form of a photon. The possible reactions, energies associated with the excited

states observed here, reaction rate, and the transition probabilities of these states are given by 4.13 and 4.14 and in table 5 [24] [28-29] [34]:

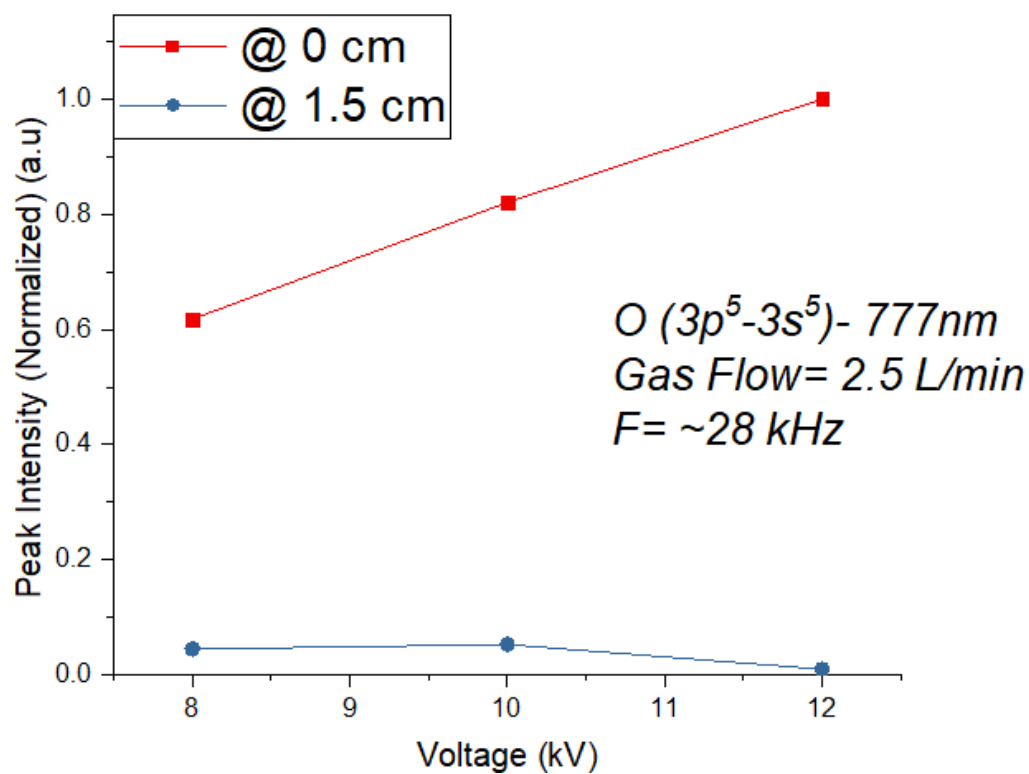


Table 5- Electronic transitions, energy states, and transition probabilities for atomic Oxygen triplet bands

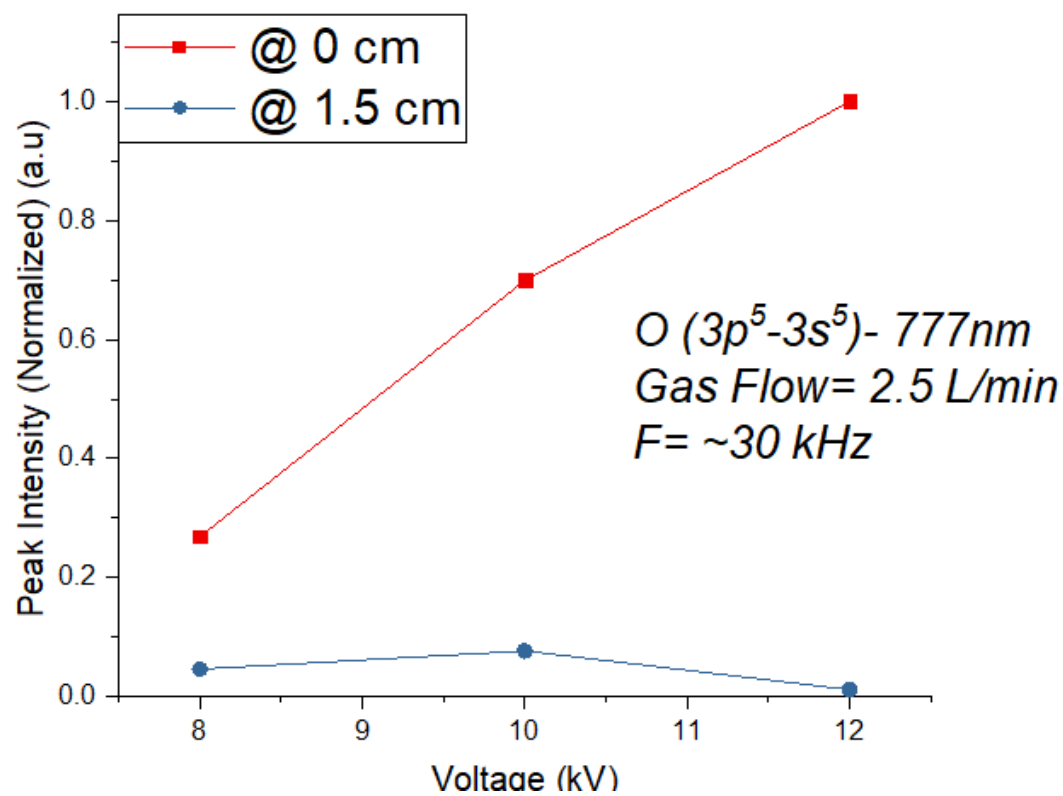
Transition	E_i (eV)	E_k (eV)	A_{ki} (s^{-1})
$4d^5-3p^5$	12.75	10.74	7.62×10^6
$3p^1-3s^1$	14.46	12.73	5.05×10^7
$3p^5-3s^5$	10.74	9.15	3.69×10^7



(a)



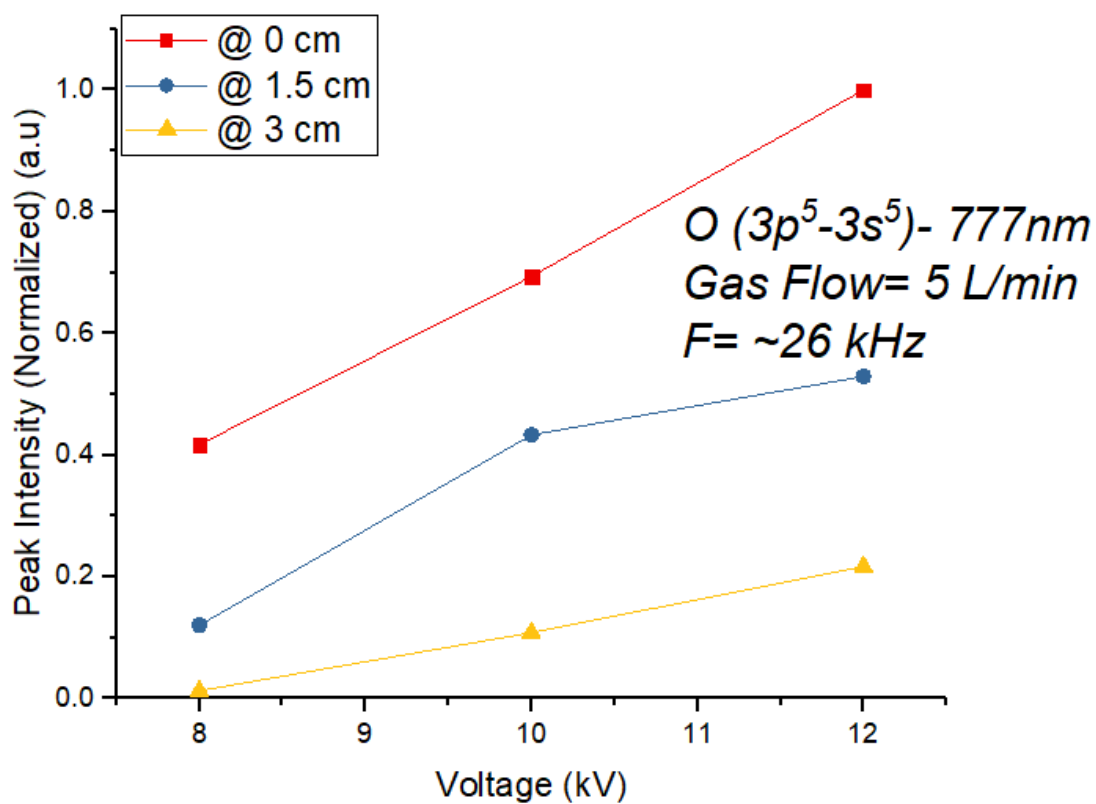
(b)



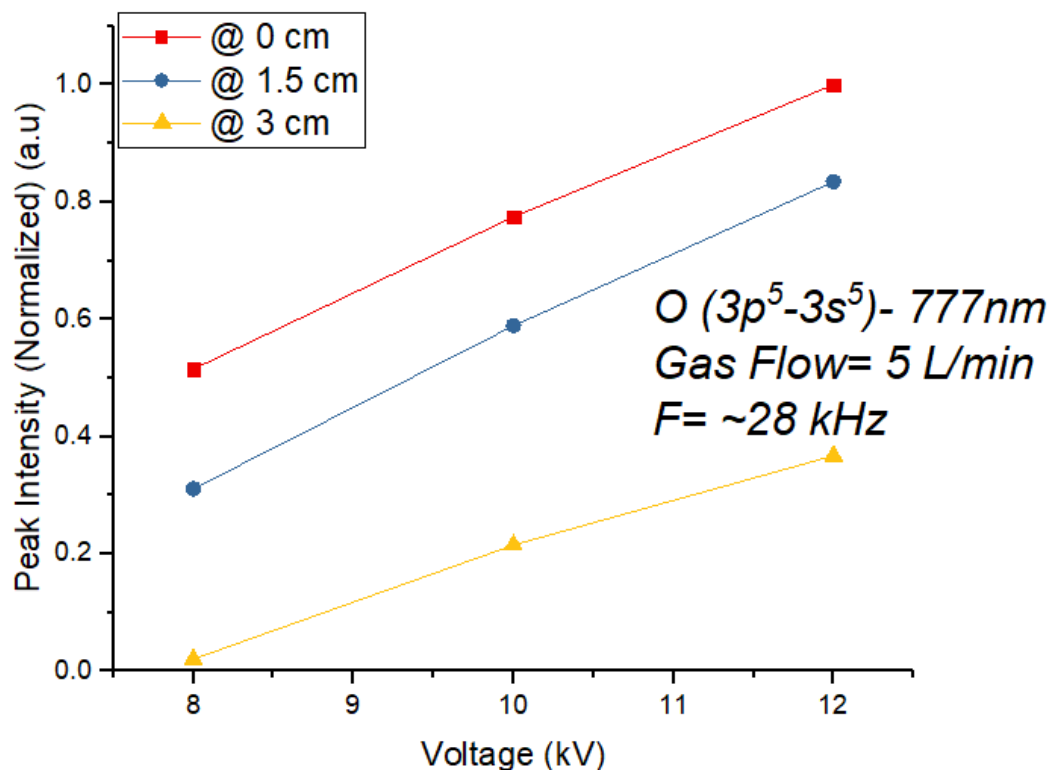
(c)

Figure 28. Dependence of atomic oxygen at (a) 26 kHz, (b) 28 kHz, (c) 30 kHz, on voltage and distance at gas flow rate 2.5 L/min.

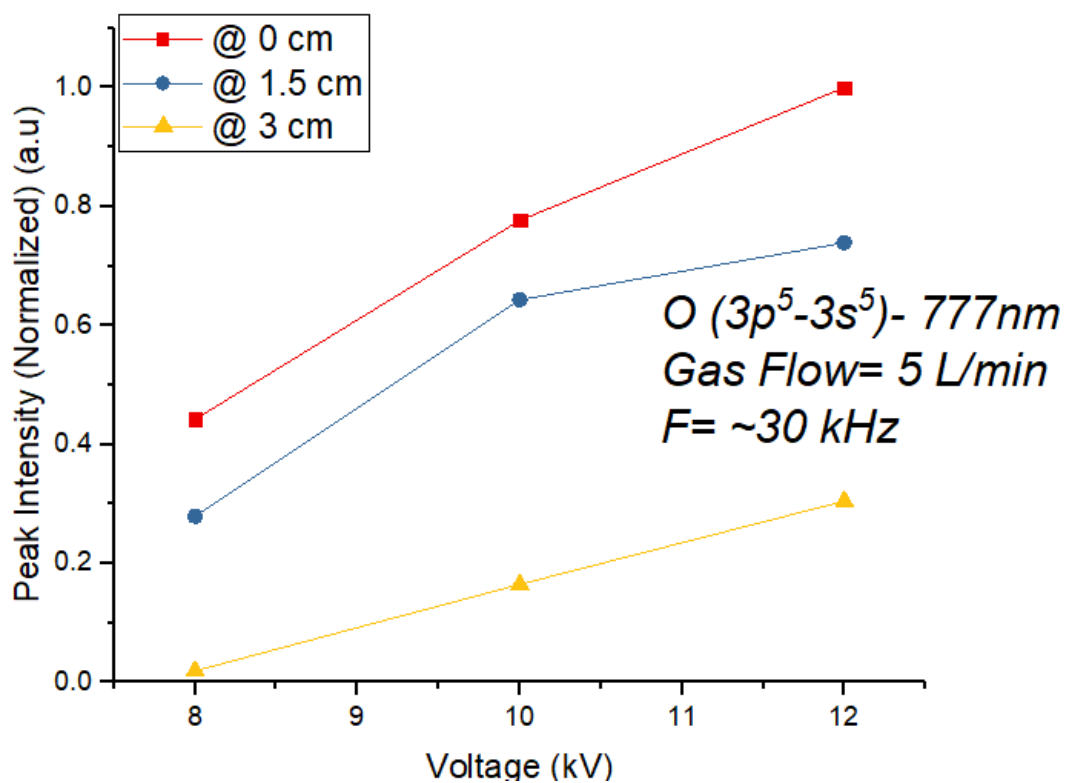
When increasing voltage, the atomic oxygen follows the same trend and increases along with it. This is due to the production mechanism that is responsible for these oxygen triplet bands. The increase in electron density and high energy electrons allow for more electron impact dissociation to occur and also allows more helium atoms to gain energy in order to provide the Penning-type reactions needed to dissociate and excite.



(a)

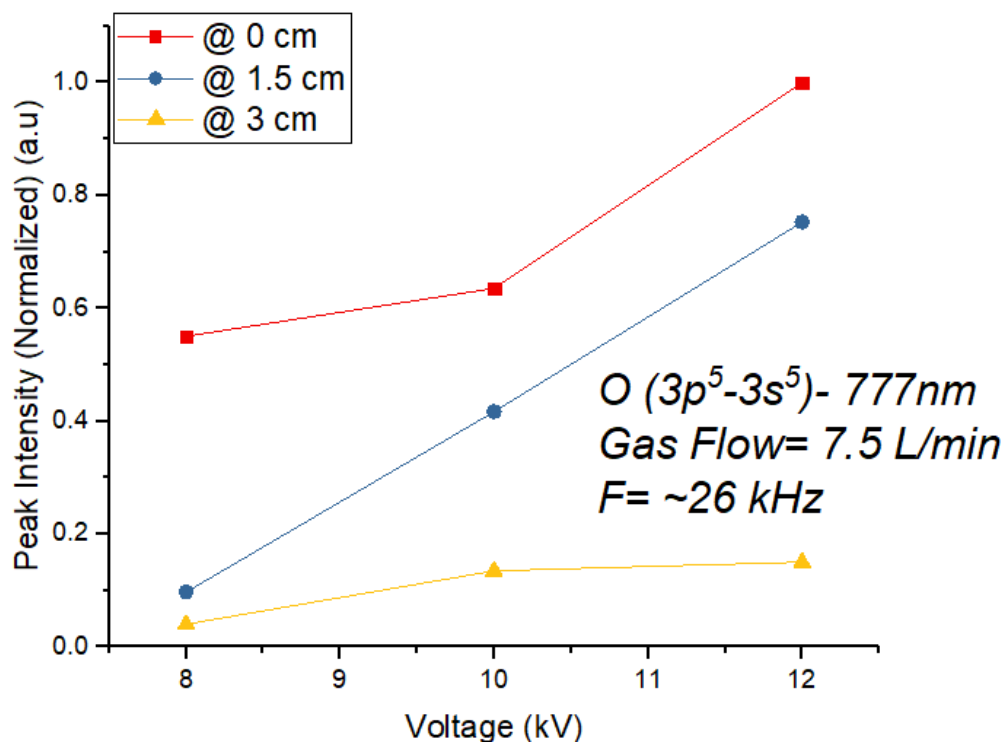


(b)

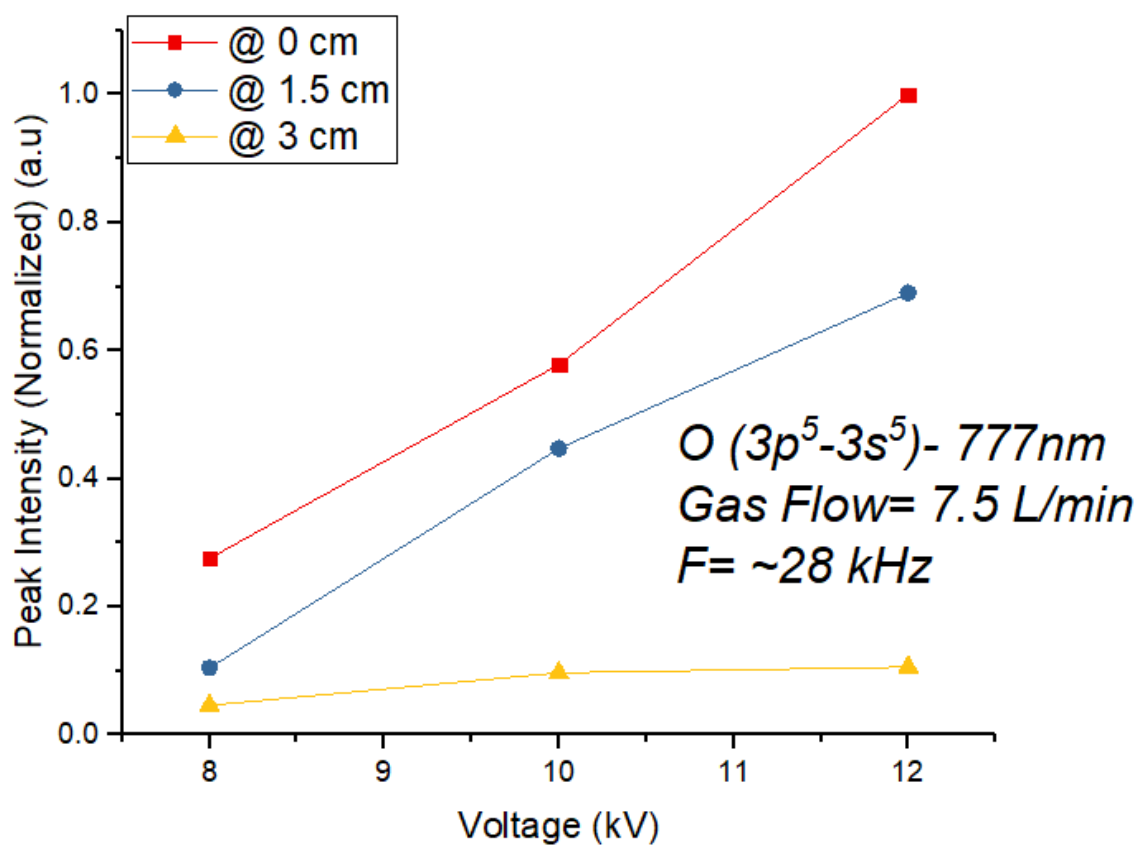


(c)

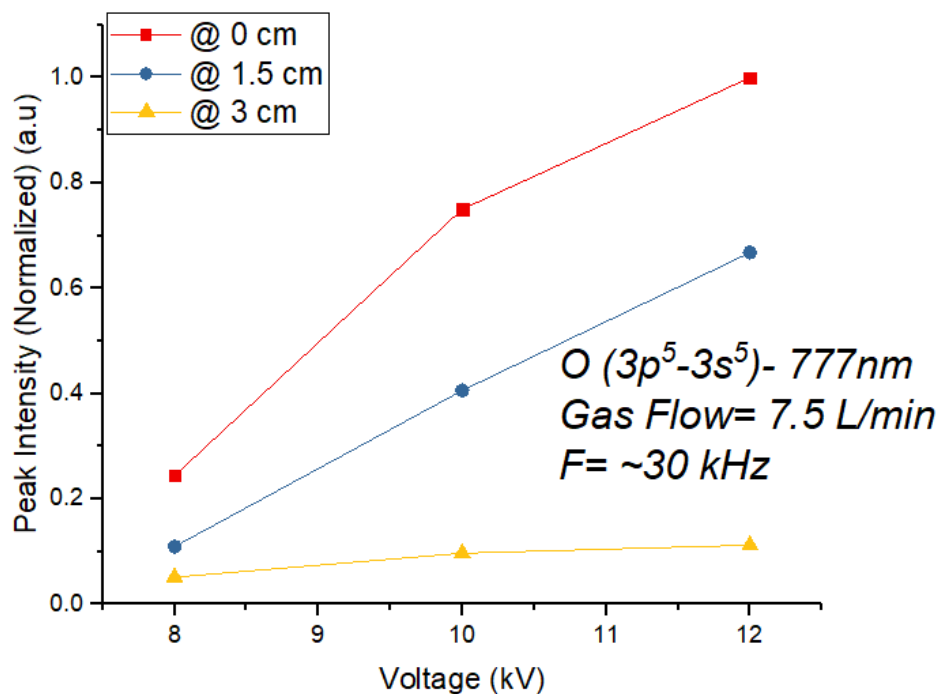
Figure 29. Dependence of atomic oxygen at (a) 26 kHz, (b) 28 kHz, (c) 30 kHz, on voltage and distance at gas flow rate 5 L/min.



(a)



(b)



(c)

Figure 30. Dependence of atomic oxygen at (a) 26 kHz, (b) 28 kHz, (c) 30 kHz, on voltage and distance at gas flow rate 7.5 L/min.

As can be seen in figures 29 and 30, the atomic oxygen triplet band is at its peak as soon as it exits the tube and then decreases as it gets further away from this point. This is seen in both the 5 L/min flow rate and the 7.5 L/min flow rate regardless of frequency. One reason for this observation concerns the mechanisms of its generation. As the jet extends out of the tube, the electron density continually decreases. Another reason for this decline is because of lack of free helium metastables to provide that Penning-type effect as the jet increases with distance. The helium metastable is responsible for this reaction as well as the ionization of N_2 which is also observed here. This is evident when comparing the reaction rate constants of both of these mechanisms. By doing this, it is seen that the helium metastables are 70 times more likely to react with the N_2 in the ambient air rather than the O_2 . Despite this, the dominant reason for this is the large instability coupled with its even higher reactivity of this excited atom. As a result, interaction with air causes it to collide, quench, and recombine primarily with O_2 to form O_3 .

(ozone). When distance increases, the interaction with the air increases, which is both good and bad. Good because it is that air interaction that paves the road for it to occur and bad because it makes it more likely to quench with the O₂ already in the air. The quenching and recombination process as well as reaction rate are given by [12]:

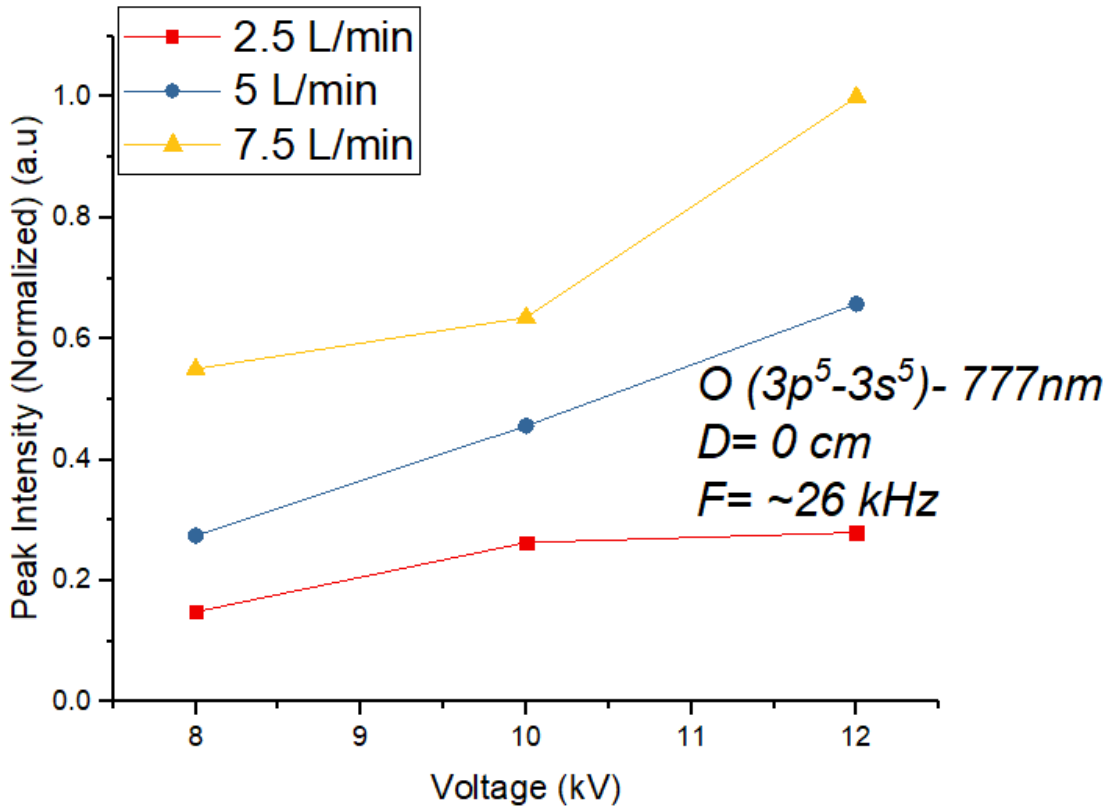
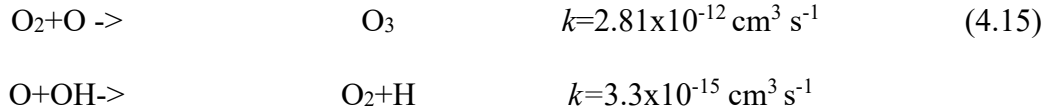


Figure 31. Dependence of atomic oxygen on gas flow rate at a frequency of 26 kHz.

As can be seen in figure 31, the production of atomic oxygen increases with an increase in flow rate. This is also noticeably seen in the emission intensity of the N₂ first negative system which also relies on the helium metastable as the method of production. With an increase in flow

rate, comes an increase of helium atoms that can be excited into the metastable state. This increase allows more O₂ to de-excite the metastables through the processes outlined above. Overall, the results reported in this subsection are in good agreement with those reported in [5] [22] [24] [28-29] [33-35].

4.1.7- Reynolds number (laminar vs turbulent flow)

Reynolds number is defined as the ration between inertial and viscous forces within a fluid and helps define whether a flow can be described as laminar or turbulent. This correlation for a helium appj was investigated by Pinchuk *et al.* [36] and it was reported that for Reynolds numbers of 300-500, the flow is in a transition sequence from laminar to turbulent and the jet length proportionality to gas flow begins to deviate [36]. Beyond a Reynolds number of 500, the flow is turbulent which leads to a mix between air and helium and the proportionality no longer holding true. The equation for the Reynolds number is given by [36]:

$$Re = \rho u d / \mu \quad (4.16)$$

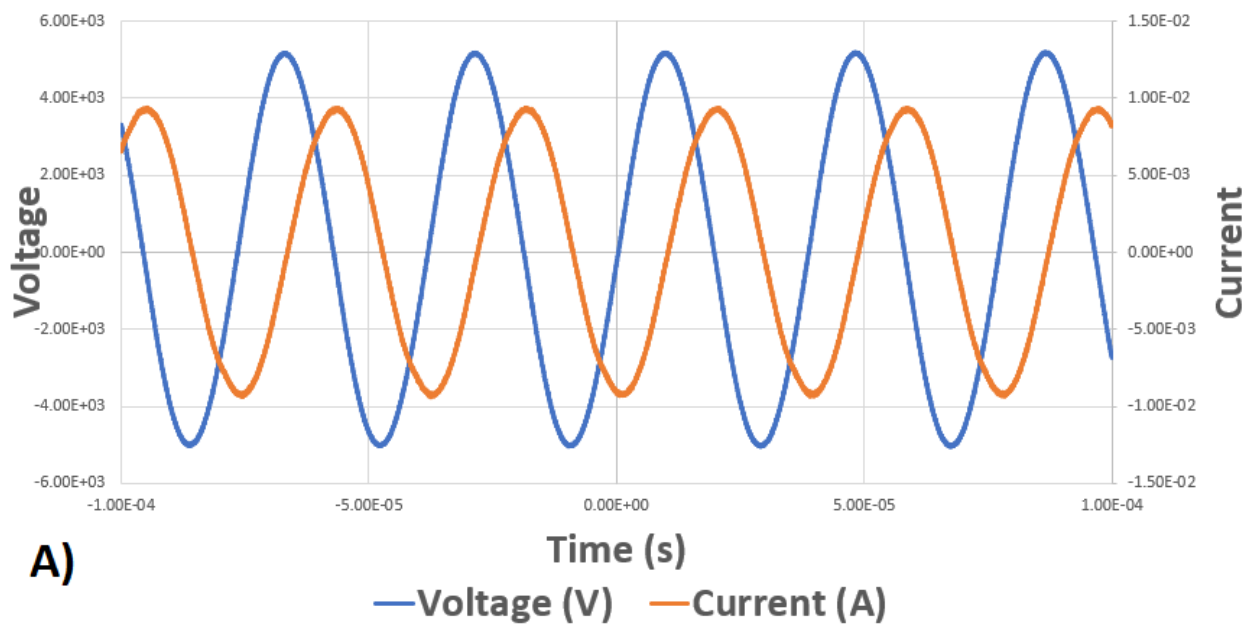
Here, ρ is the density of helium (.164 kg/m³), u is the gas flow velocity in m/s, d is the diameter of the tube in meters, and μ is the viscosity of helium (1.98 x 10⁻⁵ kg/m³). The diameter of the tube, as mentioned in Chapter 3, is 4.4 mm (.0044 m). To convert flow rate to velocity, the volume of the tube is calculated and was found to be .00233 L. Dividing flow rate by the volume of the tube gives the amount of times the gas is flushed out of the tube per minute. Dividing this value by 60 gives the amount of time the gas spends inside of the tube in seconds. Lastly,

dividing the length of the tube by the “gas residency time” gives the velocity in m/s. The calculated velocity and Reynolds numbers for this jet design is given in table 6.

Table 6- Calculated gas velocity and Reynolds numbers

Flow rate (L/min)	Velocity (m/s)	Reynolds number
2.5	2.74	99.9
5	5.47	199.4
7.5	8.2	298.8

4.2 Electrical Characteristics



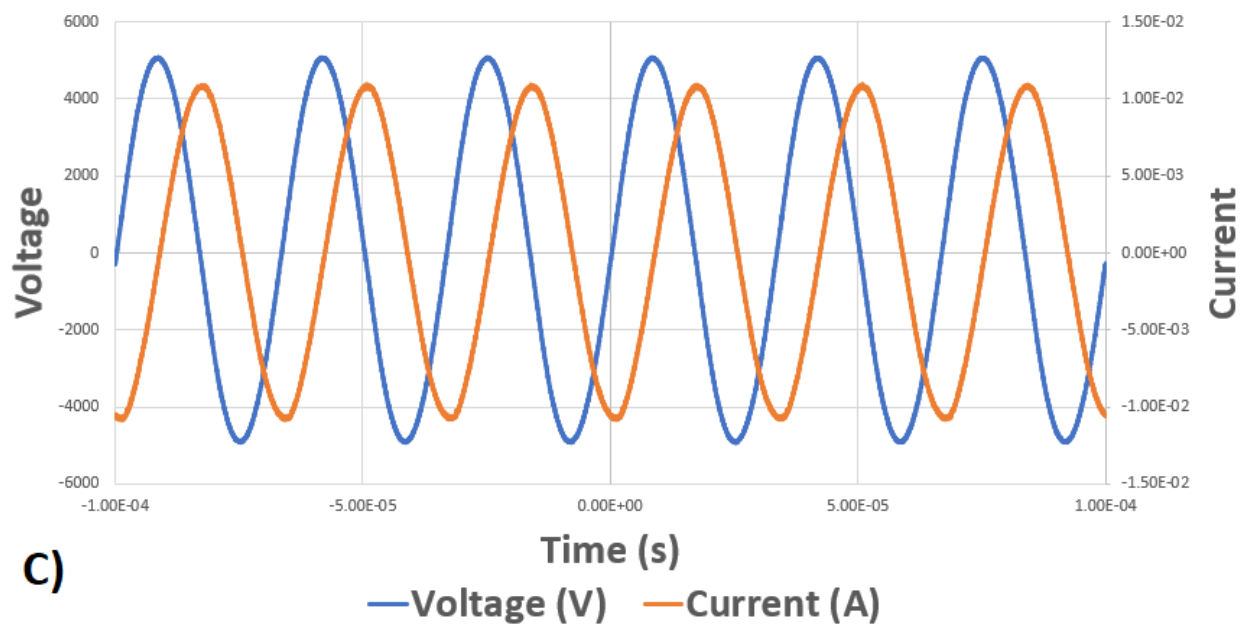
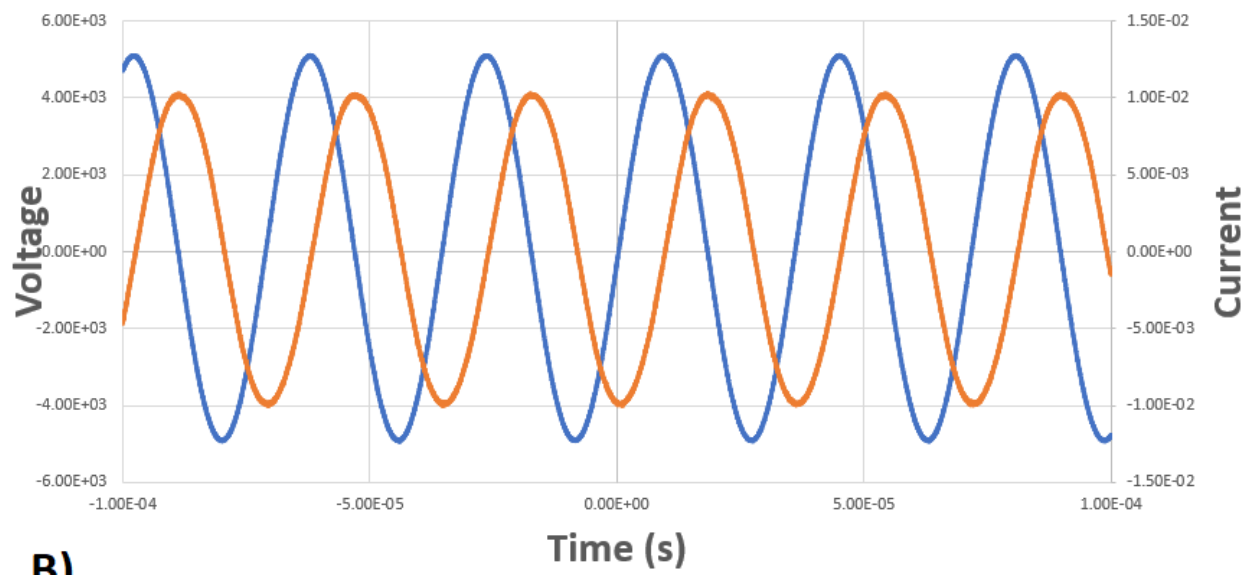
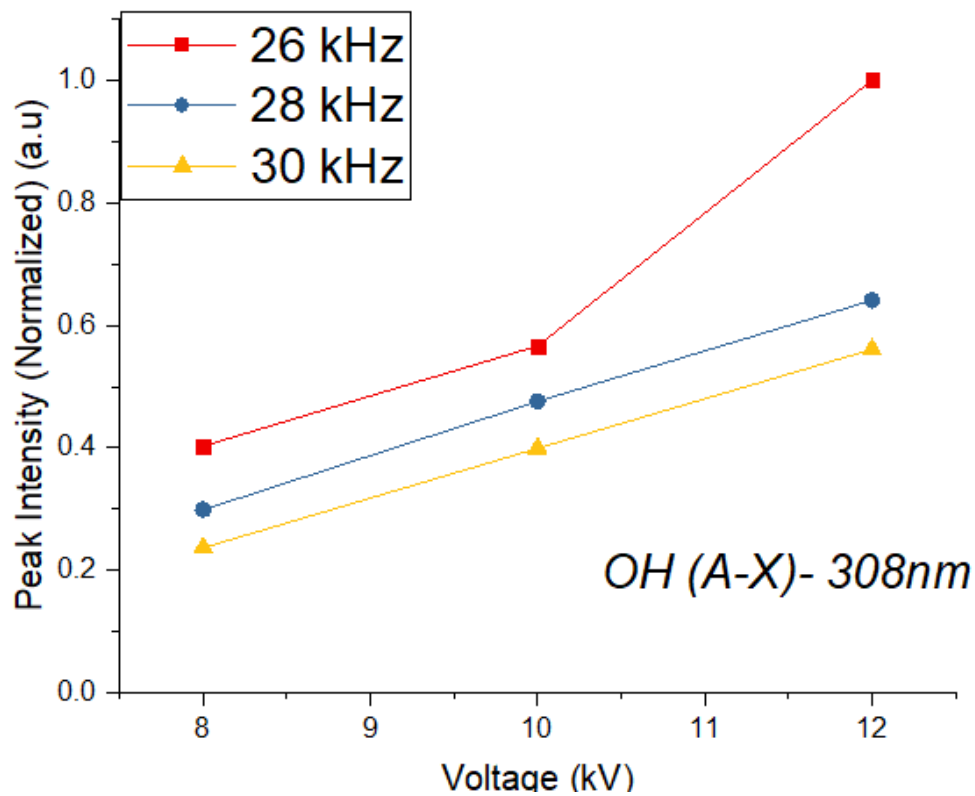


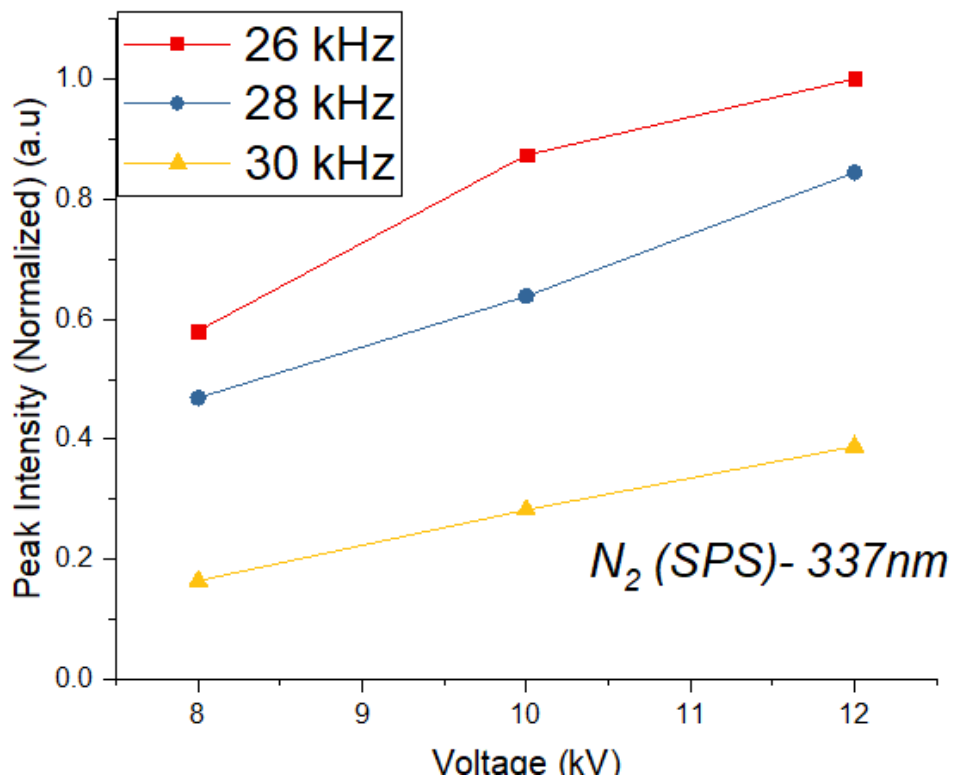
Figure 32. Applied current-voltage characteristic of the developed helium-air APPJ at 10 kV. A) 26 kHz B) 28kHz C) 30 kHz

Understanding the characteristics of the helium appj not only looks at what the jet is producing, but also how it is generating these products. In this plasma, the main energy carriers are the free electrons and the helium metastable atoms. The previous section detailed what species the jet produced and the mechanisms behind these productions such as reactions, rate constants, electron impact cross sections, electronic and vibrational state energies, and transition probabilities. However, what hasn't been discussed are the parameters and information regarding what is actually giving the energy to the electrons and helium atoms to do the producing. This section aims to discuss to the electrical data that was obtained at the time of the emission spectroscopy to examine the influence of these parameters.

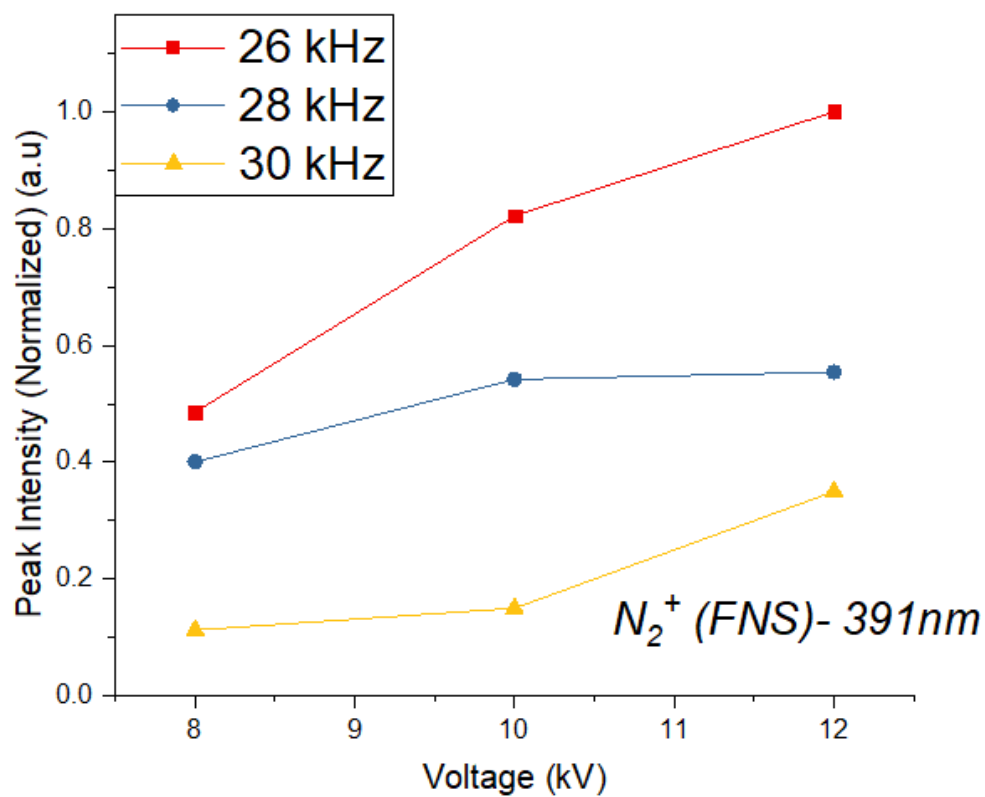
To begin, one observation that was seen during specie analysis was the fact that all species generated had the highest peak intensity at 26 kHz relative to 28 and 30 kHz for the same applied voltages and for all different flow rates. In an AC circuit, the frequency corresponds to how often the electrodes switch polarity. This causes the electron to oscillate back and forth at the rate of the applied frequency. Although this may be true, higher frequencies add more energy into the system, but the opposite is seen here.



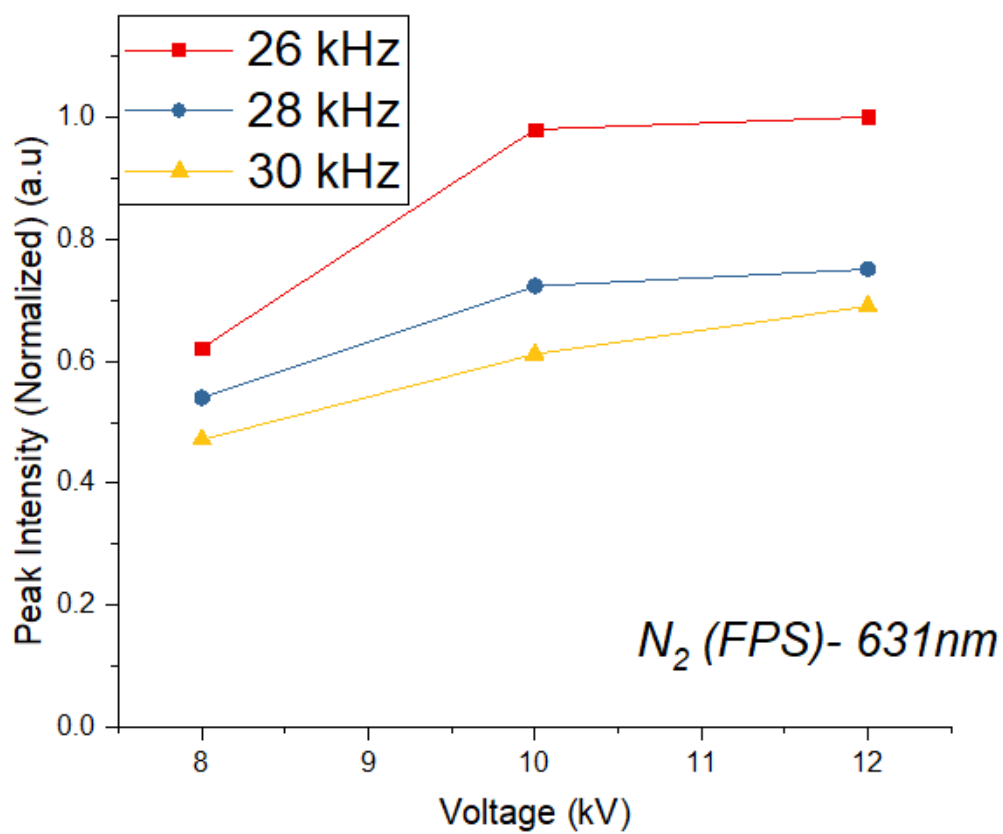
(a)



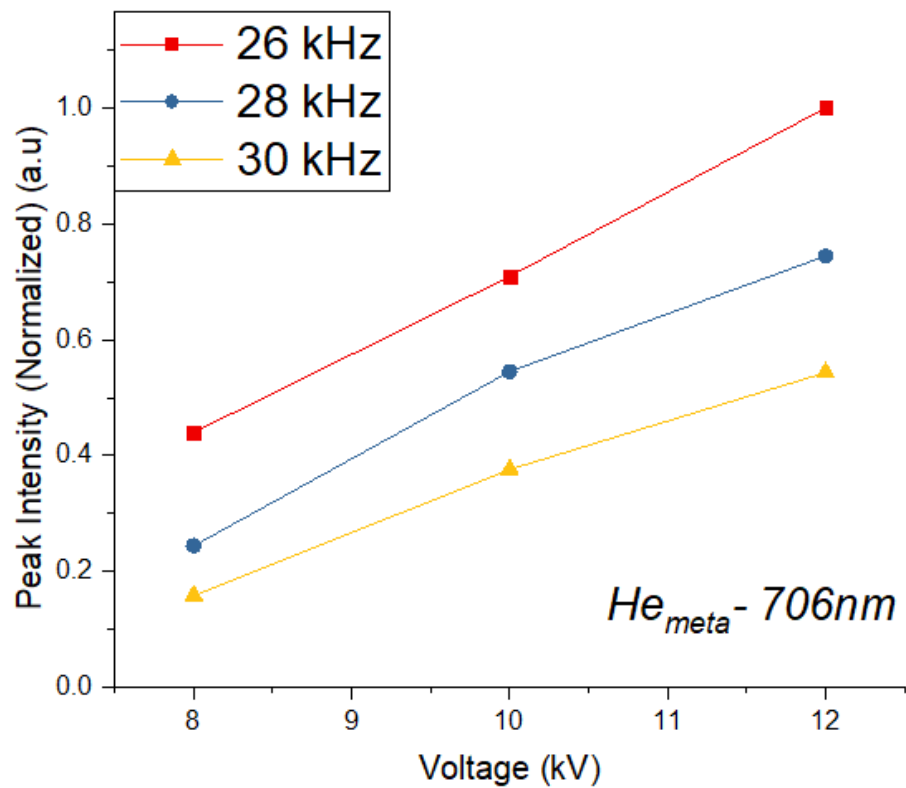
(b)



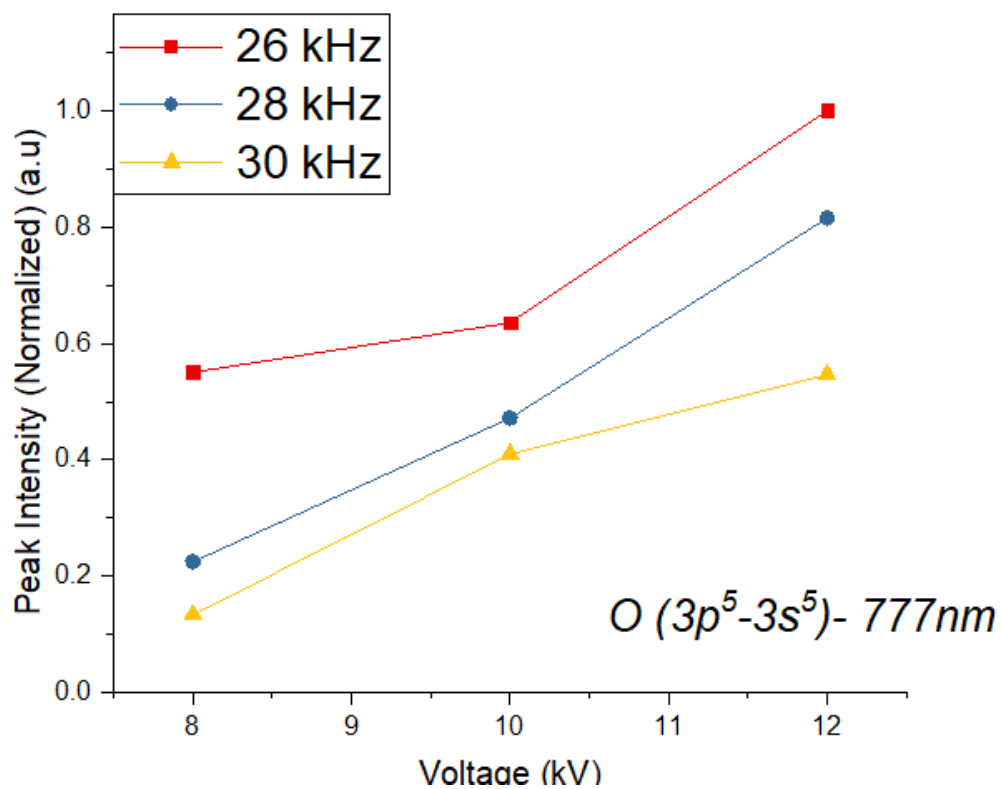
(c)



(d)



(e)



(f)

Figure 33. All species intensity as a function of frequency. (a)OH, (b) N_2 ($C^3\Pi_u-B^3\Pi_g$), (c) N_2^+ ($B^2\Sigma_u^+-X^2\Sigma_g^+$), (d) N_2 ($B^3\Pi_g-A^3\Sigma_u^+$), (e) helium metastable, (f) atomic oxygen.

As seen in figure 33, a frequency of 26 kHz shows the highest emission intensity of any other frequency used. The reason for this observation lies in the voltage parameters used. As the frequency in this experiment decreased, voltage was adjusted in order to match the voltage values at other frequencies. This meant that when going down in frequency, more power was drawn from the power supply in order to match the voltage reading at another frequency. This is supported through the measurements taken from a wattage meter that connected from the power supply to the wall outlet to provide the electrical measurements that was being drawn from the electrical outlet by the power supply. These readings are provided for all flow rates, frequencies, and voltages (tables 7-9) and shows that 26 kHz had the highest power coupling regardless of flow rate.

Table 7- Power Factor, Current, True Power, and Apparent Power of power supply at 2.5 L/min beginning with 26 kHz

Voltage (kV)	Power Factor	Current (A)	True Power (W)	Apparent Power (VA)
8	.84	.06	6.9	8.1
10	.84	.08	8.8	10.5
12	.82	.11	11.2	13.4
28 kHz				
8	.84	.06	6.4	7.7
10	.83	.08	7.7	8.5
12	.8	.1	9.6	11.8
30 kHz				
8	.84	.06	5.8	7.7
10	.81	.08	7.3	8.5
12	.8	.1	9.5	11.8

Table 8- Power Factor, Current, True Power, and Apparent Power of power supply at 5 L/min beginning with 26 kHz

Voltage (kV)	Power Factor	Current (A)	True Power (W)	Apparent Power (VA)
8	.85	.06	6.5	7.5
10	.84	.08	8.6	10.2
12	.83	.11	11.2	13.4
28 kHz				
8	.85	.05	6.3	7
10	.83	.07	7.7	8.6
12	.82	.09	9.4	11.8
30 kHz				
8	.85	.05	5.8	6.5
10	.81	.07	7.3	8
12	.79	.09	9.3	11.6

Table 9- Power Factor, Current, True Power, and Apparent Power of power supply at 7.5 L/min beginning with 26 kHz

Voltage (kV)	Power Factor	Current (A)	True Power (W)	Apparent Power (VA)
8	.85	.06	6.7	7.9
10	.83	.08	8.8	10.5
12	.83	.11	11.4	13.7
28 kHz				
8	.85	.05	6.4	6.9

10	.82	.07	7.8	8.7
12	.81	.09	9.8	12.2
30 kHz				
8	.85	.05	5.6	6.6
10	.82	.07	6.9	8.4
12	.8	.09	9.1	11.2

The information in these tables serve to confirm that an increase of power was consumed and applied a stronger electric field to those free electrons, which was then delivered to the various processes which occurred in the plasma. This led to the intensities of all species to be heightened in relation to the other frequencies. In regards to the observation made earlier that the jet length would shorten at 12 kV and 2.5 L/min, these readings do not provide an explanation as to why that occurs. Initially it was postulated that as the gas flow is the virtual ground in the system, the lower flow rate didn't compensate the polarization of the charges as efficiently as the other flow rates. However, this does not seem to be the case as the power measurements provided in tables 7-9 show a slight deviation in readings, but not enough to justify that theory which must be investigated further.

Also recorded were the values of applied peak to peak voltage and current, along with the RMS values. It was observed that the degree of the flow rate did not have any effect on these values. Despite this, a change was noticed as frequency was adjusted. As frequency increased current values increased as well. This is due to the fact that the plasma jet reactor is essentially a capacitor that builds up charge and releases it when discharge occurs. When frequency increases

along a capacitor, capacitive reactance decreases as a result. This allows more current to flow through the capacitive element and leads to the trend observed in table 10.

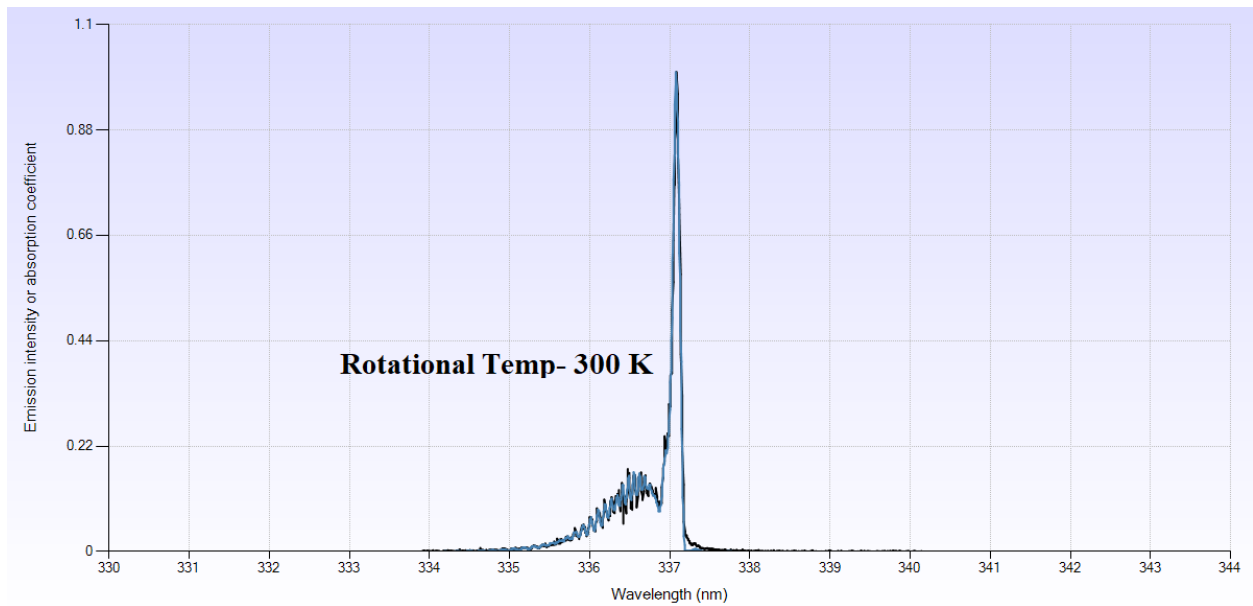
Table 10- Voltage and Current peak to peak and RMS values for different frequencies for all flow rates

V pk-to-pk (kV)	V RMS (kV)	Frequency	I pk-to-pk (mA)	I RMS (mA)
26 kHz				
8	~2.8		14.7	5.2
10	~3.5		18.7	6.7
12	~4.2		23.4	8.3
28 kHz				
8	~2.8		16	5.7
10	~3.5		20.5	7.2
12	~4.2		25	8.6
30 kHz				
8	~2.8		17.5	6.1
10	~3.5		22	7.7
12	~4.2		27	9.3

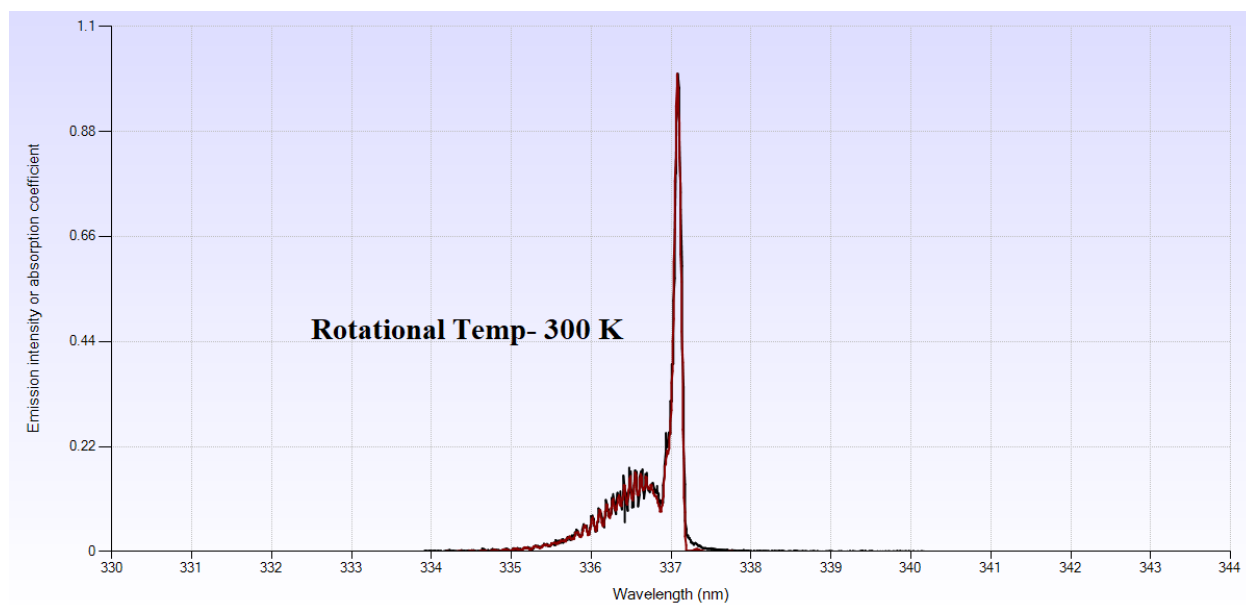
4.3- Gas Temperature Fit

The temperature of the plasma is one of its defining and most significant features of the non-thermal jet. Its relatively low temperature makes it very convenient for vital applications such as medical, biological, agricultural, and many more. Although this may be true, investigations into the dependency of gas temperature on operating parameters has not be thoroughly investigated at all. As mentioned previously throughout this work, the parameters in which the jet operates at dictates the energy values going into the system. It is assumed that as

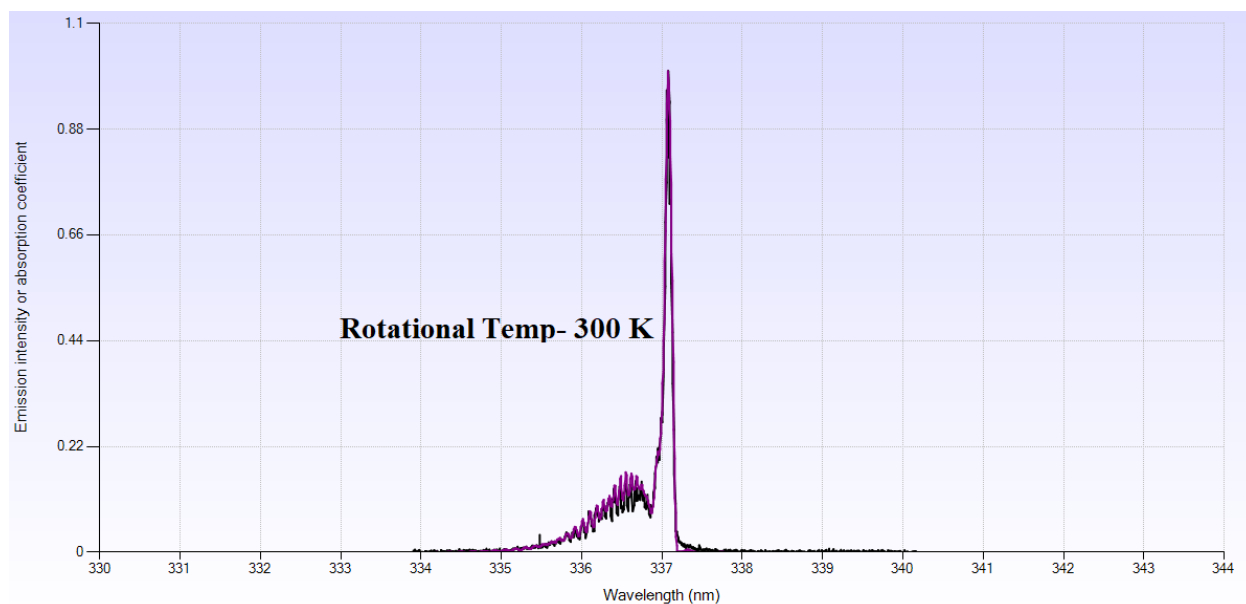
voltage and frequency is added to the system, more energy is added into the system which can possibly change the gas temperature. It is also assumed that as gas flow rate increases, this adds a cooling factor to the jet which may affect gas temperature. Through the use of Specair, which is able to simulate theoretical energies based on best fitting the experimental spectrum, this hypothesis is investigated. For our electronic temperatures, it is assumed to be at 1 eV (~12000 K) due to the low temperature nature of the plasma, while rotational temperatures are of interest and the specie simulated is the ground level N₂ Second Positive System at 337nm.



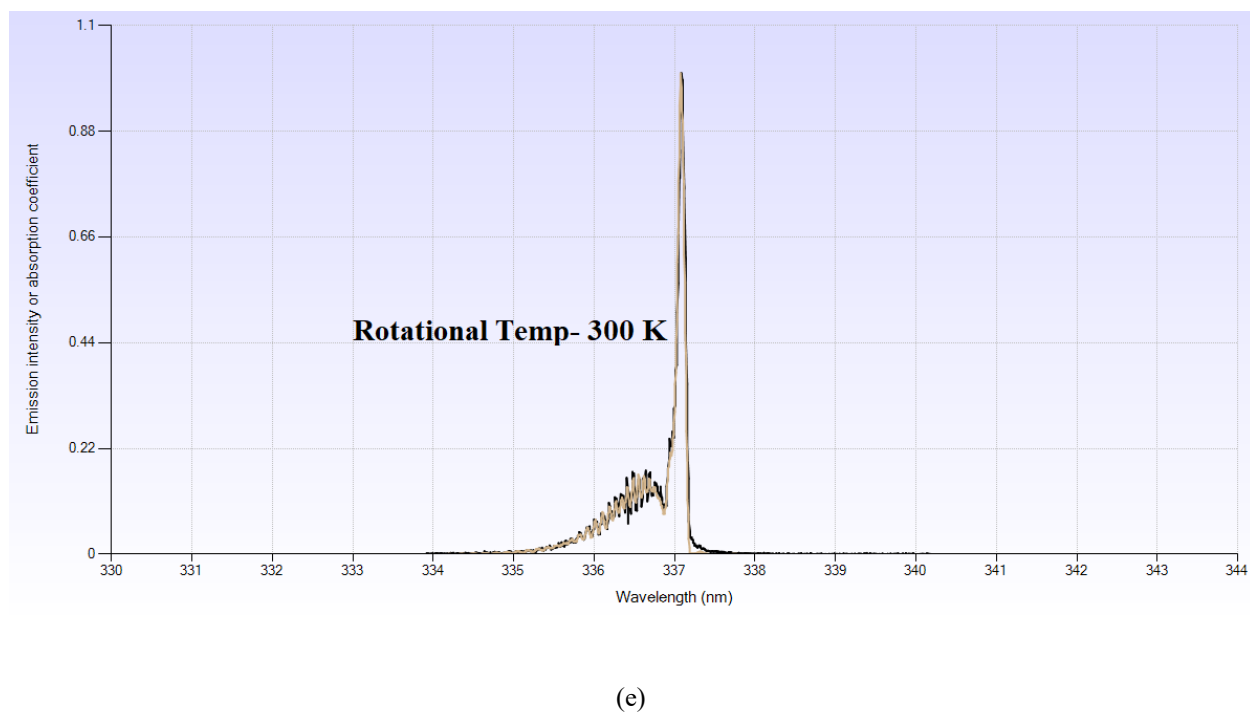
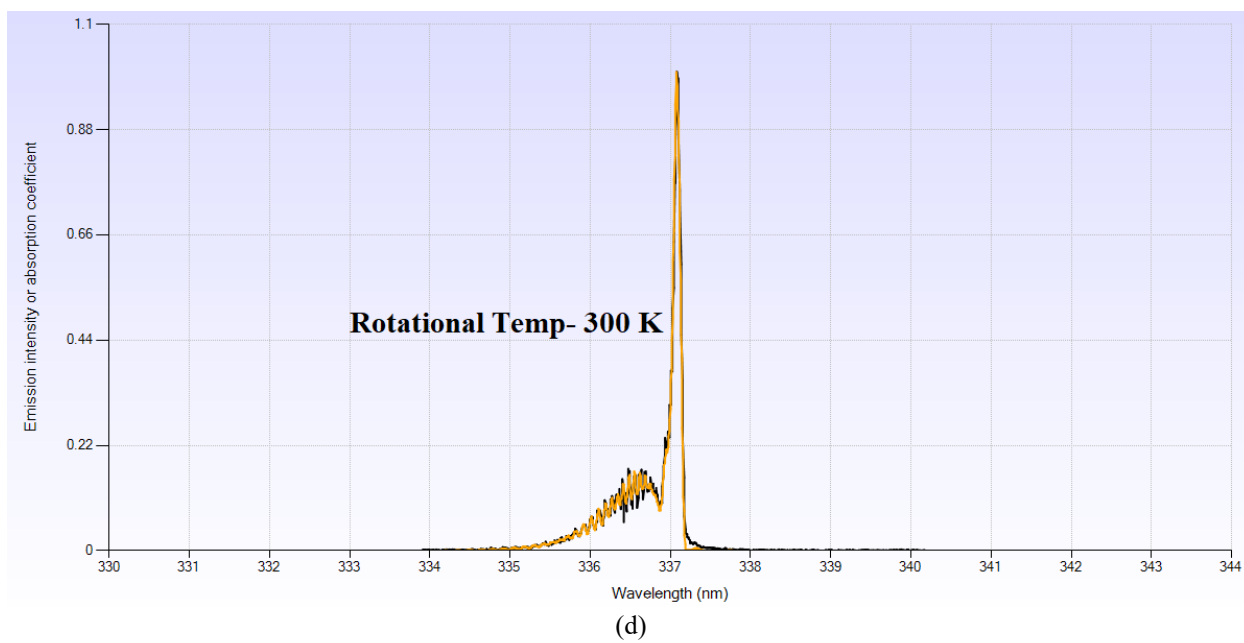
(a)

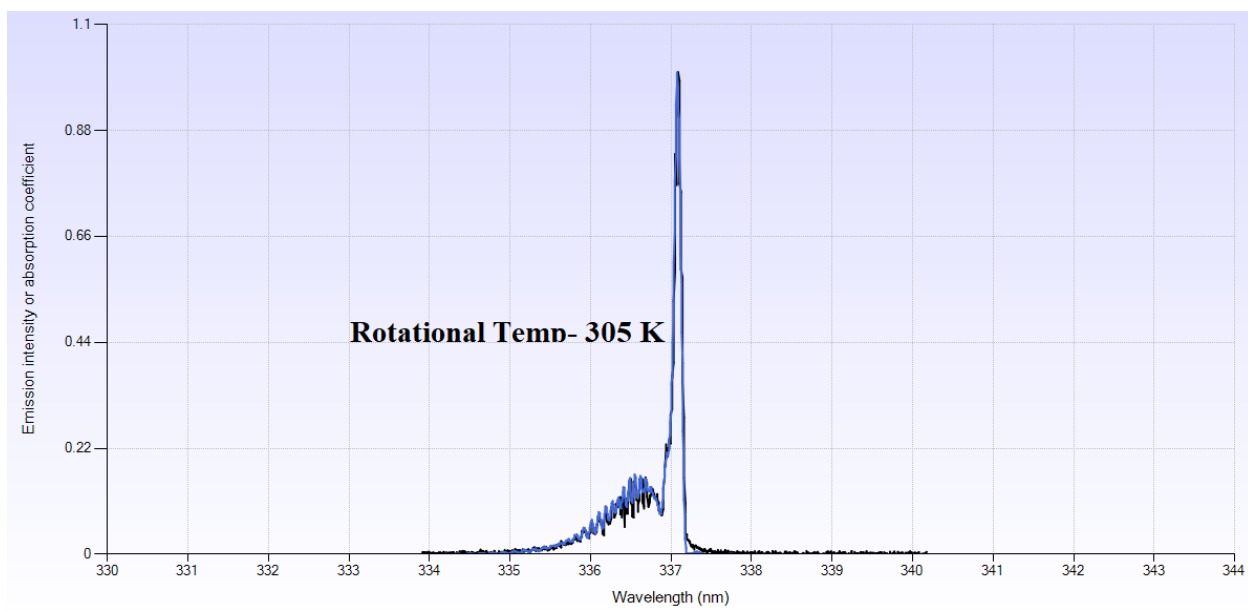


(b)

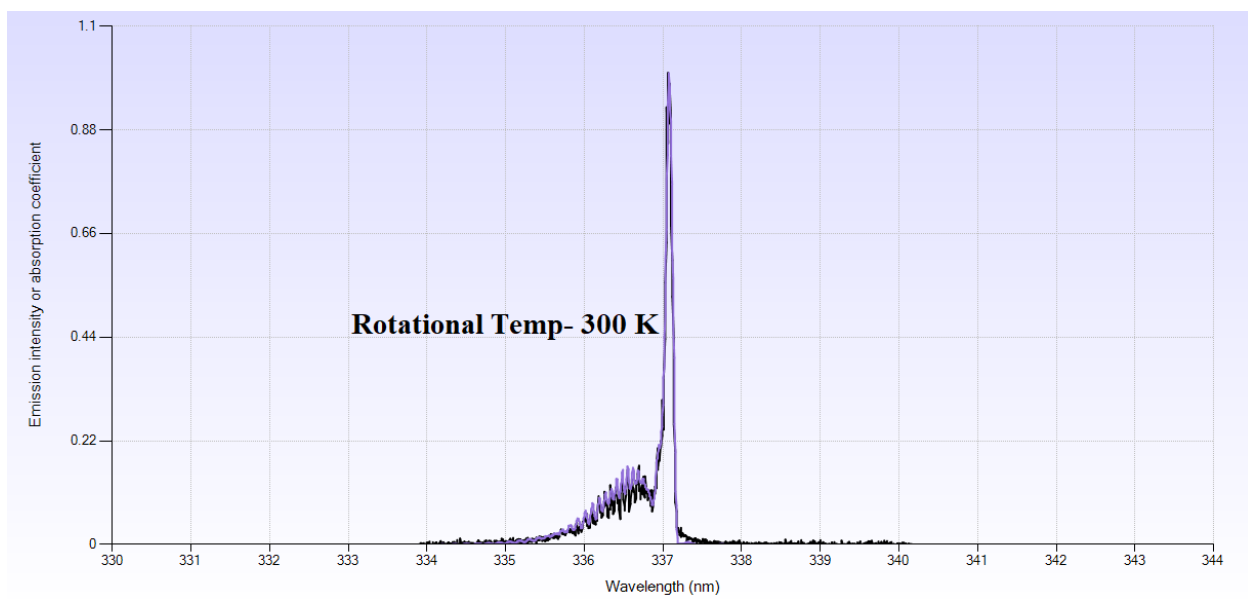


(c)

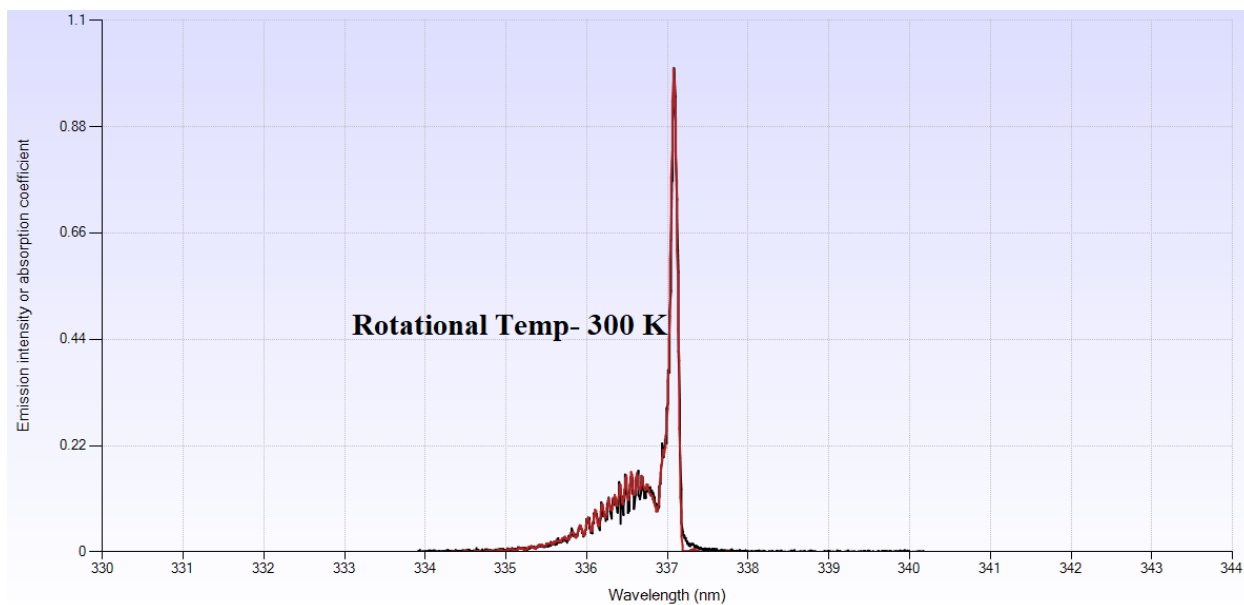




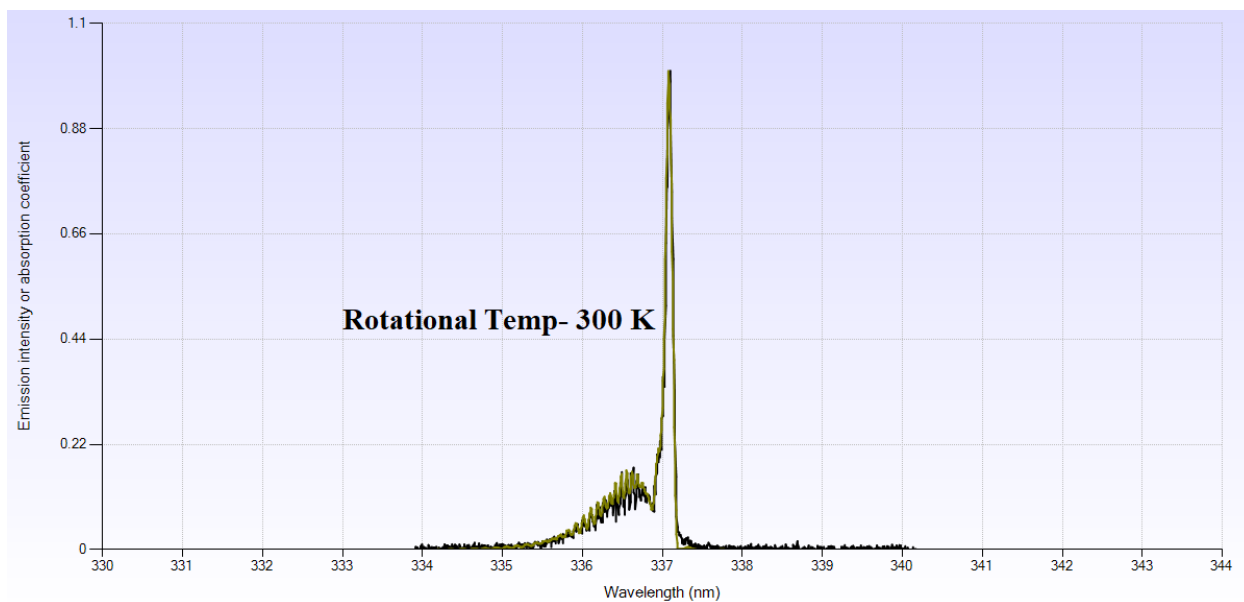
(f)



(g)



(h)



(i)

Figure 34. Specair rotational (Gas) temperature simulations for (a) 2.5 L/min 26 kHz, (b) 2.5 L/min 28 kHz, (c) 2.5 L/min 30 kHz, (d) 5 L/min 26 kHz, (e) 5 L/min 28 kHz, (f) 5 L/min 30 kHz, (g) 7.5 L/min 26 kHz, (h) 7.5 L/min 28 kHz, (i) 7.5 L/min 30 kHz.

Figure 34 shows the specair simulations of all the experimental parameters in this work and the corresponding gas temperatures as a result of best fitting the imported spectrum. It is observed that regardless of operating parameter, the gas temperature remains firmly at 300 K, with a slight deviation. This deviation is well within the uncertainty of the program which is ± 10 K. This is an indication that the energy change provided by a change in operating parameter does not affect the gas temperature in any way. As per the conservation of energy principle, this means that the energy change in the system may be going into other forms of energy such as electronic, translational, and vibrational. More studies are required in order to truly grasp the concept of energy transfer as a result of changing the operating parameters and its influence not only on the system but on the species produced.

CHAPTER 5: CONCLUSION

This work aimed to provide a detailed analysis of this jet design through OES diagnostics. Voltage and flow rate showed to have the greatest effect on specie generation, while air interaction dictated temporal evolution of the species produced. Applied frequency altered the power coupling of the system which was discussed to understand the degree of this effect. Depending on application needed, certain species are required and maximum yield of these species are investigated in this jet design. The findings here allow for optimization of the jet parameters in order to single out specific needs. Further work is needed such as accurate modelling, electron density fittings of H (β) lines, electrode and dielectric tube influence. These will allow much more comprehensive study of this jet as well as understanding how the results of this design differs from another.

REFERENCES

- [1]- Fridman, Alexander A. *Plasma Physics and Engineering*. CRC Press, 2012.
- [2]- Lu, Xinpei, et al. *Nonequilibrium Atmospheric Pressure Plasma Jets: Fundamentals, Diagnostics, and Medical Applications*. CRC Press, 2019.
- [3]- Jiang, Nan, et al. “Atmospheric Pressure Plasma Jet: Effect of Electrode Configuration, Discharge Behavior, and Its Formation Mechanism.” *Journal of Applied Physics*, vol. 106, no. 1, 2009, p. 013308., doi:10.1063/1.3159884.
- [4]- Zhu, Wen-Chao, et al. “Characteristics of Atmospheric Pressure Plasma Jets Emerging into Ambient Air and Helium.” *Journal of Physics D: Applied Physics*, vol. 42, no. 20, 2009, p. 202002., doi:10.1088/0022-3727/42/20/202002.
- [5]- Ilik, Erkan, and Tamer Akan. “Optical Properties of the Atmospheric Pressure Helium Plasma Jet Generated by Alternative Current (A.c.) Power Supply.” *Physics of Plasmas*, vol. 23, no. 5, 2016, p. 053501., doi:10.1063/1.4948718.
- [6]- Laux, C O, et al. “Optical Diagnostics of Atmospheric Pressure Air Plasmas.” *Plasma Sources Science and Technology*, vol. 12, no. 2, 2003, pp. 125–138., doi:10.1088/0963-0252/12/2/301.
- [7]- Forster, P., V. Ramaswamy, P. Artaxo, T. Berntsen, R. Betts, D.W. Fahey, J. Haywood, J. Lean, D.C. Lowe, G. Myhre, J. Nganga, R. Prinn, G. Raga, M. Schulz and R. Van Dorland, 2007: Changes in Atmospheric Constituents and in Radiative Forcing. In: *Climate Change 2007: The Physical Science Basis. Contribution of Working Group I to the Fourth Assessment Report of the Intergovernmental Panel on Climate Change* [Solomon, S., D. Qin, M. Manning, Z. Chen, M. Marquis, K.B. Averyt, M. Tignor and H.L. Miller (eds.)]. Cambridge University Press, Cambridge, United Kingdom and New York, NY, USA.
- [8]- Peter Bruggeman and Daan C Schram 2010 *Plasma Sources Sci. Technol.* **19** 045025
- [9]- Itikawa, Yukikazu, and Nigel Mason. “Cross Sections for Electron Collisions with Water Molecules.” *Journal of Physical and Chemical Reference Data*, vol. 34, no. 1, 2005, pp. 1–22., doi:10.1063/1.1799251.
- [10]- Herron, J.T., Green, D.S. Chemical Kinetics Database and Predictive Schemes for Nonthermal Humid Air Plasma Chemistry. Part II. Neutral Species Reactions. *Plasma Chemistry and Plasma Processing* **21**, 459–481 (2001). <https://doi.org/10.1023/A:1011082611822>
- [11]- NIST Chemical Kinetics Database, Standard Reference Database 17, Version 7.0 (Web Version), Release 1.6.8, Data Version 2015.09 (<http://kinetics.nist.gov/kinetics/>)

- [12]- Liu, Z., Yang, X., Zhu, A. *et al.* Determination of the OH radical in atmospheric pressure dielectric barrier discharge plasmas using near infrared cavity ring-down spectroscopy. *Eur. Phys. J. D* **48**, 365–373 (2008). <https://doi.org/10.1140/epjd/e2008-00110-7>
- [13]- R. P. Gott and K. G. Xu, "OH Production and Jet Length of an Atmospheric-Pressure Plasma Jet for Soft and Biomaterial Treatment," in *IEEE Transactions on Plasma Science*, vol. 47, no. 11, pp. 4988-4999, Nov. 2019.
- [14]- Itikawa, Yukikazu. (2006). Cross Sections for Electron Collisions with Nitrogen Molecules. *Journal of Physical and Chemical Reference Data - J PHYS CHEM REF DATA*. 35. 10.1063/1.1937426.
- [15]- Walsh, James & Shi, J. & Kong, Michael. (2006). Contrasting characteristics of pulsed and sinusoidal cold atmospheric plasma jets. *Applied Physics Letters*. 88. 171501-171501. 10.1063/1.2198100.
- [16]- N Mericam-Bourdet *et al* 2009 *J. Phys. D: Appl. Phys.* **42** 055207
- [17]- Bayram, Burcin & Freamat, Mario. (2012). Vibrational spectra of N₂ : An advanced undergraduate laboratory in atomic and molecular spectroscopy. *American Journal of Physics*. 80. 664. 10.1119/1.4722793.
- [18]- Liu, Zhinan *et al.* "A Study on Coaxial Type DBD Decomposing NO/N₂ Mixture Gas by Optical Emission Spectrum." *2012 Fifth International Conference on Intelligent Computation Technology and Automation (2010)*: 657-661.
- [19]- Lofthus, Alf, and Paul H. Krupenie. *The Spectrum of Molecular Nitrogen*. 1977.
- [20]- Asma, Begum & Laroussi, Mounir & Pervez, Mohammad. (2013). Atmospheric pressure He-air plasma jet: Breakdown process and propagation phenomenon. *AIP Advances*. 3. 10.1063/1.4811464.
- [21]- Li, Qing & Zhu, Xi-Ming & Li, Jiang-Tao & Pu, Yi-Kang. (2010). Role of metastable atoms in the propagation of atmospheric pressure dielectric barrier discharge jets. *Journal of Applied Physics*. 107. 043304 - 043304. 10.1063/1.3295914.
- [22]- Pancheshnyi, S.v., *et al.* "Measurements of Rate Constants of the N₂(C³Π_u,v'=0) and N₂+(B²Σ⁺u,v'=0) Deactivation by N₂, O₂, H₂, CO and H₂O Molecules in Afterglow of the Nanosecond Discharge." *Chemical Physics Letters*, vol. 294, no. 6, 1998, pp. 523–527., doi:10.1016/s0009-2614(98)00879-3.
- [23]- Qing Xiong *et al* 2013 *Plasma Sources Sci. Technol.* **22** 015011

- [24]- Martínez, H. & Castillo, Fernando & Martínez, H. & Villa, Mauro & Villalobos, S. & Reyes, P. & Flores, O.. (2014). Characterization of DC He-N₂ mixture plasma using optical emission spectroscopy and mass spectrometry. *Physics of Plasmas*. 21. 053502. 10.1063/1.4875343.
- [25]- Manalis, M.s., and H.p. Broida. "Vibrational Distributions of the N₂ first Positive System Produced in a Flowing Helium Afterglow." *Molecular Physics*, vol. 20, no. 5, 1971, pp. 947–951., doi:10.1080/00268977100100941.
- [26]- Paul N. Stanton and Robert M. St. John, "Electron Excitation of the First Positive Bands of N₂ and of the First Negative and Meinel Bands of N₂⁺," *J. Opt. Soc. Am.* **59**, 252-260 (1969)
- [27]- Kramida, A., Ralchenko, Yu., Reader, J., and NIST ASD Team (2019). *NIST Atomic Spectra Database* (ver. 5.7.1), [Online]. Available: <https://physics.nist.gov/asd> [2020, April 4]. National Institute of Standards and Technology, Gaithersburg, MD. DOI: <https://doi.org/10.18434/T4W30F>
- [28]- G. Uchida, K. Takenaka, K. Kawabata and Y. Setsuhara, "Influence of He Gas Flow Rate on Optical Emission Characteristics in Atmospheric Dielectric-Barrier-Discharge Plasma Jet," in *IEEE Transactions on Plasma Science*, vol. 43, no. 3, pp. 737-744, March 2015.
- [29]- Janev, R.K., & Smith, J.J. (1993). Cross sections for collision processes of hydrogen atoms with electrons, protons and multiply charged ions. International Atomic Energy Agency (IAEA): IAEA.
- [30]- Berrington, K. A., et al. "Electron Excitation Rates for Helium." *Monthly Notices of the Royal Astronomical Society*, vol. 200, no. 2, 1982, pp. 347–350., doi:10.1093/mnras/200.2.347.
- [31]- Yang, De-Zheng & Yang, Yang & Li, Shou-Zhe & Nie, Dong-Xia & Zhang, Shuai & Wang, Wenchun. (2012). A homogeneous dielectric barrier discharge plasma excited by a bipolar nanosecond pulse in nitrogen and air. *Plasma Sources Science and Technology*. 21. 10.1088/0963-0252/21/3/035004.
- [32]- K Niemi *et al* 2011 *Plasma Sources Sci. Technol.* **20** 055005
- [33]- Xiong, Qing & Lu, Xinpei & Liu, J. & Xian, Y. & Xiong, Zaiping & Zou, F. & Zou, Chengwei & Gong, W. & Hu, Jhen-Jia & Chen, K. & Pei, X. & Jiang, Zuoyu & Pan, Yijie. (2009). Temporal and spatial resolved optical emission behaviors of a cold atmospheric pressure plasma jet. *Journal of Applied Physics*. 106. 083302 - 083302. 10.1063/1.3239512.

- [34]- Milosavljević, V., et al. "Influence of Plasma Chemistry on Oxygen Triplets." *The European Physical Journal D*, vol. 64, no. 2-3, 2011, pp. 437–445.,
doi:10.1140/epjd/e2011-20213-2.